Contents

List of Figures

Introduction

The aim of this thesis is to present some macroscopic models for supply chains and networks able to reproduce the goods dynamics, successively to show, via simulations, some phenomena appearing in planning and managing such systems and, finally, to deal with optimization problems. The analyzed macroscopic models are based on the conservation laws, which are represented by special partial differential equations where the variable is a *conserved quantity*, physically a quantity which can neither be created nor destroyed. The main idea is to look at large scales so to consider the processed parts as small particles which flow in a continuous way and to assume the conservation of their density.

Depending on the observation scale supply networks modeling is characterized by different mathematical approaches: discrete event simulations and continuous models. Since discrete event models (see [11]) are based on considerations of individual parts, their main drawback is, however, an enormous computational effort. Then a cost-effective alternative to them is continuous models, described by some partial differential equation. The first proposed continuous models date back to the early 60's and started with the work of [4] and [15], but the most significant in this direction was [10], where the authors, via a limit procedure on the number of parts and suppliers, have obtained a conservation law ([3], [9]), whose flux involves either the parts density or the maximal productive capacity.

Then, in recent years continuous and homogenous product flow models have been introduced, for example in [8], [14], [10], [17], [18], and they have been built in close connection to other transport problems like vehicular traffic flow and queuing theory. Extensions on networks have been also treated in [13], [19], [20].

In this thesis, starting by the historical model of Armbruster - Degond - Ringhofer, we have compared two different macroscopic models, i.e. the Klar model,

based on a differential partial equation for density and an ordinary differential equation to capture the evolution of queues, and a continuum-discrete model, formed by a conservation law for the density and an evolution equation for processing rate. Both the models can be applied for supply chains and networks.

A supply network is characterized by a set of interconnected suppliers which, in general, consist of a processor and, if we deal with the Klar model, a buffer or a queue. Each processor is characterized by a maximum processing rate μ_j, length L_j, and processing time T_j. The quantity $\frac{L_j}{T_j}$ represents the processing velocity. To study the dynamics at the connection points or junctions, some special parameters are introduced; in particular when the number of incoming suppliers is greater than the outgoing ones, we consider the priority parameters $(q_1, ..., q_n)$, where $q_i \in]0, 1[$ determines a *level of priority* at the junction of incoming suppliers, while, on the contrary, we consider the flux distribution parameters $(\alpha_1, ..., \alpha_m)$, where $\alpha_j \in]0, 1[$, with $\sum_{j=1}^{m} \alpha_j = 1$, indicates the percentage of parts addressed from an incoming supplier to an outgoing one. At junctions, a way to solve Riemann problems, i.e. Cauchy problems with constant initial data on each arc, is prescribed for the continuum-discrete model and a solution at junctions guaranteeing the conservation of fluxes is defined.

We have to notice some differences between the Klar and continuum-discrete model. In fact, the first one considers the formation and propagation of queue, under the assumption that the processing rate μ_j is constant, while the second one do not taking account of queues but describes the evolution of μ_j which is a time-spatial dependent function. It is evident that the two models complete each other. In fact, the approach of Klar is more suitable when the presence of queue with buffer is fundamental to manage goods production. On the other hand, the mixed continuum-discrete model is useful when there is the possibility to reorganize the supply chain, i.e when the productive capacity can be readapted for some contingent necessity. In order to make a comparison of the two models, some numerical results are shown via simulations.

Moreover, an optimization problem of sequential supply chains modeled by the Klar approach has been treated. The aim is to find the configuration of production according to the supply demand minimizing the queues length, i.e. the costs of inventory, and obtaining an expected pre-assigned outflow. The control problem is

solved introducing and minimizing a cost functional which takes into account the final flux of production and the queues representing the stores. The functional is not linear, so to find its minimum, a mathematical technique has been introduced. It is based on the choice of an input flow which is a piecewise constant function, with a finite number of discontinuities. Considering on each of them an infinitesimal displacement which generates traveling temporal shifts on processors and shifts on queues, we are able to compute numerically the value of the variation of functional respect to each discontinuities. Finally, we use the steepest-descent algorithm to find, via simulations, the optimal configuration of input flow, according to the pre-fixed desired production.

This work is organized as follow.

Chapter 1 deals with hyperbolic systems of conservation laws, introducing basic definitions and giving the tools to prove existence and uniqueness of solutions. Chapter 2 presents the main macroscopic models for supply chains and networks, based on conservation laws. Chapter 3 is devoted to numerical methods used to discretize the proposed models in Chapter 2. Chapter 4, finally, compares, via simulations, the models for both chains and networks, and describes how to use the introduced optimization technique on Klar model to obtain a wished outflow minimizing the queues of the processed parts.

Chapter 1

Conservation Laws

In this chapter we present some basic definitions about system of conservation laws which are special partial differential equations where the variable is a conserved quantity. The models for supply chain networks we deal are based on conservation laws.

1.1 Definitions

Definition 1 *A system of conservation laws in one space dimension is a system of the form*

$$\begin{cases} \partial_t u_1 + \partial_x f_1(u) = 0 \\ \cdot \\ \cdot \\ \partial_t u_n + \partial_x f_n(u) = 0 \end{cases} \tag{1.1}$$

it can be written as

$$\partial_t u + \partial_x f(u) = 0, \tag{1.2}$$

where $u = (u_1, ...u_n) : [0, +\infty[\times \mathbb{R} \to \mathbb{R}^n$ *is the "conserved quantity" and* $f = (f_1, ...f_n) : \mathbb{R}^n \to \mathbb{R}^n$ *is the flux.*

Remark 2 ***(The scalar case).*** *If* $n = 1$*,* u *takes value in* $\mathbb{R}$ *and* $f : \mathbb{R} \to \mathbb{R}$*, then (1.2) is a single equation. In this case, we say that (1.2) is a scalar equation.*

In the last case, integrating (1.2) on an arbitrary space interval $[a, b]$,

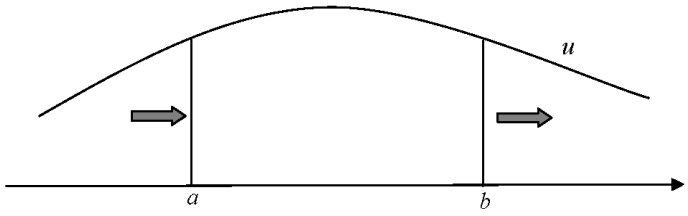

Figure 1.1: Conservation of flux.

$$\begin{aligned} \frac{d}{dt}\int_a^b u(t,x)\,dx &= -\int_a^b f(u(t,x))_x\,dx = f(u(t,a)) - f(u(t,b)) = \\ &= \text{[inflow at a]} - \text{[outflow at b]} \end{aligned}$$

holds. This relationship shows that the quantity u is neither created nor destroyed, i.e. in any interval $[a,b]$ the total amount of u can change only due to the quantity of u entering and exiting respectively at $x=a$ and $x=b$.

We always assume f to be smooth, thus, if u is a smooth function, then (1.2) can be rewritten in the quasi linear form

$$u_t + A(u)\,u_x = 0, \tag{1.3}$$

where $A(u)$ is the Jacobian matrix of f at u.

Definition 3 *The system (1.3) is said "hyperbolic" if, for every $u \in \mathbb{R}^n$, all the eigenvalues of the matrix $A(u)$ are real. Moreover (1.3) is said " strictly hyperbolic" if it is hyperbolic and if, for every $u \in \mathbb{R}^n$, the eigenvalues of the matrix $A(u)$ are all distinct.*

It is clear that equations (1.2) and (1.3) are completely equivalent for smooth solutions. Instead, if u has a jump, the (1.3) is in general not well defined, since there is a product of a discontinuous function $A(u)$ with the distributional derivative, which is in this case a Dirac measure. Hence (1.3) is meaningful only within a class of continuous functions.

Example 4 *(Gas dynamics). The Euler equations describing the evolution of a*

non viscous gas take the form

$$\begin{aligned} &\rho_t + (\rho v)_x = 0, && \textit{(conservation of mass),} \\ &(\rho v)_t + \left(\rho v^2 + p\right)_x = 0, && \textit{(conservation of momentum),} \\ &(\rho E)_t + (\rho E v + p v)_x = 0, && \textit{(conservation of energy),} \end{aligned}$$

where ρ is the mass density, v is the velocity while $E = e + \frac{v^2}{2}$ is the energy density per unit mass. The system is closed by a constitutive relation of the form $p = p(\rho, e)$, giving the pressure as a function of the density and the internal energy. The particular form of p depends on what gas we consider.

A basic feature for the nonlinear system (1.2) is that the classical solutions may not exist for some positive time, even if the initial datum is smooth. This can be shown by the method of characteristics, briefly described for a quasilinear system. Consider the Cauchy problem

$$\begin{cases} u_t + a(t,x,u)\, u_x = h(t,x,u), \\ u(0,x) = \overline{u}(x), \end{cases} \tag{1.4}$$

and, for every $y \in \mathbb{R}$, the curves $x(t,y)$, $u(t,y)$ solving

$$\begin{cases} \frac{dx}{dt} = a(t,x,u), \\ \frac{du}{dt} = h(t,x,u), \\ x(0,y) = y, \\ u(0,y) = \overline{u}(y). \end{cases} \tag{1.5}$$

The curves $t \to x(t,y)$ when $y \in \mathbb{R}$ are called characteristics.

The implicit function theorem implies that the map

$$(t,y) \to (t, x(t,y)) \tag{1.6}$$

is locally invertible in a neighborhood of $(0, x_0)$ and so it is possible to consider the map $u(t,x) = u(t, y(t,x))$ where $y(t,x)$ is the inverse of the second component of (1.6). It is easy to check that $u(t,x)$ satisfies (1.4).

Example 5 *Consider the scalar inviscid Burgers' equation*

$$u_t + \left(\frac{u^2}{2}\right)_x = 0 \tag{1.7}$$

with the initial condition

$$u(0,x) = u_0(x) = \frac{1}{1+x^2}. \tag{1.8}$$

For $t > 0$ small, the solution can be found by the method of characteristics; if u is smooth, the (1.7) can be rewritten as

$$u_t + uu_x = 0,$$

from which we get that the directional derivative of the function $u = u(t,x)$ along the vector $(1,u)$ vanishes. Therefore the solution u to this Cauchy problem must be constant along the characteristic lines in the (t,x)-plane:

$$t \to (t, x + tu_0(x)) = \left(t, x + \frac{t}{1+x^2}\right).$$

For $t < T = \frac{8}{\sqrt{27}}$, these lines do not intersect together and so the solution is classical

$$u\left(t, x + \frac{t}{1+x^2}\right) = \frac{1}{1+x^2}. \tag{1.9}$$

Indeed, at $t = \frac{8}{\sqrt{27}}$, since the characteristics intersect together, a classical solution cannot exist for $t \geq \frac{8}{\sqrt{27}}$. In fact, the map

$$x \to x + \frac{t}{1+x^2}$$

is not one-to-one and (1.9) no longer defines a single valued solution of the Cauchy problem.

According to achieve a global existence result, we must deal with weak solutions.

Definition 6 *Fix $u_0 \in L^1_{loc}(\mathbb{R};\mathbb{R}^n)$ and $T > 0$. A function $u : [0,T] \times \mathbb{R} \to \mathbb{R}^n$ is a weak solution to the Cauchy problem*

$$\begin{cases} u_t + f(u)_x = 0, \\ u(0,x) = u_0(x), \end{cases} \tag{1.10}$$

if u is continuous as a function from $[0,T]$ into L^1_{loc} and if, for every C^1 function ψ with compact support contained in the set $]-\infty, T[\times \mathbb{R}$, it holds

$$\int_0^T \int_R \{u \cdot \psi_t + f(u) \cdot \psi_x\} \, dxdt + \int_R u_0(x) \cdot \psi(0,x) \, dx = 0. \tag{1.11}$$

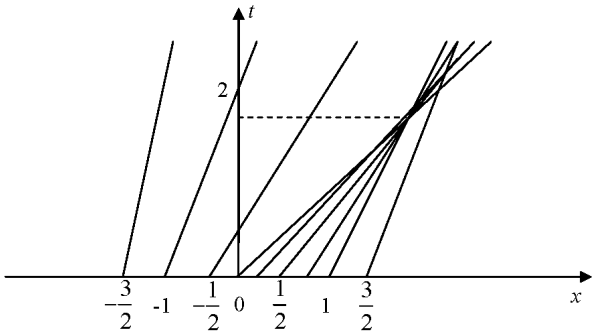

Figure 1.2: The characteristic for the Burgers equation in the (t, x)-plane.

Remark 7 *As consequence of the fact that u is continuous as a function from $[0, T]$ to L^1_{loc} and of equation (1.11), we note that a weak solution u to (1.10) satisfies*

$$u(0, x) = u_0(x) \quad \text{for a.e. } x \in \mathbb{R}$$

Since weak solutions may develop discontinuities in finite time, we introduce some notations to treat them.

Definition 8 *A function $u = u(t, x)$ has an approximate jump discontinuity at the point (τ, ξ) if there exist vectors u^-, $u^+ \in \mathbb{R}^n$ and $\lambda \in \mathbb{R}$ such that*

$$\lim_{r \to 0^+} \frac{1}{r^2} \int_{-r}^{r} \int_{-r}^{r} |u(\tau + t, \xi + x) - U(t, x)| \, dxdt = 0,$$

where

$$U(t, x) = \begin{cases} u^-, & if\ x < \lambda t, \\ u^+, & if\ x > \lambda t. \end{cases} \tag{1.12}$$

The function U is called a shock traveling wave.

The following theorem holds.

Theorem 9 *Consider a bounded weak solution u to (1.2) with an approximate jump discontinuity at (τ, ξ). Then*

$$\lambda \left(u^+ - u^-\right) = f\left(u^+\right) - f\left(u^-\right). \tag{1.13}$$

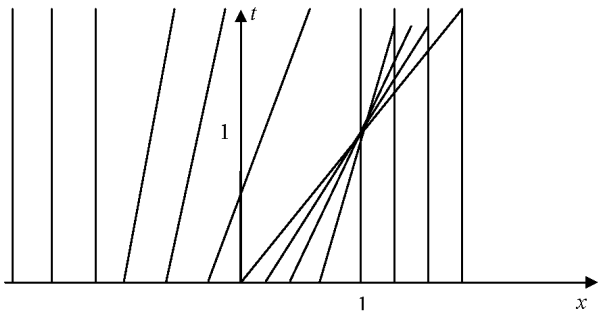

Figure 1.3: Superposition of characteristic curves for a Burgers equation.

Equation (1.13), called Rankine-Hugoniot condition, gives a condition on discontinuities of weak solutions of (1.2) relating the right and left states with the "speed" λ of the "shock". In fact considering the scalar case, (1.13) is a single equation and, for arbitrary $u^- \neq u^+$, we have

$$\lambda = \frac{f(u^+) - f(u^-)}{u^+ - u^-},$$

while for a $n \times n$ system of conservation laws, (1.13) is a system of n scalar equations.

Example 10 *Consider the Burgers equation*

$$u_t + \left(\frac{u^2}{2}\right)_x = 0 \tag{1.14}$$

with the initial condition

$$u_0(x) = \begin{cases} 1 - |x|, & if\ x \in [-1, 1], \\ 0, & otherwise. \end{cases} \tag{1.15}$$

The corresponding characteristics are shown in Fig.1.3.Therefore for $0 \leq t < 1$*, the function*

$$u(t, x) = \begin{cases} \frac{x+1}{t+1}, & if\ -1 \leq x < t, \\ \frac{1-x}{1-t}, & if\ t < x \leq < 1, \\ 0, & otherwise, \end{cases}$$

is a classical solution to 1.14. In this case the Rankine-Hugoniot condition reduces to

$$\lambda = \frac{\left[\frac{(u^+)^2}{2}\right] - \left[\frac{(u^-)^2}{2}\right]}{u^+ - u^-} = \frac{u^+ + u^-}{2}.$$

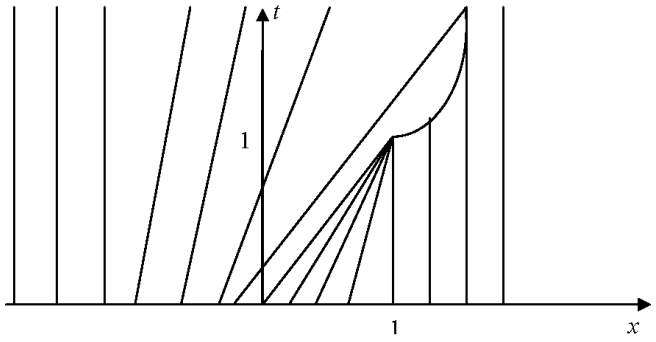

Figure 1.4: Solution to Burgers equation.

If $t \geq 1$, then the function

$$u(t,x) = \begin{cases} \frac{x+1}{t+1}, & if \quad -1 \leq x \leq -1+\sqrt{2+2t}, \\ 0, & otherwise, \end{cases}$$

satisfies the Rankine-Hugoniot condition at each point of discontinuity and so a weak solution to the Cauchy problem, given by (1.14) and (1.15), exists for each positive time (as shown in Fig.1.4).

Example 11 *Let the function u_0 defined by*

$$u_0(x) := \begin{cases} 1, & if \quad x \geq 0, \\ 0, & if \quad x < 0. \end{cases}$$

For every $0 < \alpha < 1$, the function $u_\alpha : [0, +\infty[\times \mathbb{R} \to \mathbb{R}$ defined by

$$u_\alpha := \begin{cases} 0, & if \quad x < \frac{\alpha t}{2}, \\ \alpha, & if \quad \frac{\alpha t}{2} \leq x < \frac{(1+\alpha)t}{2}, \\ 1, & if \quad x \geq \frac{(1+\alpha)t}{2}, \end{cases}$$

is a weak solution (shown in Fig.1.5) to the Burgers equation (1.14).

1.2 Admissibility conditions

As shown in the previous example, in presence of discontinuities, the definition of weak solution does not guarantee uniqueness to the Cauchy problem. Therefore, the notion of weak solution must be supplemented with admissibility conditions, motivated by physical considerations.

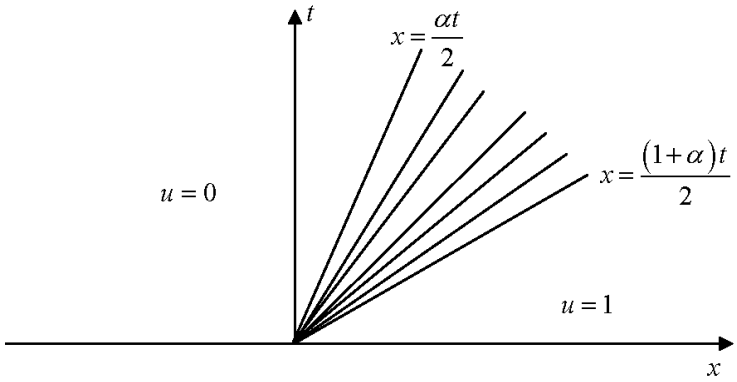

Figure 1.5: A solution u_α

1.2.1 Admissibility Condition 1

Definition 12 *(Vanishing viscosity) A weak solution $u = u(t,x)$ to the Cauchy problem*

$$\begin{cases} u_t + f(u)_x = 0, \\ u(0,x) = u_0(x), \end{cases} \tag{1.16}$$

is admissible if there exists a sequence of smooth solutions u^ε to

$$u_t^\varepsilon + A(u^\varepsilon)\, u_x^\varepsilon = \varepsilon u_{xx}^\varepsilon \qquad (A = Df) \tag{1.17}$$

which converges to u in L^1_{Loc} as $\varepsilon \to 0^+$.

Unfortunately, it is very difficult to provide uniform estimates to the parabolic system (1.17) and characterize the corresponding limits as $\varepsilon \to 0^+$. From the above condition, however, it can be deduced other conditions which can be more easily verified in practice.

1.2.2 Admissibility Condition 2

Now, arising from physical considerations, we introduce the entropy-admissibility condition.

Definition 13 *A C^1 function $\eta : \mathbb{R}^n \to \mathbb{R}$ is an entropy for (1.2) if it is convex and there exists a C^1 function $q : \mathbb{R}^n \to \mathbb{R}$ such that*

$$D\eta(u) \cdot Df(u) = Dq(u) \tag{1.18}$$

for every $u \in \mathbb{R}^n$. The function q is said an "entropy flux" for η. The pair (η, q) is said "entropy-entropy flux pair" for (1.2).

Definition 14 *(Entropy inequality) A weak solution $u = u(t,x)$ to the Cauchy problem (1.16) is said entropy admissible if, for every C^1 function $\varphi \geq 0$ with compact support in $[0,T[\times \mathbb{R}$ and for every "entropy-entropy flux pair" (η, q), it holds*

$$\int_0^T \int_{\mathbb{R}} (\ \eta(u)\,\varphi_t + q(u)\ \ \varphi_x)\,dxdt \geq 0 \tag{1.19}$$

We consider now an entropy admissible solution u and a sequence of entropy-entropy flux pairs (η_ν, q_ν) such that $\eta_\nu \to \eta$ and $q_\nu \to q$ locally uniformly in $u \in \mathbb{R}^n$. If $\varphi \geq 0$ is a C^1 function with compact support in $[0,T[\times \mathbb{R}$, then

$$\int_0^T \int_{\mathbb{R}} (\ \eta_\nu(u)\,\varphi_t + q_\nu(u)\ \ \varphi_x)\,dxdt \geq 0 \tag{1.20}$$

for every $\nu \in \mathbb{N}$. Passing to the limit as $\nu \to +\infty$ in (1.20), we obtain that

$$\int_0^T \int_{\mathbb{R}} (\ \eta(u)\,\varphi_t + q(u)\ \ \varphi_x)\,dxdt \geq 0 \tag{1.21}$$

From this, we can call a C^0 function η an entropy if there exists a sequence of entropies η_ν converging to η locally uniformly. Moreover a C^0 function q an entropy if there exists a sequence of entropies q_ν, entropy flux of η_ν, converging to q locally uniformly.

Remark 15 *Consider the scalar Cauchy problem as in (1.16), where $f : \mathbb{R} \to \mathbb{R}$ is a C^1 function. Then the relation between C^1 entropy and entropy flux is given by*

$$\eta'(u)\,f'(u) = q'(u). \tag{1.22}$$

Therefore if we take a C^1 entropy η, every corresponding entropy flux q has the following expression

$$q(u) = \int_{u_0}^{u} \eta'(s)\,f'(s)\,ds,$$

where u_0 is an arbitrary element of $\mathbb{R}$.

Definition 16 *A weak solution $u = u(t,x)$ to the scalar Cauchy problem (1.16) satisfies the Kruzkov entropy admissibility condition if*

$$\int_0^T \int_{\mathbb{R}} \{|u-k|\ \ \varphi_t + sgn(u-k)\,(f(u) - f(k))\,\varphi_x\}\,dxdt \geq 0$$

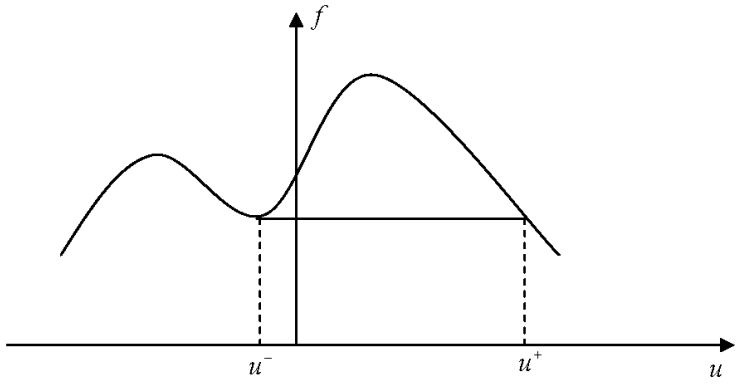

Figure 1.6: The condition (1.23) in the case $u^- < u^+$.

for every $k \in \mathbb{R}$ *and every* C^1 *function* $\varphi \geq 0$ *with compact support in* $[0,T[\times \mathbb{R}$.

Theorem 17 *Let* $u = u(t,x)$ *be a piecewise* C^1 *solution to the scalar equation (1.16). Then* u *satisfies the Kruzkov entropy admissible condition if and only if along every line of jump* $x = \xi(t)$ *the following condition holds. For every* $\alpha \in [0,1]$

$$\begin{cases} f(\alpha u^+ + (1-\alpha)u^-) \geq \alpha f(u^+) + (1-\alpha) f(u^-), & if\ u^- < u^+, \\ f(\alpha u^+ + (1-\alpha)u^-) \leq \alpha f(u^+) + (1-\alpha) f(u^-), & if\ u^- > u^+, \end{cases} \tag{1.23}$$

where $u^- := u(t, \xi(t)-)$ *and* $u^+ := u(t, \xi(t)+)$.

The (1.23) implies that, if $u^- < u^+$ (respectively $u^- > u^+$) then the graph of f remains above (below) the segment connecting $(u^-, f(u^-))$ to $(u^+, f(u^+))$ as shown in Fig.1.6 (Fig.1.7).

1.2.3 Admissibility Condition 3

Definition 18 *(Lax Condition) A bounded weak solution* $u = u(t,x)$ *to the Cauchy problem (1.16) is Lax admissible if, at every point of approximate jump, the speeds corresponding to the left and right states* u^-, u^+ *satisfy*

$$\lambda_i(u^-) \geq \lambda_i(u^-, u^+) \geq \lambda_i(u^+) \tag{1.24}$$

for some $i \in \{1, ..., n\}$.

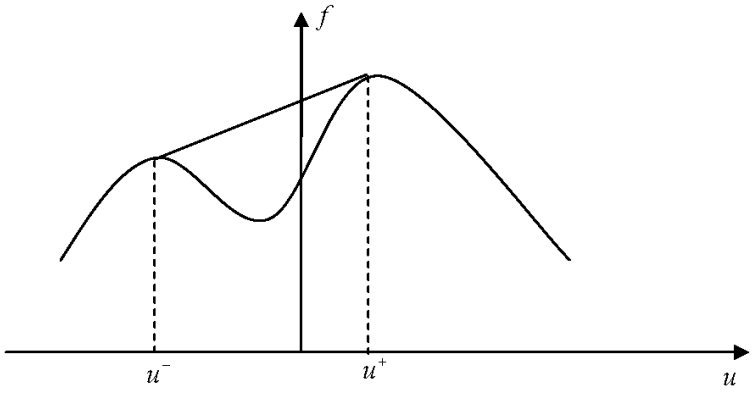

Figure 1.7: The condition (1.23) in the case $u^- > u^+$.

1.3 Riemann Problem

Let $\Omega \subseteq \mathbb{R}^n$ be an open set, let $f : \Omega \to \mathbb{R}^n$ a smooth flux and consider the system of conservation laws

$$u_t + f(u)_x = 0, \tag{1.25}$$

supposed to be strictly hyperbolic.

Definition 19 *A Riemann problem for the system (1.25) is the Cauchy problem for the initial datum (*Heaviside*)*

$$u_0(x) = \begin{cases} u^-, & if\ x < 0, \\ u^+, & if\ x > 0, \end{cases} \tag{1.26}$$

where $u^-, u^+ \in \Omega \subseteq \mathbb{R}^n$.

To solve Cauchy problems, the solution of Riemann problem assumes a key role. In fact, to prove existence we use the *wave-front tracking method* consisting in the following steps:

1. approximate the initial condition with piecewise constant solutions;

2. at every point of discontinuity, solve the corresponding Riemann problem;

3. approximate the exact solution to Riemann problems with piecewise constant functions and piece them together to get a function defined until two wave fronts interact together;

4. repeat inductively the previous construction, starting from the interaction time;

5. prove that the functions so constructed converge to a limit function and prove that this limit function is an entropy admissible solution.

Denote by $A(u)$ the Jacobian matrix of the flux f and with $\lambda_1(u) < \cdots < \lambda_n(u)$ the n eigenvalues of the matrix $A(u)$. For strictly hyperbolic systems, one can find bases of right and left eigenvectors, $\{r_1(u), ..., r_n(u)\}$ and $\{l_1(u), ..., l_n(u)\}$ depending strictly on u, such that

1. $|r_i(u)| \equiv 1$ for every $u \in \Omega$ and $i \in \{1, ..., n\}$;

2. for every $i, j \in \{1, ..., n\}$,

$$l_i \cdot r_j := \begin{cases} 1, & if\ i = j, \\ 0, & if\ i \neq j. \end{cases}$$

We introduce the following notation. If $i \in \{1, ..., n\}$, then the directional derivative of $\lambda_j(u)$ in the direction of $r_i(u)$ is given by

$$r_i \cdot \lambda_j(u) := \lim_{\varepsilon \to 0} \frac{\lambda_j(u + \varepsilon r_i(u)) - \lambda_j(u)}{\varepsilon}.$$

Definition 20 *We say that the i-characteristic field, $i \in \{1, ..., n\}$, is genuinely nonlinear if*

$$r_i \cdot \lambda_i(u) \neq 0 \quad \forall u \in \Omega.$$

We say that the i-characteristic field, ($i \in \{1, ..., n\}$) is linearly degenerate if

$$r_i \cdot \lambda_i(u) = 0 \quad \forall u \in \Omega.$$

If the i-th characteristic field is genuinely nonlinear, then, for simplicity, we assume that $r_i \cdot \lambda_i(u) > 0$ for every $u \in \Omega$.

We consider three cases.

1. Centered rarefaction waves. For $u^- \in \Omega$, $i \in \{1, ..., n\}$ and $\sigma > 0$, we denote by $R_i(\bar{\sigma})(u^-)$ the solution to

$$\begin{cases} \frac{du}{d\sigma} = r_i(u), \\ u(0) = u^-. \end{cases} \tag{1.27}$$

Let $\bar{\sigma} > 0$. Define $u^+ = R_i(\bar{\sigma})(u^-)$ for some $i \in \{1, ..., n\}$. If the i-th characteristic field is genuinely nonlinear, then the function

$$u(t,x) := \begin{cases} u^-, & if\ x < \lambda_i(u^-)t, \\ R_i(\sigma)(u^-), & if\ x = \lambda_i(R_i(\sigma)(u^-))t,\ \sigma \in [0, \bar{\sigma}], \\ u^+, & if\ x > \lambda_i(u^+)t, \end{cases} \tag{1.28}$$

is an entropy admissible solution to the Riemann problem

$$\begin{aligned} &u_t + f(u)_x = 0, \\ &u(0,x) = u_0(x), \end{aligned}$$

with u_0 defined in (1.26). The function $u(t,x)$ is called a centered rarefaction wave.

2. Shock waves. Fix $u^- \in \Omega$ and $i \in \{1, ..., n\}$. For some σ_0, there exist smooth functions $S_i(u_-) = S_i : [-\sigma_0, \sigma_0] \to \Omega$ and $\lambda_i : [-\sigma_0, \sigma_0] \to \mathbb{R}$ such that:

   (a) $f(S_i(\sigma)) - f(u^-) = \lambda_i(\sigma)(S_i(\sigma) - u^-)$ for every $\sigma \in [-\sigma_0, \sigma_0]$;
   (b) $\left|\frac{dS_i}{d\sigma}\right| \equiv 1$;
   (c) $S_i(0) = u^-$, $\lambda_i(0) = \lambda_i(u^-)$;
   (d) $\frac{dS_i(\sigma)}{d\sigma}|_{\sigma=0} = r_i(u^-)$;
   (e) $\frac{d\lambda_i(\sigma)}{d\sigma}|_{\sigma=0} = \frac{1}{2} r_i \cdot \lambda_i(u^-)$;
   (f) $\frac{d^2 S_i(\sigma)}{d\sigma^2}|_{\sigma=0} = \frac{1}{2} r_i \cdot r_i(u^-)$.

Let $\bar{\sigma} < 0$. Define $u^+ = S_i(\bar{\sigma})$. If the i-th characteristic field is genuinely nonlinear, then the function

$$u(t,x) := \begin{cases} u^-, & if\ x < \lambda_i(\bar{\sigma})t, \\ u^+, & if\ x > \lambda_i(\bar{\sigma})t, \end{cases} \tag{1.29}$$

is an entropy admissible solution to the Riemann problem

$$\begin{cases} u_t + f(u)_x = 0, \\ u(0,x) = u_0(x), \end{cases}$$

with u_0 defined in (1.26). The function $u(t,x)$ is called a shock wave.

(a) **Remark 21** *If we consider $\bar{\sigma} < 0$, then (1.29) is again a weak solution, but it does not satisfy the entropy condition.*

3. Contact discontinuities. Fix $u^- \in \Omega$, $i \in \{1, ..., n\}$ and $\sigma \in [-\sigma_0, \sigma_0]$. Define $u^+ = S_i(\bar{\sigma})$. If the i-th characteristic field is linearly degenerate, then the function

$$u(t,x) := \begin{cases} u^-, & if\ x < \lambda_i(u^-)\, t, \\ u^+, & if\ x > \lambda_i(u^-)\, t, \end{cases} \tag{1.30}$$

is an entropy admissible solution to the Riemann problem

$$\begin{cases} u_t + f(u)_x = 0, \\ u(0,x) = u_0(x), \end{cases}$$

with u_0 defined in (1.26). The function $u(t,x)$ is called a contact discontinuity.

Remark 22 *If the i-th characteristic field is linearly degenerate, then*

$$\lambda_i\left(u^-\right) = \lambda_i\left(u^+\right) = \lambda_i(\sigma)$$

for every $\sigma \in [-\sigma_0, \sigma_0]$.

Definition 23 *The waves defined in (1.28), (1.29) and (1.30) are called waves of the i-th family.*

For each $\sigma \in \mathbb{R}$ and $i \in \{1, ..., n\}$, let us consider the function

$$\psi_i(\sigma)(u_0) := \begin{cases} R_i(\sigma)(u_0), & if\ \sigma \geq 0, \\ S_i(\sigma)(u_0), & if\ \sigma < 0, \end{cases} \tag{1.31}$$

where $u_0 \in \Omega$. The value σ is called the strength of the wave of the i-th family, connecting u_0 to $\psi_i(\sigma)(u_0)$. It follows that $\psi_i(\cdot)(u_0)$ is a smooth function. Moreover let us consider the composite function

$$\Psi(\sigma_1, ..., \sigma_n)\left(u^-\right) := \psi_n(\sigma_n) \circ \cdots \circ \psi_1(\sigma_1)\left(u^-\right), \tag{1.32}$$

where $u^- \in \Omega$ and $(\sigma_1, ..., \sigma_n)$ belongs to a neighborhood of 0 in $\mathbb{R}^n$. It is possible to calculate the Jacobian matrix of the function Ψ and to prove that it is invertible in a neighborhood of $(0, ..., 0)$. Hence we can apply the Implicit Function Theorem and prove the following result.

Theorem 24 *For every compact set $K \subseteq \Omega$, there exists $\delta > 0$ such that, for every $u^- \in K$ and for every $u^+ \in \Omega$ with $|u^+ - u^-| \leq \delta$ there exists a unique $(\sigma_1, ..., \sigma_n)$ in a neighborhood of $0 \in \mathbb{R}^n$ satisfying*

$$\Psi(\sigma_1, ..., \sigma_n)(u^-) = u^+.$$

Moreover the Riemann problem connecting u^- with u^+ has an entropy admissible solution, constructing by piecing together the solutions of n Riemann problems.

Example 25 *The 2×2 system of conservation laws*

$$[u_1]_t + \left[\frac{u_1}{1+u_1+u_2}\right]_x = 0, \;\; [u_2]_t + \left[\frac{u_2}{1+u_1+u_2}\right]_x = 0, \;\; u_1, u_2 > 0. \tag{1.33}$$

is justified by the study of two components chromatography. Writing (1.33) in the quasi linear form (1.3), the eigenvalues and the eigenvectors of the corresponding 2×2 matrix $A(u)$ are found to be

$$\begin{array}{ll} \lambda_1(u) = \frac{1}{(1+u_1+u_2)^2}, & \lambda_2(u) = \frac{1}{1+u_1+u_2}, \\ r_1(u) = \frac{1}{\sqrt{u_1+u_2}} \begin{pmatrix} -u_1 \\ -u_2 \end{pmatrix}, & r_2(u) = \frac{1}{\sqrt{2}} \begin{pmatrix} -1 \\ -1 \end{pmatrix}. \end{array}$$

The first characteristic field is genuinely nonlinear, the second is linearly degenerate. In this example, the two shock and rarefaction curves S_i, R_i always coincide, for $i = 1, 2$. Their computation is easy, because they are straight line (see Fig.1.8):

$$R_1(\sigma)(u) = u + \sigma r_1(u), \quad R_2(\sigma)(u) = u + \sigma r_2(u). \tag{1.34}$$

Observe that the integral curves of the two vector fields r_1 and r_2 are respectively the rays through the origin and the lines with slope -1. Now consider two states $u^- = (u_1^-, u_2^-)$ and $u^+ = (u_1^+, u_2^+)$. To solve the Riemann problem (1.26) for the system (1.25) we first compute an intermediate state u^* such that $u^* = R_1(\sigma)(u^-)$, $u^+ = R_1(\sigma)(u^*)$ for some σ_1, σ_2. By (1.34), the components of u^* satisfy

$$u_1^* + u_2^* = u_1^+ + u_2^+, \quad u_1^* u_2^- = u_1^- u_2^*.$$

The solution of the Riemann problem thus takes two different forms, depending on the sign of

$$\sigma = \sqrt{(u_1^-)^2 + (u_2^-)^2} - \sqrt{(u_1^*)^2 + (u_2^*)^2}.$$

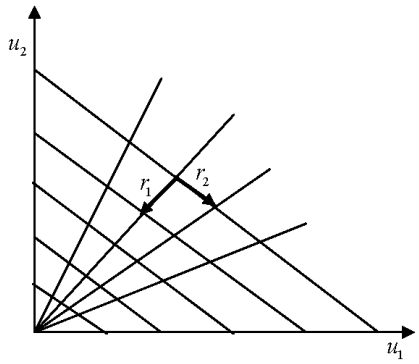

Figure 1.8: Shock and rarefaction curves.

Case 1: $\sigma_1 > 0$. *Then, the solution consists of centered rarefaction waves of the first family and of a constant discontinuity of the second family:*

$$u(t,x) = \begin{cases} u^-, & if\ \frac{x}{t} < \lambda_1(u^-), \\ su^* + (1-s)u^*, & if\ \frac{x}{t} = \lambda_1(su^* + (1-s)u^-), \\ u^*, & if\ \lambda_1(u^*) < \frac{x}{t} < \lambda_2(u^+), \\ u^+, & if\ \frac{x}{t} \geq \lambda_2(u^+), \end{cases} \tag{1.35}$$

where $s \in [0,1]$.

Case 2: $\sigma_1 \leq 0$. *Then, the solution contains a compressive shock of the first family (which vanishes if* $\sigma_1 = 0$*) and a contact discontinuity of the second family:*

$$u(t,x) = \begin{cases} u^-, & if\ \frac{x}{t} < \lambda_1(u^-, u^*), \\ u^*, & if\ \lambda_1(u^-, u^*) \leq \frac{x}{t} < \lambda_2(u^+), \\ u^*, & if\ \lambda_1(u^*) < \frac{x}{t} < \lambda_2(u^+), \end{cases} \tag{1.36}$$

Observe that $\lambda_2(u^*) = \lambda_2(u^+) = (1 + u_1 + u_2)^{-1}$, *because the second characteristic field is linearly degenerate. In this special case since the integral curves of* r_1 *are straight lines, the shock speed in (1.36) can be computed as*

$$\begin{aligned} \lambda_1(u^-, u^*) &= \int_0^1 \lambda_1\left(su^* + (1-s)u^-\right) ds = \\ &= \int_0^1 \left[\left(1 + s(u_1^* + u_2^*) + (1-s)\left(u_1^- + u_2^-\right)\right)\right]^{-2} ds = \\ &= \frac{1}{\left(1 + u_1^* + u_2^*\right)\left(1 + u_1^- + u_2^-\right)}. \end{aligned}$$

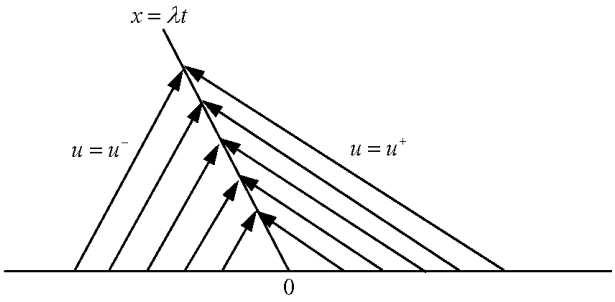

Figure 1.9: Shock wave

1.3.1 The Non-Convex Scalar Case

Consider now the Riemann Problem (1.35)-(1.36) assuming f as uniformly convex function and $G = (f')^{-1}$.

Theorem 26 *(Solution of Riemann's problem)*

- *If $u^- > u^+$, the unique weak solution of the Riemann Problem is*

$$u(t,x) = \begin{cases} u^-, & \frac{x}{t} < \lambda, \\ u^+, & \frac{x}{t} > \lambda, \end{cases} \tag{1.37}$$

  where

$$\lambda = \frac{f(u^+) - f(u^-)}{u^+ - u^-}. \tag{1.38}$$

- *If $u^- < u^+$, the unique weak solution of the Riemann Problem is*

$$u(t,x) = \begin{cases} u^-, & \frac{x}{t} < f'(u^-), \\ G\left(\frac{x}{t}\right), & f'(u^-) < \frac{x}{t} < f'(u^+), \\ u^+, & \frac{x}{t} > f'(u^+). \end{cases} \tag{1.39}$$

Remark 27 *In the first case the states u^-, u^+ are separated by a shock wave with constant speed λ. In the second case the states u^-, u^+ are separated by a (centered) rarefaction wave.*

Remark 28 *Assume f is uniformly concave. In this case, if $u^- > u^+$ (respectively $u^- < u^+$) the unique weak solution of the Riemann Problem is a rarefaction wave (a shock wave).*

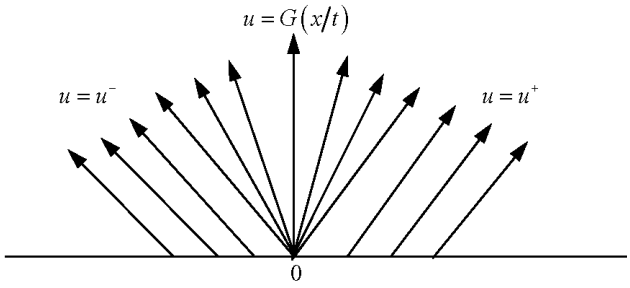

Figure 1.10: Rarefaction waves.

In the scalar case, the construction of solutions to Riemann problems can be done not only in the genuinely nonlinear case, i.e. for convex or concave flux or linearly degenerate case, i.e. affine flux.

Then, consider a scalar conservation law:

$$u_t + f(u)_x = 0,$$

with $f : \mathbb{R} \to \mathbb{R}$ smooth. Given (u_-, u_+) the solution to the corresponding Riemann problem is done in the following way.

If $u_- < u_+$ we let $\tilde{f}$ be the largest convex function such that for every $u \in [u_-, u_+]$, it holds:

$$\tilde{f}(u) \leq f(u);$$

If $u_- > u_+$ we let $\tilde{f}$ be the smallest concave function such that for every $u \in [u_+, u_-]$, it holds:

$$\tilde{f}(u) \geq f(u);$$

Both the cases are shown in Fig.1.11.

Then the solution to the Riemann problem with data (u_-, u_+) is the solution for the flux $\tilde{f}$ to the same Riemann problem. As we can see in this case, the flux $\tilde{f}$ is in general not strictly convex or concave but may contain some linear part. Then the solution to the corresponding Riemann problems may contain combinations of rarefactions and shocks.

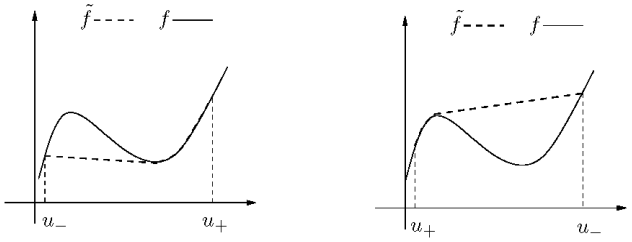

Figure 1.11: Definition of $\tilde{f}$.

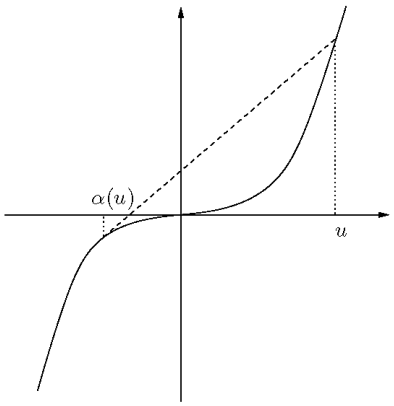

Figure 1.12: Definition of α

For simplicity we will show the following special case.

Fix the scalar conservation law:

$$u_t + (u^3)_x = 0,$$

and $u_- > 0$.

If $u_+ > u_-$, then $\tilde{f}$ coincides with f and the solution to the corresponding Riemann problem is given by a single rarefaction wave.

If $u_+ < u_-$, then we have to distinguish two cases. First, for every u define $\alpha(u) \leq u$ to be the point such that the secant from $(\alpha(u), f(\alpha(u))$ to $(u, f(u))$ is tangent to the graph of $f(u) = u^3$ at $\alpha(u)$ (Fig.1.12);

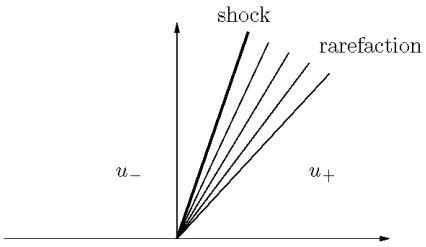

Figure 1.13: Solution to the Riemann problem with $u_- > 0$ and $u^+ < \alpha(u)$.

In formulas:

$$\frac{f(u) - f(\alpha(u))}{u - \alpha(u)} = f'(\alpha(u)),$$

then

$$\frac{u^3 - \alpha^3(u)}{u - \alpha(u)} = 3\alpha^2(u),$$

and one can easily get two solutions, i.e. the trivial one $\alpha(u) = u$ and $\alpha(u) = -\frac{u}{2}$.

Now if $u_+ \geq \alpha(u_-)$ then again $\tilde{f}$ coincides with f and the solution is given by a single shock. Instead, if $u_+ < \alpha(u_-)$, the solution to the Riemann problem is given by the function:

$$u(t,x) = \begin{cases} u_-\,, & if\ x < \frac{3}{4}u_-\,t, \\ -\sqrt{\frac{x}{3t}}\,, & if\ \frac{3}{4}u_-\,t \leq x \leq 3(u_+)^2\,t, \\ u_+\,, & if\ x > 3(u_+)^2\,t. \end{cases}$$

which is formed by a shock followed by a rarefaction attached to it, as shown in Fig.1.13.

In the case $u_- < 0$, the construction is symmetric with respect to the case $u_- > 0$, while for $u_- = 0$ the solution is always given by a rarefaction.

1.4 Functions with Bounded Variation

Now we give some basic notions about functions with bounded variation.

If we consider an interval $J \subseteq \mathbb{R}$ and a function $w : J \to \mathbb{R}$, the total variation of w is defined by

$$\text{Tot.Var. } w = \sup \left\{ \sum_{j=1}^{N} |w(x_j) - w(x_{j-1})| \right\}, \tag{1.40}$$

where $N \geq 1$, the points x_j belong to J for every $j \in \{0, \ldots, N\}$ and satisfy $x_0 < x_1 < \cdots < x_N$.

Definition 29 *We say that the function $w : J \to \mathbb{R}$ has bounded total variation if Tot.Var. $w < +\infty$. We denote with $BV(J)$ the set of all real functions $w : J \to \mathbb{R}$ with bounded total variation.*

The total variation of a function w is a positive number. Moreover if w is a function with bounded total variation, this implies that it is a bounded function, but the converse is false. The following Lemma and Theorems show important properties of such functions.

Lemma 30 *Let $w : J \to \mathbb{R}$ be a function with bounded total variation and $\bar{x}$ be a point in the interior of J. Then, the limits*

$$\lim_{x \to \bar{x}^-} w(x), \qquad \lim_{x \to \bar{x}^+} w(x)$$

exist. Moreover, the function w has at most countably many points of discontinuity.

Theorem 31 ***(Helly)*** *Consider a sequence of functions $w_n : J \to \mathbb{R}^m$. Assume that there exist positive constants, C and M, such that:*

1. *Tot.Var. $w_n \leq C$ for every $n \in \mathbb{N}$;*
2. *$|w_n(x)| \leq M$ for every $n \in \mathbb{N}$ and $x \in J$.*

Then there exist a function $w : J \to \mathbb{R}^m$ and a subsequence w_{n_k} such that

1. *$\lim_{k \to +\infty} w_{n_k}(x) = w(x)$ for every $x \in J$;*
2. *Tot.Var. $w \leq C$;*
3. *$|w(x)| \leq M$ for every $x \in J$.*

Theorem 32 *Consider a sequence of functions $w_n : [0, +\infty[\times J \to \mathbb{R}^n$. Assume that there exist positive constants C, L and M such that:*

1. *Tot.Var. $w_n(t, \cdot) \leq C$ for every $n \in \mathbb{N}$ and $t \geq 0$;*
2. *$|w_n(t, x)| \leq M$ for every $n \in \mathbb{N}$ and $x \in J$ and $t \geq 0$;*
3. *$\int_J |w_n(t, x) - w_n(s, x)|\, dx \leq L\,|t - s|$ for every $n \in \mathbb{N}$ and $t, s \geq 0$.*

Then there exist a function $w \in L^1_{loc}([0, +\infty \times J; \mathbb{R}^n)$ and a subsequence w_{n_k} such that

1. *$w_{n_k} \to w$ in $L^1_{loc}([0, +\infty \times J; \mathbb{R}^n)$ as $k \to +\infty$;*
2. *$\int_J |w(t, x) - w(s, x)|\, dx \leq L\,|t - s|$ for every $t, s \geq 0$.*

Moreover the values of w can be uniquely determined by setting

$$w(t, x) = \lim_{y \to x^+} w(t, y)$$

for every $t \geq 0$ and $x \in$Int J. In this case we have

1. *Tot.Var. $w(t, \cdot) \leq C$ for every $t \geq 0$;*
2. *$|w(t, x)| \leq M$ for every $x \in J$ and $t \geq 0$.*

1.5 BV Functions in $\mathbb{R}^n$

Now, we describe briefly the L^1 theory for BV functions (CitaZion). Let Ω be an open subset of $\mathbb{R}^n$ and consider $w : \Omega \to \mathbb{R}$. We denote with $\mathcal{B}(\Omega)$ the σ-algebra of Borel sets of Ω and with $\mathcal{B}_c(\Omega)$ the set

$$\{B \in \mathcal{B}(\Omega) : B \text{ compactly embedded in } \Omega\}. \tag{1.41}$$

Definition 33 *We say that $\mu : \mathcal{B}_c(\Omega) \to \mathbb{R}$ is a Radon measure if it is countable additive and $\mu(\emptyset) = 0$. We denote with $\mathfrak{M}(\Omega)$ the set of all Radon measures on Ω.*

The following theorem holds.

Theorem 34 *Fix a Radon measure $\mu \in \mathfrak{M}(\Omega)$. There exist two positive and unique Borel measures $\mu^+, \mu^- : \mathcal{B}(\Omega) \to [0, +\infty]$ such that*

$$\mu(E) = \mu^+(E) - \mu^-(E) \tag{1.42}$$

for every $E \in \mathcal{B}_c(\Omega)$.

Definition 35 *Fix a Radon measure $\mu \in \mathfrak{M}(\Omega)$ and consider the total variation of μ defined by $|u| := \mu^+ + \mu^-$. We say that μ has bounded total variation if $|u|(\Omega) < +\infty$ and we denote with $\mathfrak{M}_b(\Omega)$ the set of all Radon measures with bounded total variation.*

Remark 36 *Notice that $\mathfrak{M}_b(\Omega)$ is a Banach space with respect to the norm*

$$||u||_{\mathfrak{M}_b(\Omega)} = |u|(\Omega).$$

Definition 37 *We say that $w : \Omega \to \mathbb{R}$ has bounded total variation if*

1. *$w \in L^1(\Omega)$;*
2. *the i-th partial derivative $D_i w$ exists in the sense of distributions and belongs to $\mathfrak{M}_b(\Omega)$, for every $i = 1, \ldots, n$.*

The total variation of w is given by

$$\sum_{i=1}^{n} |D_i w|(\Omega).$$

We denote with $BV(\Omega)$ the set of all functions defined on Ω with bounded total variation.

Remark 38 *The space $BV(\Omega)$ is a Banach space with respect to the norm*

$$||w||_{L^1(\Omega)} + \sum_{i=1}^{n} |D_i w|(\Omega).$$

Remark 39 *Let $w \in L^1(\Omega)$. Then $w \in BV(\Omega)$ if and only if there exists $c \in (0, +\infty)$ such that*

$$\left| \int_\Omega w \operatorname{div} \varphi dx \right| \leq c \sup_{x \in \Omega} |\varphi(x)|$$

for every $\varphi \in C_c^\infty(\Omega; \mathbb{R}^n)$. In this case one can choose the constant c equal to the total variation of w.

Remark 40 *If Ω is an interval of $\mathbb{R}$, then the two descriptions of BV functions are not completely equivalent. The most important difference is that if we change the values of a BV function w in a finite set, then the total variation of w changes but remain finite if we consider the first description, while it does not vary in the second case. Therefore, if we are interested only in the L^1 equivalence class, then we can assume that a BV function w is right continuous or left continuous.*

1.6 Wave-Front Tracking and Existence of Solutions

This section deals with the existence of an entropy admissible solution to the Cauchy problem

$$\begin{cases} u_t + [f(u)]_x = 0, \\ u(0,\cdot) = \bar{u}(\cdot), \end{cases} \tag{1.43}$$

where $f : \mathbb{R}^n \to \mathbb{R}^n$ is a smooth flux and $\bar{u} \in L^1(\mathbb{R}^n)$ is bounded in total variation. In order to prove existence, we construct a sequence of approximate solutions using the method called wave-front tracking algorithm.

We start considering the scalar case, while, for the system case, we will give some references.

1.6.1 The Scalar Case

We assume the following conditions:

(C1) $f : \mathbb{R} \to \mathbb{R}$ is a scalar smooth function;

(C2) the characteristic field is either genuinely nonlinear or linearly degenerate.

The construction starts at time $t = 0$ by choosing a sequence of piecewise constant approximations $(\bar{u}_\nu)_\nu$ of $\bar{u}$ such that

$$\text{Tot.Var.}\{\bar{u}_v\} \leq \text{Tot.Var.}\{\bar{u}\}, \tag{1.44}$$

$$||\bar{u}_v||_{L^\infty} \leq ||\bar{u}||_{L^\infty} \tag{1.45}$$

and

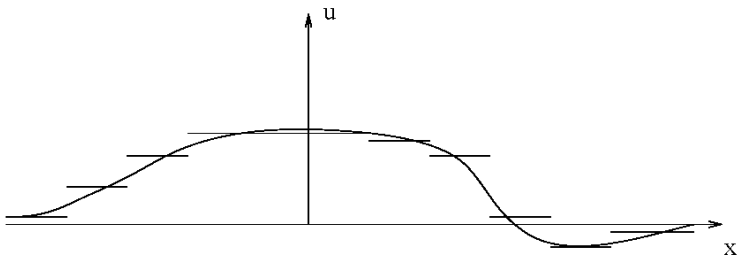

Figure 1.14: A piecewise constant approximation of the initial datum satisfying (1.45) and (1.46).

$$||\bar{u}_v - \bar{u}||_{L^1} < \frac{1}{\nu}, \tag{1.46}$$

for every $\nu \in \mathbb{N}$ (see Fig.1.14).

Fix $\nu \in \mathbb{N}$. By (1.44), $\bar{u}_v$ has a finite number of discontinuities, say $x_1 < \cdots < x_N$. For each $i = 1, \ldots, N$, we approximately solve the Riemann Problem generated by the jump $(\bar{u}_\nu(x_i-), \bar{u}_\nu(x_i+))$ with piecewise constant functions of the type $\varphi(\frac{x-x_i}{t})$, where $\varphi : \mathbb{R} \to \mathbb{R}$. More precisely, if the Riemann Problem generated by $(\bar{u}_\nu(x_i-), \bar{u}_\nu(x_i+))$ admits an exact solution containing just shocks or contact discontinuities, then $\varphi(\frac{x-x_i}{t})$ is the exact solution, while if a rarefaction wave appears, then we split it in a centered rarefaction fan, containing a sequence of jumps of size at most $\frac{1}{\nu}$, traveling with a speed between the characteristic speeds of the states connected. In this way, we are able to construct an approximate solution $u_\nu(t, x)$ until a time t_1, where at least two wave fronts interact together (see Fig.1.15).

Remark 41 *In the scalar case, if the characteristic field is linearly degenerate, then all the waves are contact discontinuities and travel at the same speed. Therefore, the previous construction can be done for every positive time.*

Remark 42 *Notice that it is possible to avoid that three of more wave fronts interact together at the same time slightly changing the speed of some wave fronts. This may introduce a small error of the approximate solution with respect to the exact one.*

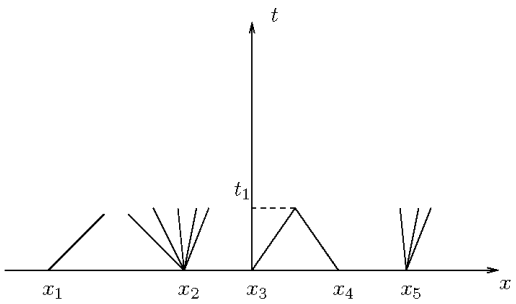

Figure 1.15: The wave front tracking construction until first time of interaction.

At time $t = t_1$, $u_\nu(t_1, \cdot)$ is clearly a piecewise constant function. So we can repeat the previous construction until a second interaction time $t = t_2$ and so on. In order to prove that a wave-front tracking approximate solution exists for every $t \in [0, T]$, where T may be also $+\infty$, we need to estimate

1. the number of waves;
2. the number of interactions between waves;
3. the total variation of the approximate solution.

The first two estimates are concerned with the possibility to construct a piecewise constant approximate solution. The third estimate, instead, is concerned with the convergence of the approximate solutions towards an exact solution.

Remark 43 *The two first bounds are nontrivial for the vector case and it is necessary to introduce simplified solutions to Riemann problems and/or non-physical waves.*

The next lemma shows that the number of interactions is finite.

Lemma 44 *The number of wave fronts for the approximate solution u_ν is not increasing with respect to the time and so u_ν is defined for every $t \geq 0$. Moreover the number of interactions between waves is bounded by the number of wave fronts.*

Lemma 45 *The total variation of $u_\nu(t, \cdot)$ is not increasing with respect the time. Therefore for each $t \geq 0$*

$$Tot.Var.\, u_\nu(t, \cdot) \leq Tot.Var.\, \bar{u} \tag{1.47}$$

The following theorem holds.

Theorem 46 *Let $f : \mathbb{R} \to \mathbb{R}$ be smooth and $\bar{u} \in L^1(\mathbb{R})$ with bounded variation. Then there exists an entropy-admissible solution $u(t,x)$ to the Cauchy problem (1.43) defined for every $t \geq 0$. Moreover,*

$$||\bar{u}(t,\cdot)||_{L^\infty} \leq ||\bar{u}(\cdot)||_{L^\infty} \tag{1.48}$$

for every $t \geq 0$.

1.6.2 The System Case

For systems, since more types of interaction may happen, the construction of wave-front tracking approximations is more complex. In particular the bounds on number of waves, interactions and BV norms are no more directly obtained.

In this case, in order to show the basic ideas for obtaining the needed bounds, we start giving some total variations estimates for interaction of waves along a wave-front tracking approximation.

The constants in the estimates depend on the total variation of the initial datum, which is assumed to be sufficiently small.

Consider a wave of the i-th family of strength σ_i, $i \neq j$, and indicate by σ'_k ($k \in \{1, ..., n\}$) the strengths of the new waves produced by the interaction.

Then it holds

$$\left|\sigma_i - \sigma'_i\right| + \left|\sigma_j - \sigma'_j\right| + \sum_{k \neq i,j} \left|\sigma'_k\right| \leq C \left|\sigma_i\right| \left|\sigma_j\right|, \tag{1.49}$$

For the case $i = j$, let us indicate by $\sigma_{i,1}$ and $\sigma_{i,2}$ the strengths of the interacting waves, then it holds

$$\left|\sigma_{i,1} + \sigma_{i,2} - \sigma'_i\right| + \sum_{k \neq i} \left|\sigma'_k\right| \leq C \left|\sigma_{i,1}\right| \left|\sigma_{i,2}\right|. \tag{1.50}$$

It is possible now, fixing a parameter δ_v, to split rarefactions in rarefaction fans with shocks of strength at most δ_v. Also, only if the product of interacting waves is bigger than δ_v, at each interaction time, the new Riemann Problem can be exactly solved eventually splitting the rarefaction waves in rarefaction fans. Otherwise, the Riemann Problem is only solved with waves of the same families

of the interacting ones, the error being transported along a *non-physical wave*, traveling at a speed bigger than all waves. In this way, it is possible to control the number of waves and interactions and then let δ_v go to zero [6].

Consider now a wave-front tracking approximate solution u_v and let $x_\alpha(t)$, of family i_α and strength σ_α, indicate the discontinuities of $u_v(t)$. We say two discontinuities are interacting if $x_\alpha < x_\beta$ and either $i_\alpha > i_\beta$ or $i_\alpha = i_\beta$ and at least one of the two waves is a shock. Define the Glimm functional computed at $u_v(t)$ as:

$$Y(u_v(t)) = \text{Tot.Var.}(u_v(t)) + C_1 Q(u_v(t)),$$

where C_1 is a constant to be chosen suitably and

$$Q(u_v(t)) = \sum |\sigma_\alpha| |\sigma\beta|$$

where the sum is over interacting waves. It can be proved that Y is equivalent to the functional measuring the total variation. Clearly such functional changes only at interaction times.

Using the interaction estimates (1.49) and (1.50), at an interaction time $\bar{t}$, we get

$$|\text{Tot.Var.}(u_v(\bar{t}+)) - \text{Tot.Var.}(u_v(\bar{t}-))| \leq C|\sigma_i||\sigma_j|,$$

$$Q(u_v(\bar{t}+)) - Q(u_v(\bar{t}-)) \leq -C_1|\sigma_i||\sigma_j| + C|\sigma_i||\sigma_j| \,\text{Tot.Var.}(u_v(\bar{t}-)).$$

Therefore

$$Y(u_v(\bar{t}+)) - Y(u_v(\bar{t}-)) \leq |\sigma_i||\sigma_j|[C - C_1 + C\ \text{Tot.Var.}u_v(\bar{t}-)].$$

On the other side, for every t:

$$\text{Tot.Var.}(u_v(t)) \leq Y(u_v(t)).$$

Then choosing $C_1 > C$ and assuming that Tot.Var.$(u_v(0))$ is sufficiently small, one has that Y is decreasing along a wave-front tracking approximate solution and so the total variation is controlled.

1.7 Uniqueness and Continuous Dependence

In this section it will show a method, based on a Riemannian type distance on L^1, to prove uniqueness and Lipschitz continuous dependence by initial data for solutions to the Cauchy problem, controlling how their distance varies in time for any two approximate solutions u, u'. For simplicity we only consider the scalar case, while for the system case the approach is illustrated in [7]. By existing various alternative methods, this one presented here is more suitable to be used for networks.

The basic idea is to estimate the L^1-distance viewing L^1 as viewing L^1 as a Riemannian manifold. We consider the subspace of piecewise constant functions and "generalized tangent vectors" consisting of two components (v, ξ), where $v \in L^1$ and $\xi \in \mathbb{R}^n$ describe respectively the L^1 infinitesimal displacement and the infinitesimal displacement of discontinuities.

For example, take a family of piecewise constant functions $\theta \to u^\theta$, $\theta \in [0,1]$, each of which has the same number of jumps, say at the points $x_1^\theta < ..... < x_N^\theta$. Assume that the following functions are well defined (see Fig.1.16)

$$L^1 \ni v^\theta(x) = \lim_{h \to 0} \frac{u^{\theta+h}(x) - u^\theta(x)}{h},$$

and also the numbers

$$\xi_\beta^\theta = \lim_{h \to 0} \frac{x_\beta^{\theta+h} - x_\beta^\theta}{h}, \qquad \beta = 1, ..., N.$$

Then we say that γ admits tangent vectors

$$\left(v^\theta, \xi^\theta\right) \in T_{u^\theta} \doteq L^1(\mathbb{R}; \mathbb{R}^n) \times \mathbb{R}^n.$$

In general such path $\theta \to u^\theta$ is not differentiable w.r.t. the usual differential structure of L^1, in fact if $\xi_\beta^\theta \neq 0$, as $h \to 0$ the ratio $\frac{\left[u^{\theta+h}(x) - u^\theta(x)\right]}{h}$ does not converge to any limit in L^1.

The L^1-length of the path $\gamma : \theta \to u^\theta$ can be computed in the following way:

$$||\gamma||_{L^1} = \int_0^1 \left|\left|v^\theta\right|\right|_{L^1} d\theta + \sum_{\beta=1}^{N} \int_0^1 \left|u^\theta(x_\beta+) - u^\theta(x_\beta-)\right| \left|\xi_\beta^\theta\right| d\theta. \tag{1.51}$$

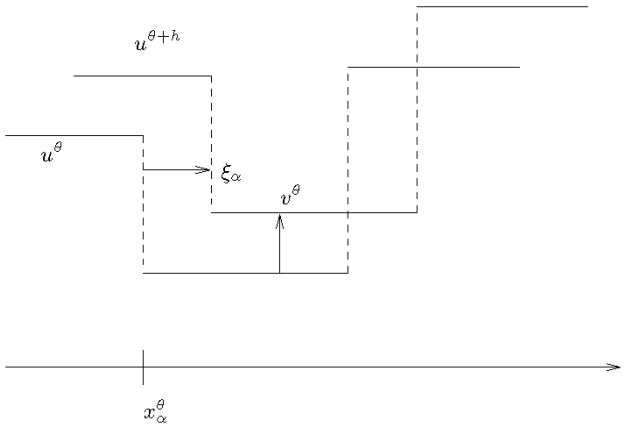

Figure 1.16: Construction of "generalized tangent vectors".

According to (1.51), in order to compute the L^1-length of the path γ, we integrate the norm of its tangent vector which is defined as follows:

$$||(v,\xi)|| \doteq ||v||_{L^1} + \sum_{\beta=1}^{N} |\Delta u_\beta| \left|\xi_\beta\right|,$$

where $\Delta u_\beta = u(x_\beta+) - u(x_\beta-)$ is the jump across the discontinuity x_β. Let us introduce the following definition.

Definition 47 *We say that a continuous map $\gamma : \theta \to u^\theta \doteq \gamma(\theta)$ from $[0,1]$ into L^1_{loc} is a regular path if the following holds. All functions u^θ are piecewise constant, with the same number of jumps, say at $x_1^\theta < ..... < x_N^\theta$ and coincide outside some fixed interval $]-M, M[$. Moreover, γ admits a generalized tangent vector $D\gamma(\theta) = \left(v^\theta, \xi^\theta\right) \in T_{\gamma(\theta)} = L^1(\mathbb{R};\mathbb{R}^n) \times \mathbb{R}^N$, continuously depending on θ.*

Let $\Omega(u,u')$ the family of all regular paths $\gamma : [0,1] \to \gamma(t)$ with $\gamma(0) = u$, $\gamma(1) = u'$, where u and u' are two piecewise functions. The Riemannian distance between u and u' is given by

$$d\left(u,u'\right) \doteq \inf\left\{||\gamma||_{L^1}, \gamma \in \Omega\left(u,u'\right)\right\}.$$

To define d on all L^1, for given $u, u' \in L^1$ we set

$$d\left(u,u'\right) \doteq \inf\left\{||\gamma||_{L^1}+||u-\tilde{u}||_{L^1}+\left|\left|u'-\tilde{u}'\right|\right|_{L^1}: \right.$$
$$\left. \tilde{u},\tilde{u}' \text{ piecewise constant functions, } \gamma\in\Omega\left(u,u'\right)\right\}$$

It is easy to check that this distance coincides with that one of L^1. (For the system case, see [7]).

Now, studying the evolution of norms of tangent vectors along wave-front tracking approximations, let us estimate the L^1 distance among solutions. Let $\gamma_0(\theta)=u^\theta$ be a regular path joining $u=u^0$ with $u'=u^1$, where u, u' are piecewise constant functions. Define $u^\theta(t,x)$ to be a wave-front tracking approximate solution with initial data u^θ and let $\gamma_t(\theta)=u^\theta(t,\cdot)$.

It is possible to check that γ_t is a regular path for each regular path γ_0 and $t\geq 0$. If we can prove

$$||\gamma_t||_{L^1}\leq||\gamma_0||_{L^1}, \tag{1.52}$$

then for every $t\geq 0$

$$\left|\left|u(t,\cdot)-u'(t,\cdot)\right|\right|_{L^1}\leq\inf_{\gamma_t}||\gamma_t||_{L^1}\leq\inf_{\gamma 0}||\gamma_0||_{L^1}=\left|\left|u(0,\cdot)-u'(0,\cdot)\right|\right|_{L^1}. \tag{1.53}$$

To obtain (1.52), hence (1.53), it is enough to prove that, for every tangent vector $(v,\xi)(t)$ to any regular path γ_t, one has:

$$||(v,\xi)(t)||\leq||(v,\xi)(0)||, \tag{1.54}$$

i.e. the norm of a tangent vector does not increase in time. Moreover, if (1.53) is established, then uniqueness and Lipschitz continuous dependence of solutions to Cauchy problems is straightforwardly achieved passing to the limit on the wave-front tracking approximate solutions.

Let us now estimate the increase of the norm of a tangent vector. In order to achieve (1.54), we fix a time $\bar{t}$ and treat the following cases:

Case 1. no interaction of waves takes place at $\bar{t}$;

Case 2. two waves interact at $\bar{t}$;

In Case 1, denote by x_β, σ_β and ξ_β, respectively, the positions, sizes and shifts of the discontinuities of a wave-front tracking approximate solution. Following [7] we get:

$$\begin{aligned}
&\frac{d}{dt}\left\{\int |v(t,x)|\,dx + \sum_\beta \left|\xi_\beta\right| |\sigma_\beta|\right\} = \\
&-\left\{\sum_\beta \left(\lambda\left(\rho^-\right) - \dot{x}_\beta\right)\left|v^-\right| + \sum_\beta \left(\dot{x}_\beta - \lambda\left(\rho^+\right)\right)\left|v^+\right|\right\} + \\
&+\sum_\beta D\lambda\left(\rho^-,\rho^+\right)\cdot\left(v^-,v^+\right)\left(sign\xi_\beta\right)|\sigma_\beta|,
\end{aligned}$$

where $\sigma_\beta = \rho^+ - \rho^-$, $\rho^\pm \doteq \rho(x_\beta \pm)$ and similarly for $v^\pm$. If the waves respect the Rankine-Hugoniot conditions, then

$$\sum_\beta D\lambda\left(\rho^-,\rho^+\right)\cdot\left(v^-,v^+\right) = \left(\lambda\left(\rho^-\right) - \dot{x}_\beta\right)\frac{v^-}{|\sigma_\beta|} + \left(\dot{x}_\beta - \lambda\left(\rho^+\right)\right)\frac{v^+}{|\sigma_\beta|}$$

and

$$\frac{d}{dt}\left\{\int |v(t,x)|\,dx + \sum_\beta \left|\xi_\beta\right| |\sigma_\beta|\right\} \leq 0. \tag{1.55}$$

In the wave-front tracking algorithm the Riemann-Hugoniot condition may be violated for rarefaction fans. However, this results in an increase of the distance which is controlled in terms of $\frac{1}{v}$ (the size of a rarefaction shock) and tends to zero when $v \to \infty$.

For the Case 2, first, we have the following:

Lemma 48 *Consider two waves, with speed λ_1 and λ_2 respectively, that interact together at $\bar{t}$ producing a wave with speed λ_3. If the first wave is shifted by ξ_1 and the second one by ξ_2, then the shift of the resulting wave is given by*

$$\xi_3 = \frac{\lambda_3 - \lambda_2}{\lambda_1 - \lambda_2}\xi_1 + \frac{\lambda_1 - \lambda_3}{\lambda_1 - \lambda_2}\xi_2 \tag{1.56}$$

Moreover we have that

$$\Delta\rho_3\xi_3 = \Delta\rho_1\xi_1 + \Delta\rho_2\xi_2 \tag{1.57}$$

where $\Delta\rho_i$ are the signed strengths of the corresponding waves.

Finally, we observe that from (1.57) it follows

$$|\Delta\rho_3\xi_3| = |\Delta\rho_1|\,|\xi_1| + |\Delta\rho_2|\,|\xi_2|\,,$$

from which

$$\left|\left|(v,\xi)\left(t^+\right)\right|\right| \leq \left|\left|(v,\xi)\left(t^-\right)\right|\right|. \tag{1.58}$$

Chapter 2

Macroscopic models for supply chain and networks

In this chapter, starting by the Armbruster-Degond-Ringhofer model, we present the Göttlich-Herty-Klar model and a continuum-discrete model for supply chains and networks.

2.1 The Armbruster-Degond-Ringhofer model

Consider a production line formed by M suppliers $S_0, ...S_M$, in which a certain good is processed by each supplier and is fed in the next one.

Labeling the processed part by index n, we denote by $\tau(m,n)$ the time at which the part n passes from $m-1$ to m supplier. Then, in order to model generic supply chain, the goal is to derive rules governing the evolution of each $\tau(m,n)$. A hierarchy of models is available for this purpose, but the focus is centralized on the so called fluid models, which replace the individual parts by a continuum and use rate equations for the flow of product through a supplier (see [1], [5] for an overview). For a large number of parts, these are computationally much less expensive than discrete event simulation models, but they necessarily represent an approximation to the actual situation.

Then we derive a fluid dynamic model, namely a conservation law for a partial differential equation, out of very simple principles governing the evolution of the times $\tau(m,n)$. Basically we assume that each supplier works as a single processor

characterized by its processing time $T(m)$ as well as its maximal production rate (capacity) $\mu(m)$ and a buffer queue in front of it. The processing policy is supposed to be 'first come first served'; $T(m)$ represents the time which is needed to produce a single part while $\mu(m)$ is defined as the maximal amount of parts per unit time which can handled by each single processor $m = 0, ...M-1$. In this model both $T(m)$ and $\mu(m)$ are fixed.

We denote by a_n, $n = 1, 2, ..$, the time part number n arrives at the end of queue and by b_n the 'release time', i.e. the time part number n reaches the front of the queue and is fed into the processor. If the queue is full, the interval between two consecutive times b_n will be given by the processing rate $\mu(m)$, i.e.

$$b_n = b_{n-1} + \frac{1}{\mu(m)}$$

will hold as long as $a_n \leq b_{n-1} + \frac{1}{\mu(m)}$ holds, meaning that part number n has already arrived when we want to feed it into the processor m. Instead, if the queue is empty, we wait that part n arrives to the end of queue and immediately feed it into the processor. In this case the condition $a_n > b_{n-1} + \frac{1}{\mu(m)}$ will imply $b_n = a_n$. Then, combining the two previous, we obtain the relation:

$$b_n = \max\left\{a_n, b_{n-1} + \frac{1}{\mu(m)}\right\}. \tag{2.1}$$

If $T(m)$ is the processing time to finish the part, we denote by $e_n = b_n + T(m)$ the time the part leaves the processor and enters the next queue. So, the (2.1) can be re-write as:

$$e_n = \max\left\{a_n + T(m), e_{n-1} + \frac{1}{\mu(m)}\right\}. \tag{2.2}$$

which represents the basic relationship between the arrival times a_n and the exit times e_n.

Referring now to the previous definition of $\tau(m, n)$ and using the obvious change of notation $a_n \to \tau(m, n)$ and $e_n \to \tau(m+1, n)$ we obtain from (2.2)

$$\begin{aligned} \tau(m+1, n) &= \max\left\{\tau(m, n) + T(m), \tau(m+1, n-1) + \frac{1}{\mu(m)}\right\}, \\ n &\geq 1,\ m = 0, .., M-1. \end{aligned} \tag{2.3}$$

The (2.3) needs initial and boundary conditions which are:

$$\tau(0,n) = \tau^A(n),\ n \geq 0, \quad \tau(m,0) = \tau^I(m),\ m = 0,...M, \tag{2.4}$$

where $\tau^A(n)$ simply denotes the arrival time of part n in the first processor and $\tau^I(m)$ denotes the time the first part has arrived at supplier S_m. The (2.3) and (2.4) define completely a discrete event simulation model. So, $\tau^I(m+1) - \tau^I(m) - T(m)$ denotes the time the first part has waited in the buffer in front of processor at S_m, while, assuming a constant service rate μ in the past,
$\mu(m,0)\left[\tau^I(m+1) - \tau^I(m) - T(m)\right]$ would be the number of parts in the queue at the time part number 0 arrives. This definition indicates that, for an actual simulation, we have to start somewhere. But this issue will be resolved once the problem is formulated in terms of a conservation law. Then, given the times $\tau(m,n)$, conservation of the number of parts is expressed via the introduction of the Newell-curves (see [10], [24]), which describe how the information of (2.3) can be organized to facilitate the computation of performance measures, e.g. the Work in Progress (WIP). In this context, the N-curve $U(m,t)$ at supplier S_m is given by the number of parts which have passed from processor S_{m-1} to S_m at any time t, i.e by

$$U(m,t) = \sum_{n=0}^{\infty} H(t - \tau(m,n)),\ t > 0, \tag{2.5}$$

where H is the Heavyside function, i.e.

$$H(y) = \begin{cases} 0 & if\ y < 0 \\ 1 & if\ \ y \geq 0 \end{cases}.$$

The WIP $W(m,t)$ of processor S_m, the total number of parts (including all parts in the queue as well) actually produced at S_m at time t, is given by the difference of two consecutive N-curves:

$$W(m,t) = U(m,t) - U(m+1,t) + K(m),\ \ m = 0,...M, \tag{2.6}$$

where the time independent constants $K(m)$ are determinated by initial situation. If each of processors S_m has a given minimal processing time $T(m)$ then

$\tau(m+1,n) \geq \tau(m,n) + T(m)$ will hold and this implies that $W(m,t)$ can never become negative.

Considering the first derivative of $W(m,t)$ with respect to t, we obtain:

$$\begin{aligned} \frac{d}{dt}W(m,t) &= \frac{d}{dt}U(m,t) - \frac{d}{dt}U(m+1,t) = \\ &\sum_{n=0}^{\infty}\delta(t-\tau(m,n)) - \sum_{n=0}^{\infty}\delta(t-\tau(m+1,n)) = \\ &= F(m,t) - F(m+1,t), \end{aligned} \tag{2.7}$$

where, by definition, the flux $F(m,t)$ from processor S_{m-1} to S_m is given by the first derivative of $U(m,t)$ and it can be interpreted as a superposition of δ-distributions. To avoid this inconvenience, the (2.7) is replaced by a conservation law with a simple constitutive relation between the density ρ and the flux f, in which continuous averaged quantities are considered and the dependence on individual parts is completely removed.

By a reformulation of the problem, necessary to prevent analytical difficulties, it can be shown that the asymptotic limit leads to a partial differential equation. First, we map (2.7) onto a grid in an artificial spatial variable x, called the 'Degree of Completion' (DOC). We define a mesh $0 = x_0 < ..... < x_M = X$ and replace $F(m,t)$ by $F(x_m,t)$. So the parts enter and leave the supply chain respectively at the DOC $x = 0$ and DOC $x = X$. Next, multiplying the flux by an arbitrary smooth test function $\psi(t)$, the integral

$$\int_{\tau^I(m)}^{\infty}\psi(t)\,F(x_m,t)\,dt = \sum_{n=0}^{\infty}\int_{\tau^I(m)}^{\infty}\psi(t)\,\delta(t-\tau(m,n))\,dt = \sum_{n=0}^{\infty}\psi(\tau(m,n)) \tag{2.8}$$

holds. Then we can rewrite the (2.8) into a Riemann sum as

$$\int_{\tau^I(m)}^{\infty}\psi(t)\,F(x_m,t)\,dt = \sum_{n=0}^{\infty}\psi(\tau(m,n))\,\Delta_n\tau(m,n)\,f(x_m,\tau(m,n))$$

where the increment is given by the difference of $\tau(m,n)$ in the index n, i.e. $\Delta_n\tau(m,n) = \tau(m,n+1) - \tau(m,n)$, and, as consequence from (2.8), the function

$f(x_m, \tau(m,n))$ is provided by the inverse of $\Delta_n\tau(m,n)$. For a $\Delta_n\tau(m,n)$ small, i.e. $\Delta_n\tau(m,n) \to 0$, we obtain the approximate relation

$$\int_{\tau^I(m)}^{\infty} \psi(t) F(x_m, t)\, dt \approx \int_{\tau^I(m)}^{\infty} \psi(t) f(x_m, t)\, dt$$

where the function f is the approximate flux for $t = \tau(m,n)$ and $x = x_m$, i.e.

$$f(x_m, \tau(m,n)) = \frac{1}{\tau(m,n+1) - \tau(m,n)}, \qquad n \geq 0,\ m = 0, ..., M. \tag{2.9}$$

Assuming now that the arrival times τ are continuously distributed, i.e. expressed in terms of continuous variables such as $\tau(x,y)$, we rewrite the approximate flux as $f(x, \tau(x,y)) = \frac{1}{\partial_y \tau(x,y)}$. In the similar way, it is possible to find an approximate of part density ρ.

We can observe that the N-function $U(x,t)$, the antiderivative of the flux, satisfies the relations

$$\begin{aligned} (a)\ \frac{d}{dy}U(x, \tau(x,y)) &= \partial_t U(x,\tau)\, \partial_y \tau = 1, \\ (b)\ \frac{d}{dx}U(x, \tau(x,y)) &= \partial_x U(x,\tau) + \partial_t U(x,\tau)\, \partial_x \tau. \end{aligned} \tag{2.10}$$

In analogy to (2.6) setting $\rho(x,t) = K(x) - \partial_x U(x,t)$, with K an arbitrary function, and since $\partial_t U(x,\tau) = f(x,\tau)$, the (2.10) becomes

$$\frac{d}{dx}U(x, \tau(x,y)) = K(x) - \rho(x,t) + f(x,\tau)\, \partial_x \tau.$$

Moreover the (2.10-a) implies that $\frac{d}{dy}U(x, \tau(x,y))$ can be set to an arbitrary chosen function $K(x)$, since it is a function of the DOC variable x only. So for a continuum $\tau(x,y)$ we set $\rho(x,t) = \frac{\partial_x \tau}{\partial_y \tau}$. ρ and f satisfy a conservation law of the form $\partial_t \rho + \partial_x f = 0$.

Thus, on a discrete level, the approximate density is given by

$$\rho(x_m, \tau(m+1,n)) = \frac{\tau(m+1,n+1) - \tau(m,n+1)}{h_m\left(\tau(m+1,n+1) - \tau(m+1,n)\right)} \tag{2.11}$$

with $n \geq 0$, $m = 0, ..., M-1$, $h_m := x_{m+1} - x_m$.

The definitions in (2.9) and (2.11) allow to derive a simple constitutive relation between flux and density as shown in the following theorem.

Theorem 49 *Let the arrival times $\tau(m,n)$ satisfy the time recursion (2.3) and let the approximate density ρ and flux f be defined by (2.11) and (2.9). Then the approximate flux can be written in terms of the approximate density via a constitutive relation of the form*

$$f(x_m, \tau(m,n)) = \min\left\{\mu(m-1,n), \frac{h_{m-1}\rho(x_{m-1}, \tau(m,n))}{T(m-1)}\right\},$$

with $n \geq 0$, $m = 1, 2, ...$

Proof. The proof was done by Armbruster et al. and it can be found in [2]. ■

Now, it will be shown that the approximate density ρ and flux f, defined by (2.11) and (2.9), satisfy a conservation law of the form $\partial_t \rho + \partial_x f = 0$, asymptotically, i.e. for a large time and nodes scales ($N, M \to \infty$). Moreover the asymptotic validity can be divided into three parts: scaling, interpolation and weak formulation.

2.1.1 Scaling and dimensionless formulation

We define the average processing time T_0 as

$$T_0 = \frac{1}{M}\sum_{m=0}^{M-1} T(m),$$

and so MT_0 describes the time a part spent to be processed in the empty system without any waiting times. Then, T_0 is used as a scale basis over all time scales, and we denote all scaled variables and functions by the subindex s.

$$\begin{aligned} \tau(m,n) &= MT_0\tau_s(m,n), \quad T(m) = T_0 T_s(x_m), \quad \mu(m,n) = \\ &= \frac{\mu_s(x_m, \tau_s(m+1,n))}{T_0}. \end{aligned} \tag{2.12}$$

Consider a regime where $M >> 1$ and set $\varepsilon = \frac{1}{M} << 1$. Inserting (2.12) into (2.3), for $n = 0, 1, ..$ and $m = 0, ..M-1$ we get:

$$\begin{aligned} &\tau_s(m+1, n+1) = \\ &\max\left\{\tau_s(m,n+1) + \varepsilon T_s(x_m), \tau_s(m+1,n) + \frac{\varepsilon}{\mu_s(x_m, \tau_s(m+1,n))}\right\}, \end{aligned} \tag{2.13}$$

where the initial and boundary condition, respectively $\tau_s^A = \tau_s(0,n)$ and $\tau_s^I = \tau_s(m,0)$, are scaled in the same way as $\tau(m,n)$.

It is assumed that the differences between two consecutive arrival times τ are of the same order as the average processing time T_0. This is reasonable since otherwise the total WIP would either go to zero or infinity. So it is set

$$\begin{aligned}\Delta_n\tau(m,n) &= \tau(m,n+1)-\tau(m,n) = T_0\Delta_{ns}\tau_s(m,n),\\ \Delta_m\tau(m,n) &= \tau(m+1,n)-\tau(m,n) = T_0\Delta_{ms}\tau_s(m,n),\end{aligned}$$

giving

$$\begin{aligned}\tau_s(m+1,n) &= \tau_s(m,n)+\varepsilon\Delta_{ms}\tau_s(m,n),\\ \tau_s(m,n+1) &= \tau_s(m,n)+\varepsilon\Delta_{ns}\tau_s(m,n).\end{aligned}$$

Then, scaling the density ρ (2.11) and the flux f (2.9) we get

$$\begin{aligned}f(x,t) &= \frac{1}{T_0}f_s\left(x,\frac{t}{MT_0}\right),\\ \rho(x,t) &= \frac{M}{X}\rho_s\left(x,\frac{t}{MT_0}\right),\end{aligned}$$

where X is the length of the DOC interval. Finally

$$\begin{aligned}&f_s(x_m,\tau_s(m,n)) = \tfrac{1}{\Delta_{ns}\tau_s(m,n)}, && m=0,..,M,\ n=0,1,..\\ &\rho_s(x_m,\tau_s(m+1,n)) = \tfrac{\varepsilon X\Delta_{ms}\tau_s(m,n+1)}{h_m\Delta_{ns}\tau_s(m+1,n)}, && m=0,..,M,\ n=0,1,...\end{aligned} \tag{2.14}$$

2.1.2 Interpolation and weak formulation

In this section, it will be show the asymptotic validity of a conservation law in the regime situation, which is considered supposing $M >> 1$ or $\varepsilon = \frac{1}{M} << 1$. The goal is an initial boundary value problem for the conservation law

$$\partial_t\rho+\partial_x f = 0,\quad f=\min\{\mu(x,t),\rho\},\quad f(0,t)=f^A(t), \tag{2.15}$$

together with some initial condition $\rho(x,0)=\rho_0(t)$.

Several complications appear in this approach; in fact, the main difficulty arising from $M \to \infty$, or equivalently $\varepsilon \to 0$, is that the flux function f can become discontinuous due to the assumption of different maximal capacities. Consider the following bottleneck scenario: if processor x_m has a higher capacity than x_{m+1}, i.e. $\mu(x_{m+1}) < \mu(x_m)$, a queue in front of x_{m+1} will grow. But, since mass still has to be conserved, this discontinuity has to be compensated by a δ-distribution in the density ρ which, hence, will not be a classical function. To deal with this issue, an asymptotic analysis for the Newell-curve $U(m,t)$ (2.5) is performed. Denoting the approximation of U by u, setting $\rho(x,t) = -\partial_x u(x,t)$ and integrating the (2.15) once respect to x, we get

$$\partial_t u(x,t) - \min\{\mu(x,t), -\partial_x u\}, \quad \lim_{x\to 0^-} u(x,t) = g^A(t), \quad \frac{d}{dt} g^A(t) = f^A(t) \tag{2.16}$$

The last equation allows for shock solutions appearing as a δ-distribution in u. In this case, although the x-derivative of u becomes unbounded, the flux (i.e. $\partial_t u(x,t)$) will be bounded because of the $min-$function. It is possible to show that, in the limit $\varepsilon \to 0$, u satisfies the hyperbolic problem in (2.16) weakly in space x and time t. First we have to define the interpolants in the form of scaled functions $\widetilde{u}_s$ and $\widetilde{f}_s$. An effective method towards a continuum is a piecewise constant interpolation in space and time. Then, the next theorem will show that the N-curve $\widetilde{u}_s$ satisfies the (2.16) weakly in x and t as $\varepsilon \to 0$.

Theorem 50 *Given the scaled density and flux at the discrete points $x_m, \tau_s(m,n)$, as defined in (2.13). Let the scaled throughput times $T_s(x_m)$ stay uniformly bounded, i.e. $h_m = O(\varepsilon)$ holds uniformly in m. Assume finitely many bottlenecks for a finite amount of time, i.e. let $\Delta_m \tau_s(m,n)$ be bounded for $\varepsilon \to 0$ expect for a certain number of nodes m and a finite number of parts n, which stays bounded as $\varepsilon \to 0$. Then, for $\varepsilon \to 0$, and $\max h_m \to 0$ the interpolated N-function and flux $\widetilde{u}_s$, $\widetilde{f}_s$ satisfy the initial boundary value problem*

$$\begin{gathered} \partial_t \widetilde{u}_s = \widetilde{f}_s, \quad \widetilde{f}_s = \min\{\mu, -\partial_x \widetilde{u}_s\}, \quad t > \widetilde{\tau}_s^I(x), \quad 0 < x < X, \\ \widetilde{u}_s\left(x, \widetilde{\tau}_s^I(x)\right) = 0, \quad \lim_{x\to 0^-} \widetilde{u}_s(x,t) = \int_{\widetilde{\tau}_s(0,0)}^{t} f^A(s)\, ds \end{gathered} \tag{2.17}$$

in the limit $\varepsilon \to 0$, weakly in x and t.

Proof. The proof was done by Armbruster et al. and it can be found in [2]. ■

Then, through this theorem, it is proved the asymptotic validity of the integrated conservation law (2.17), for any N-curve u and any flux f, derived from an arbitrary sequence τ via the definitions (2.9) and (2.11) and the interpolants $\widetilde{u}_s$, $\widetilde{f}_s$.

Moreover, considering the unscaled variables, Theorem (50) implies that density $\rho(x,t)$ can be approximately computed as $\rho = -\partial_x u$.

2.2 The Göttlich-Herty-Klar model

In this section, we present a model for large queuing supply chain networks based on the work of Armbruster, Degond and Ringhofer [2]. Mainly, we formulate a PDE network problem and a separate modeling of the queues, taking advantage of existence theory of the network problem.

First, we state the definition of a supply chain network describing the connection between it and the suppliers.

Definition 51 . *A supply chain network is a finite, connected directed, simple graph consisting of arcs $J = \{1, ..., N\}$ and vertices $V = \{1, ..., N-1\}$. Each supplier j is modeled by an arc j, which is again parameterized by an interval $[a_j, b_j]$. We use $a_1 = -\infty$ and $b_N = +\infty$ for the first respectively the last supplier in the supply chain.*

First we consider the special case where each vertex is connected to exactly two arcs. As shown in Fig.2.1, we conventionally assume that $b_j = a_{j-1}$. Then, we state that a supplier j is defined by a processor and a queue in front of it, i.e. at $x = a_j$ (for simplicity we assume that the first supplier consists of a processor only).

Each processor j is characterized by a maximum processing capacity μ_j, its length L_j and the processing time T_j. The rate $\frac{L_j}{T_j}$ defines the processing velocity. The evolution of parts inside the processor j is modeled by the function $\rho_j(x,t)$ indicating the density of parts in j at point x and time t.

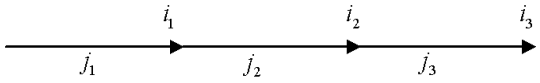

Figure 2.1: Example of a simple network structure

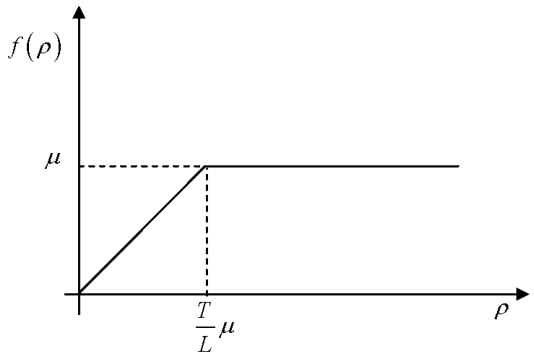

Figure 2.2: Relation between flow and density

The dynamics of each processor on an arc j are governed by an advection equation as in ((the previous Section)):

$$\begin{cases} \partial_t \rho_j(x,t) + \partial_x \min\left\{\mu_j, \frac{L_j}{T_j}\rho_j(x,t)\right\} = 0, & \forall x \in [a_j, b_j],\ t \in \mathbb{R}^+ \\ \rho_j(x,0) = \rho_{j,0}(x), & \forall x \in [a_j, b_j] \end{cases} \tag{2.18}$$

Note that we use the flux functions derived in ((the previous Section))

$$f : \mathbb{R}_0^+ \to [0,\mu], \quad f(\rho) = \min\left\{\mu, \frac{L}{T}\rho\right\}, \tag{2.19}$$

where the maximal rate for the processor is a positive constant μ. Clearly, f is Lipschitz with constant $L_f = \frac{L}{T}$.

Remark 52 *Usually, an inflow profile $f_1(t)$ for the supply chain is given. This profile can be translated into initial data $\rho_1(x,0) := \rho_{1,0}(b_1 - t) = f_1(t)$ on artificial first arc, where it's assumed $\mu_1 > \max f_1$ and $\frac{L_1}{T_1} = 1$.*

Each queue is a time-dependent function $t \to q_j(t)$ and buffered demands for the generic processor j when the capacity of processor $j-1$ is different from the demand of processor j (in fact, in this case the queue q_j increases or decreases its buffer).

Mathematically, we require each queue q_j to satisfy the following equation:

$$\partial_t q_j(t) = f_{j-1}\left(\rho_{j-1}(b_{j-1}, t)\right) - f_j\left(\rho_j(a_j, t)\right), \quad j = 2, ..., N \tag{2.20}$$

Due to the advection, we can define the flux on the outgoing arc j as

$$f_j\left(\rho_j(a_j, t)\right) = \begin{cases} \min\left\{f_{j-1}\left(\rho_{j-1}(b_{j-1}, t)\right), \mu_j\right\} & q_j(t) = 0 \\ \mu_j & q_j(t) > 0 \end{cases} \tag{2.21}$$

where the flux $f_j\left(\rho_j(a_j, t)\right)$ is dependent on the capacity of the queue. The (2.21) allows for the following interpretation: if the outgoing buffer is empty, we process as many parts as possible but at most μ_j, while if it contains some parts, then we process at maximal possible rate, i.e. again μ_j.

Finally, we have the following coupled system of partial and ordinary differential equations on a network

$$\partial_t \rho_j(x, t) = -\partial_x \min\left\{\mu_j, \frac{L_j}{T_j}\rho_j(x, t)\right\} \tag{2.22a}$$

$$\rho_j(x, 0) = \rho_{j,0}(x) \tag{2.22b}$$

$$\partial_t q_j(t) = f_{j-1}\left(\rho_{j-1}(b_{j-1}, t)\right) - f_j\left(\rho_j(a_j, t)\right) \tag{2.22c}$$

$$q_j(0) = q_{j,0} \tag{2.22d}$$

$$f_j\left(\rho_j(a_j, t)\right) = \begin{cases} \min\left\{f_{j-1}\left(\rho_{j-1}(b_{j-1}, t)\right), \mu_j\right\} & q_j(t) = 0 \\ \mu_j & q_j(t) > 0 \end{cases} \tag{2.22e}$$

Consider the very special flux function in (2.19), the Riemann problem for (2.18) and $(x, t) \in \mathbb{R} \times \mathbb{R}^+$ admits one of the following two solutions. Let the initial data such as

$$\rho_{j,0}(x) = \begin{cases} \rho_l & \text{for } x < 0 \\ \rho_r & \text{for } x \geq 0 \end{cases},$$

with $\rho_l, \rho_r \in \mathbb{R}_0^+$. Then, for $\rho_l < \rho_r$ the solution ρ_j is given by

$$\rho_j(x,t) = \begin{cases} \rho_l & -\infty < \frac{x}{t} \leq \frac{f_j(\rho_r)-f_j(\rho_l)}{\rho_r-\rho_l} \\ \rho_r & \frac{f_j(\rho_r)-f_j(\rho_l)}{\rho_r-\rho_l} < \frac{x}{t} < \infty \end{cases} \tag{2.23}$$

while for $\rho_r < \rho_l$, if $\rho_l \leq \mu_j$ or $\rho_r \geq \mu_j$ the solution is the same, i.e. (2.23). Otherwise, in the case $\rho_r < \mu_j < \rho_l$, the solution will be

$$\rho(x,t) = \begin{cases} \rho_l & -\infty < \frac{x}{t} \leq \frac{f_j(\rho_l)-\mu_j}{\rho_l-\mu_j} \\ \mu_j & \frac{f_j(\rho_l)-\mu_j}{\rho_l-\mu_j} < \frac{x}{t} \leq \frac{\mu_j-f_j(\rho_r)}{\mu_j-\rho_r} \\ \rho_r & \frac{\mu_j-f_j(\rho_r)}{\mu_j-\rho_r} < \frac{x}{t} < \infty \end{cases} \tag{2.24}$$

where it holds $\frac{\mu_j-f_j(\rho_r)}{\mu_j-\rho_r}$ and $\frac{f_j(\rho_l)-\mu_j}{\rho_l-\mu_j} = 1$.

We can introduce the following definition:

Definition 53 (Network solution) *A family of functions $\{\rho_j, q_j\}_{j\in J}$ is called an admissible solution for a network as in 2.1 if, for all j, ρ_j is a weak entropic solutions [22] to (2.18), q_j is absolutely continuous and, in the sense of traces for ρ_js, equations (2.20) and (2.21) hold for a.e. t.*

In particular, considering a single vertex $v \in V$ with incoming arc $j = 1$ and outgoing arc $j = 2$ and constant initial data $\rho_{j,0}(x) \leq \mu_j$, there exists an admissible solution $\{\rho_1, \rho_2, q_2\}$ which has the form:

$$\rho_1(x,t) = \rho_{1,0} \tag{2.25a}$$

$$\rho_2(x,t) = \begin{cases} f_1(\rho_{1,0}) < \mu_2 \begin{cases} \rho_{1,0} & 0 \leq \frac{x-t_0}{t} < 1 = \frac{f_2(\mu_2)-f_2(\rho_{1,0})}{\mu_2-\rho_{1,0}} \\ \mu_2 & 1 \leq \frac{x-t_0}{t} \text{ and } \frac{x}{t} < 1 \\ \rho_{2,0} & 1 \leq \frac{x}{t} < \infty \end{cases} \\ f_1(\rho_{1,0}) \geq \mu_2 \begin{cases} \mu_2 & 0 \leq \frac{x}{t} < 1 = \frac{f_2(\mu_2)-f_2(\rho_{2,0})}{\mu_2-\rho_{2,0}} \\ \rho_{2,0} & 1 \leq \frac{x}{t} < \infty \end{cases} \end{cases} \tag{2.25b}$$

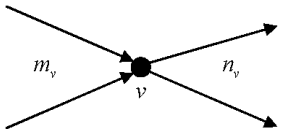

Figure 2.3: Geometry of a vertex with multiple incoming and outcoming arcs

$$q_2(t) = q_{2,0} + \int_0^t f_1\left(\rho_{1,0}\right) - f_2\left(\rho_2\left(a_2+,\tau\right)\right) d\tau \tag{2.25c}$$

where $t_0 = \frac{q_{2,0}}{\mu_2 - f_1\left(\rho_{1,0}\right)}$.

For a network as in Fig.2.1 with initial values $q_j(0) = 0$ and initial data $\left\{\rho_{j,0}(x)\right\}_j$ where each $\rho_{j,0}$ is a step function, there exists an admissible solution $\left\{\rho_j, q_j\right\}_j$ to the network problem (2.22a) to (2.22e) whose construction is based on wave-front tracking algorithm.

2.2.1 Modeling general networks

Consider now a generic number of vertices $v \in V$ with m_v incoming and n_v outcoming arcs (as, for example, in Fig.2.3).

We denote by δ_v^- and δ_v^+ the set of arc indexes of incoming and outcoming arcs. If we have more than one outgoing arc, we need to define and successively to model the distribution of the goods from the incoming arcs. Assuming that for each vertex v a matrix $A_v := A(\alpha_{i,j}) \in \mathbb{R}^{m_v \times n_v}$ is given, hence, the total flux willing to go to arc $j \in \delta_v^+$ is given by

$$\sum_{i \in \delta_v^-} \alpha_{i,j} f_i\left(\rho_i\left(b_i-,t\right)\right).$$

Moreover we assume that, for all $i \in \delta_v^-$ and $j \in \delta_v^+$, the matrix A satisfies:

$$0 \leq \alpha_{i,j} \leq 1,$$

$$\sum_{j \in \delta_v^+} \alpha_{i,j} = 1.$$

Then, the supply chain network is modeling by (2.18) and,for each junction (vertex) v, by the following equation for the queues

$$\forall j \in \delta_v^+ \ : \ \partial_t q_j(t) = \sum_{i \in \delta_v^-} \alpha_{i,j} f_i(\rho_i(b_i-,t)) - f_j\left(\rho_j(a_j+,t)\right), \tag{2.26}$$

and the boundary values $\forall j \in \delta_v^+$,

$$f_j\left(\rho_j(a_j+,t)\right) = \begin{cases} \min\left\{\sum_{i \in \delta_v^-} \alpha_{i,j} f_i(\rho_i(b_i-,t)), \mu_j\right\} & q_j(t) = 0 \\ \mu_j & q_j(t) > 0 \end{cases}. \tag{2.27}$$

Starting by the empty queue, if the outgoing flux is a percentage of the sum of all incoming fluxes given by A_v the queue remains empty, while if it is equal to the maximal processing capacity, the queue increases. Finally if the queue is full, it is always reduced with a capacity determined by A_v and the capacities of the connected arcs.

Note that due to the positive velocity of the occurring waves the boundary conditions are well-defined. Moreover, due to (2.26) and the assumptions on A, the total flux at each vertex v is conserved for all times $t > 0$, i.e.

$$\sum_{j \in \delta_v^+} \left(\partial_t q_j(t) + f_j\left(\rho_j(a_j+,t)\right)\right) = \sum_{i \in \delta_v^-} f_i(\rho_i(b_i-,t)).$$

The construction of a solution to the network problem given by (2.18), (2.26), (2.27) is as before.

Now, let $\eta = \min_j(b_j - a_j)$ be the minimum length of a supplier; since all waves move at positive velocity at most equal to 1, two interactions with vertices of the same wave can happen at most every η units of time. If N is the number of suppliers, than there is at most a multiplication by N every η unit of time, thus we can control the number of waves and interactions.

Therefore, for given piecewise constant initial data $\rho_{j,0}^\delta$ on a network, a solution $\left(\rho^\delta, q^\delta\right)$ can be defined by the wave-tracking method up to any time T.

2.3 A continuum-discrete model for supply chain network

In this section we introduce a supply chains model extending the Armbruster, Degond and Ringhofer one presented in the section [2.1], in which each arc is modeled by a conservation law for the good density ρ and an evolution equation for the processing rate μ.

Starting by the approach used in [12],once introduced the model, we discuss about possible choices of solutions at nodes guaranteeing the conservation of fluxes given by the general equation

$$\rho_t + f_\varepsilon(\rho, \mu)_x = 0,$$

where, for $\varepsilon > 0$ the flux f_ε is given by:

$$f_\varepsilon(\rho, \mu) = \begin{cases} m\rho, & if\ \rho \leq \mu, \\ m\mu + \varepsilon(\rho - \mu), & if\ \rho \geq \mu, \end{cases}$$

with m the processing velocity.

Keeping the analogy to Riemann problems, we call the latter Riemann Solver at nodes. The first choice is to fix the rule:

SC1 The incoming density flux is equal to the outgoing density flux. So, if a solution with only waves in the density ρ exists, then such solution is taken, otherwise the minimal μ wave is produced.

Rule **SC1** corresponds to the case in which processing rate adjustments are done only if necessary, while the density ρ can be regulated more freely. In particular, it is justified in all situations in which processing rate adjustments require re-building of the supply chain, while density adjustments are operated easily (e.g. by stocking).

Even if rule **SC1** is the most natural also from a geometric point of view, in the space of Riemann data, it produces waves only to lower the value of μ and this involves, as consequence, that, in some cases, the value of the processing rate does not increase and it is not possible to maximize the flux.

In order to avoid this problem, two additional rules to solve dynamics at a node are analyzed:

SC2 The objects are processed in order to maximize the flux with minimal value of the processing rate.

SC3 The objects are processed in order to maximize the flux. Then, if a solution with only waves in the density ρ exists, then such solution is taken, otherwise the minimal μ wave is produced.

The Riemann Problems are solved fixing two "routing" algorithms:

RA1 Goods from an incoming arc are sent to outgoing ones according to their final destination in order to maximize the flux over incoming arcs. Goods are processed ordered by arrival time (FIFO policy).

RA2 Goods are processed by arrival time (FIFO policy) and are sent to outgoing arcs in order to maximize the flux over incoming and outgoing arcs.

For both routing algorithms the flux of goods is maximized considering one of the two additional rules, **SC2** and **SC3**.

In order to understand the mechanism of the two previous rules, a simple example is shown.

Suppose to have a supply chain network for assembling orange and lemon fruit juice bottles as in Fig.2.4-a

Bottles coming from the first arc are sterilized in node v^1 and are re-direct with a certain probability α to node v^2 where some is filled with lemon fruit juice and with probability $1-\alpha$ to node v^3 where some is filled with orange fruit juice. Assume that lemon and orange fruit juice bottles have two different shapes. In nodes v^4 and v^5, bottles are labeled as their own fruit juice. Finally in node v^6, produced bottles are corked. In this situation the dynamics at node v^1 is solved using the **RA1** algorithm. In fact, the redirection of bottles in order to maximize the production is not possible, since bottles have different shapes for any kind of juice.

Consider now a supply network as shown in Fig.2.4-b in which the white cups are addressed towards n arcs (or sub-chains) to be colored using different colors. Since the aim is to maximize the cups production independently from the colors, a mechanism is realized which addresses the cups on the outgoing sub-chains taking into account their loads in such way as to maximize flux on both incoming and

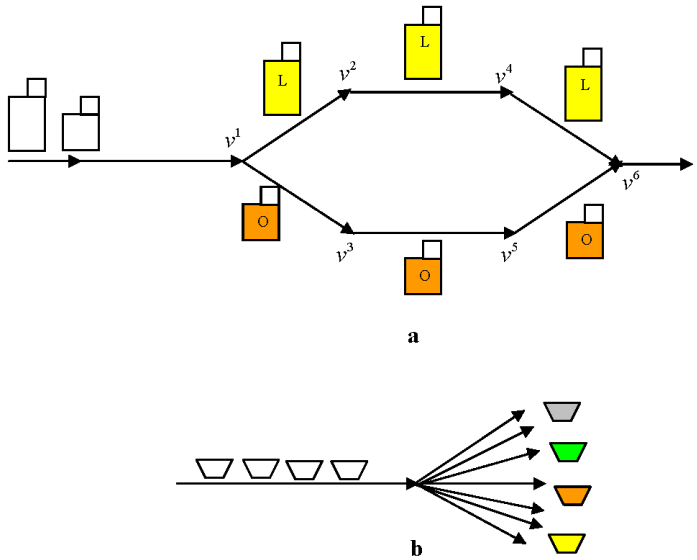

Figure 2.4: Supply network

outgoing sub-chains. So, a model based on rule **RA2** is realized to capture the behavior of this network.

2.3.1 Basic Definitions

We start from the conservation law model

$$\rho_t + \left(\min\left\{\mu\left(t,x\right),\rho\right\}\right)_x = 0. \tag{2.28}$$

To avoid problems of existence of solutions, we assume μ piecewise constant and an evolution equation of semi-linear type:

$$\mu_t + \bar{V}\mu_x = 0, \tag{2.29}$$

where $\bar{V}$ is some constant velocity. Taking $\bar{V} = 0$, it can be no solution to a Riemann Problem for the system (2.28)-(2.29) with data (ρ_l, μ_l) and (ρ_r, μ_r) if $\min\{\rho_l, \mu_l\} > \mu_r$. Since we expect the chain to influence backward the processing rate we assume $\bar{V} < 0$ and for simplicity we set $\bar{V} = -1$.

A supply network consists of $N+1$ sub-chains $I_1, ..., I_{N+1}$, modeled by real intervals $\left[a^k, b^k\right] \subset \mathbb{R}$, $k = 1, ..., N+1$, $a_k < b_k$, possible with either $a_k = -\infty$ or

$b_k = +\infty$ and M suppliers or processors $P_1, ..., P_M$ with certain throughput times and capacity.

Each supplier processes a certain good, measured in units of parts. It is assumed that a node P consists of a processor, which decides how to manage the flow among sub-chains, with a maximal processing rate μ.

The evolution on each arc is given by (2.28)-(2.29), while at each nodes vertex the evolution is given by solving Riemann Problems for the density equation (2.28) with μs as parameters. Since such Riemann Problems may still admit no solution keeping the values of μs constant, then we expect μ waves to be generated following equation (2.29). Moreover the vanishing of the characteristic velocity for (2.28), in case $\rho > \mu$, can provoke resonances with the nodes (which can be presented schematically as waves with zero velocities). Then, for this reason, the model is modified as follows.

Each sub-chain I_k is characterized by a maximum density $\rho_k^{\max}$, a maximum processing rate $\mu_k^{\max}$ and a flux f_ε^k. Then the dynamics is given by:

$$\begin{cases} \rho_t + f_\varepsilon^k(\rho,\mu)_x = 0, \\ \mu_t - \mu_x = 0. \end{cases} \tag{2.30}$$

The flux is defined as:

$$\textbf{(F)} \quad f_\varepsilon^k(\rho,\mu) = \begin{cases} \rho, & 0 \le \rho \le \mu, \\ \mu + \varepsilon(\rho - \mu), & \mu \le \rho \le \rho_k^{\max}, \end{cases}$$

$$f_\varepsilon^k(\rho,\mu) = \begin{cases} \varepsilon\rho + (1-\varepsilon)\mu, & 0 \le \mu \le \rho, \\ \rho, & \rho \le \mu \le \mu_k^{\max}, \end{cases}$$

as shown in (Fig.2.5)

The conservation law for the good density in (2.30) is a ε perturbation of (2.28) in the sense that $||f - f\varepsilon||_\infty \le C\varepsilon$ where f is the flux of (2.30). The equation has the advantage of producing waves with always strictly positive speed, thus avoiding resonance with the "boundary" problems at each node.

From now on, fixing $\varepsilon > 0$ and dropping the indices, the flux will be indicated by $f(\rho,\mu)$.

Remark 54 *It is possible to generalize all following definitions and results to the case of different fluxes $f_{\varepsilon_k}^k$ for each sub-chain I_k (also choosing ε dependent on*

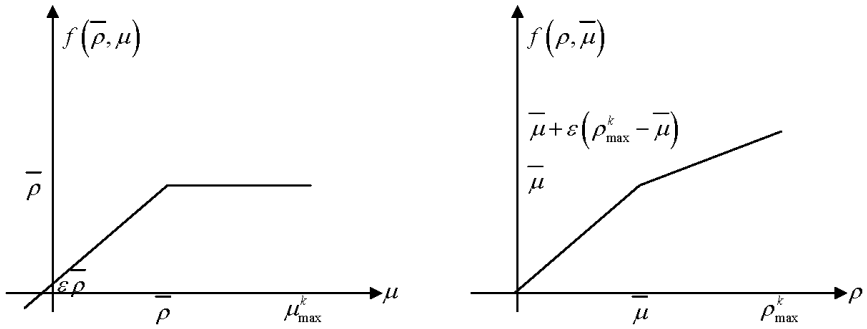

Figure 2.5: Flux (F): Left, $f(\bar{\rho},\mu)$. Right, $f(\rho,\bar{\mu})$.

k). In fact, all statements are in terms of values of fluxes at endpoints of the sub-chains, thus it is sufficient that the ranges of fluxes intersect. Moreover, we can consider different slopes m_k for each sub-chain I_k, considering the following flux

$$f^k_\varepsilon(\rho,\mu)=\begin{cases} m_k\rho, & 0\le\rho\le\mu,\\ m_k\mu+\varepsilon(\rho-\mu), & \mu\le\rho\le\rho^{\max}_k,\end{cases}$$

where $m_k\ge 0$ represents the velocity of each processor and is given by

$$m_k=\frac{L_k}{T_k},$$

with L_k and T_k, respectively, fixed length and processing time of processor k.

Assuming that the sub-chains are connected by some junction J, each of them is given by a finite number of incoming and outgoing sub-chains, then J is identified with $((i_1,...,i_n),(j_1,...,j_m))$ (see Fig.2.6) where the first n-tuple and the second m-tuple indicate respectively the set of incoming and outgoing sub-chains. Moreover, each sub-chain can be incoming or outgoing at most for one junction. Hence, the complete model is given by a couple (I,P), where $I=\{I_k : k=1,...,N+1\}$ is the collection of sub-chains and P is the collection of junctions.

The supply network evolution is described by a finite set of functions ρ_k, μ_k defined on $[0,+\infty[\times I_k$. On each sub-chain I_k, we say that $U_k:=(\rho_k,\mu_k):[0,+\infty[\times I_k\to\mathbb{R}$ is a weak solution to (2.30) if, for every C^∞-function $\varphi:[0,+\infty[\times I_k\to\mathbb{R}^2$ with compact support in $]0,+\infty[\times]a_k,b_k[$,

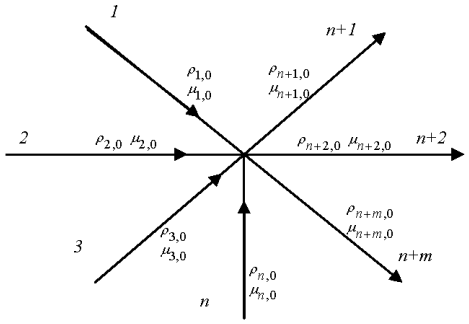

Figure 2.6: A junction.

$$\int_0^{+\infty} \int_{a_k}^{b_k} \left(U_k \frac{\partial \varphi}{\partial t} + f\left(U_k\right) \frac{\partial \varphi}{\partial x} \right) dxdt = 0,$$

where

$$f\left(U_k\right) = \begin{pmatrix} f\left(\rho_k, \mu_k\right) \\ -\mu_k \end{pmatrix},$$

is the flux function of the system (2.30). For definition of entropic solution, see at [6].

For a scalar conservation law, a Riemann Problem (RP) is a Cauchy problem for an initial data of Heavyside type, that is a piecewise constant with only one discontinuity. The solutions are formed by continuous waves called rarefactions and by traveling discontinuities called shocks.

Analogously, we call Riemann problem for a junction the Cauchy problem corresponding to an initial data which is constant on each supply sub-chain.

Definition 55 *A Riemann Solver (RS) for the junction P with n incoming sub-chains and m outgoing ones consists in a map that associates to a Riemann data $(\rho_0, \mu_0) = \left(\rho_{1,0}, \mu_{1,0}, ..., \rho_{n,0}, \mu_{n,0}, \rho_{n+1,0}, \mu_{n+1,0}, ..., \rho_{n+m,0}, \mu_{n+m,0}\right)$ at P a vector $(\hat{\rho}_0, \hat{\mu}_0) = \left(\hat{\rho}_1, \hat{\mu}_1, ..., \hat{\rho}_n, \hat{\mu}_n, \hat{\rho}_{n+1}, \hat{\mu}_{n+1}, ..., \hat{\rho}_{n+m}, \hat{\mu}_{n+m}\right)$ so that the solution is given by the waves $\left(\rho_{i,0}, \hat{\rho}_i\right)$ and $\left(\mu_{i,0}, \hat{\mu}_i\right)$ on the sub-chain I_i, $i = 1, ..., n$ and*

by the waves $\left(\hat{\rho}_j, \rho_{j,0}\right)$ *on the sub-chain* I_j, $j = n+1, ..., n+m$. *We require the consistency condition*

(CC) $RS\left(RS\left((\rho_0, \mu_0)\right)\right) = RS\left((\rho_0, \mu_0)\right)$.

Once a Riemann Solver is assigned, we can define admissible solutions at P.

Definition 56 *Assume a Riemann Solver RS is assigned for the supplier* P. *Let* $U = (U_1, ..., U_{n+m})$ *be such that* U *is of bounded variation for every* $t \geq 0$. *Then* U *is an admissible weak solution of (2.30) related to RS at the junction* P *if and only if the following property holds for almost every* t. *Setting*

$$\tilde{U}_p(t) = \left(U_1(\cdot, b_1-), ..., U_n(\cdot, b_n-), U_{n+1}(\cdot, a_{n+1}+), ..., U_{n+m}(\cdot, a_{n+m}+)\right)$$

we have $RS\left(\tilde{U}_p(t)\right) = \tilde{U}_p(t)$.

The aim is to solve the Cauchy problem on $[0, +\infty[$ for a given initial and boundary data as in next definition.

Definition 57 *Given* $U_k : I_k \to [0,1]$, $k = 1, ...N+1$, *measurable BV functions, a collection of functions* $U = (U_1, ..., U_{N+1})$, *with* $U_k : [0, +\infty[\times I_k \to [0,1]$ *continuous as functions from* $[0, +\infty[$ *into* L^1_{loc} *and* $U_k(t, \cdot)$ *BV function for almost every* t, *is an admissible solution to the Cauchy problem on the supply chain if* U_k *is a weak entropic solution to (2.30) on* I_k, $U_k(0, x) = \bar{U}_k(x)$ *a.e., and, at each supplier* P_k, U *is an admissible weak solution.*

2.3.2 Riemann Solvers for suppliers

Fixing a sub-chain I_k, we analyze system (2.30) as a system of conservation laws in the variables $U = (\rho, \mu)$:

$$U_t + F(U)_x = 0, \tag{2.31}$$

with flux function given by $F(U) = (f(\rho, \mu), -\mu)$, thus the Jacobian matrix of the flux is:

$$DF(\rho, \mu) = \begin{cases} \begin{pmatrix} 1 & 0 \\ 0 & -1 \end{pmatrix}, & \text{if } \rho < \mu, \\ \begin{pmatrix} \varepsilon & 1-\varepsilon \\ 0 & -1 \end{pmatrix}, & \text{if } \rho > \mu. \end{cases}$$

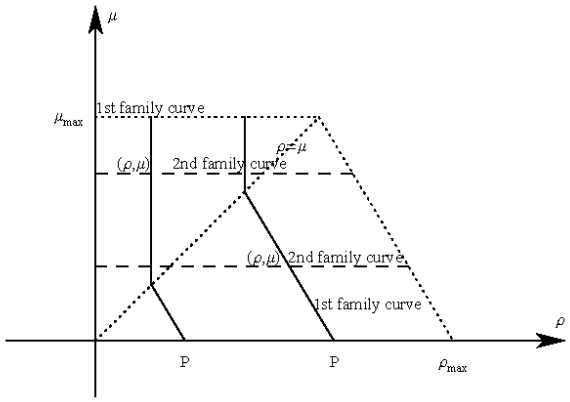

Figure 2.7: First and second family curves

The eigenvalues and eigenvectors are given by:

$$\lambda_1(\rho,\mu) \equiv -1, \qquad r_1(\rho,\mu) = \begin{cases} \begin{pmatrix} 0 \\ 1 \end{pmatrix}, & \text{if } \rho < \mu, \\ \begin{pmatrix} -\frac{1-\varepsilon}{1+\varepsilon} \\ 1 \end{pmatrix}, & \text{if } \rho > \mu, \end{cases}$$

$$\lambda_2(\rho,\mu) = \begin{cases} 1 & \text{if } \rho < \mu, \\ \varepsilon & \text{if } \rho > \mu, \end{cases} \qquad r_1(\rho,\mu) \equiv \begin{pmatrix} 0 \\ 1 \end{pmatrix}.$$

Hence the Hugoniot curves for the first family are vertical lines above the secant $\rho = \mu$ and lines with slope close to $-\frac{1}{2}$ below the same secant. The Hugoniot curves for the second family are just horizontal lines. Since we consider positive and bounded values for the variables, we fix the invariant region (see Fig.2.7):

$$\begin{aligned} D \;=\; & \{(\rho,\mu) : 0 \le \rho \le \rho_{\max},\ 0 \le \mu \le \mu_{\max}, \\ & 0 \le (1+\varepsilon)\,\rho + (1-\varepsilon)\,\mu \le (1+\varepsilon)\,\rho_{\max} = 2\,(1-\varepsilon)\,\mu_{\max}\} \end{aligned}$$

Observe that

$$\rho_{\max} = \mu_{\max}\frac{2}{1+\varepsilon}. \tag{2.32}$$

First, some results, widely proved for sequential supply chains in [12], are reported.

Proposition 58 *Given (ρ_0, μ_0), the minimal value of the flux at points of the curve of the first family passing through (ρ_0, μ_0) is given by:*

$$f_{\min}\left((\rho_0, \mu_0)\right) = \begin{cases} \frac{2\varepsilon}{1+\varepsilon}\rho_0, & if\ \rho_0 \leq \mu_0, \\ \varepsilon\rho_0 + \frac{\varepsilon(1-\varepsilon)}{1+\varepsilon}\mu_0, & if\ \rho_0 > \mu_0. \end{cases}$$

Lemma 59 *Given an initial datum (ρ_0, μ_0), the maximum value of the density of the curve of the second family passing through (ρ_0, μ_0) and belonging to the invariant region is given by*

$$\rho^M(\mu_0) = \rho_{\max} - \mu_0 \frac{\rho_{\max} - \mu_{\max}}{\mu_{\max}}. \tag{2.33}$$

Proof. From 2.7 the maximum value is obtained by the intersection of the curve of the second family passing through (ρ_0, μ_0) and the line connecting the points $(\rho_{\max}, 0)$ and $(\mu_{\max}, \mu_{\max})$:

$$\rho^M(\mu_0) = \rho_{\max} - \mu_0 \frac{\rho_{\max} - \mu_{\max}}{\mu_{\max}}.$$

From (2.32) we get

$$\rho^M(\mu_0) = \frac{2}{1+\varepsilon}\mu_{\max} - \frac{(1-\varepsilon)}{1+\varepsilon}\mu_0.$$

■

The following estimate holds [12]:

Proposition 60 *Assume that a second family wave $((\rho_l, \mu_l), (\rho_m, \mu_m))$ interacts with a first family wave $((\rho_m, \mu_m), (\rho_r, \mu_r))$. If $\mu_r < \mu_m$ then the flux variation decreases.*

Considering now a node P with n and m respectively incoming and outgoing sub-chains and a Riemann initial datum $\left(\rho_{1,0}, \mu_{1,0}, ..., \rho_{n,0}, \mu_{n,0}\right)$ and $\left(\rho_{n+1,0}, \mu_{n+1,0}, ..., \rho_{m+n,0}, \mu_{m+n,0}\right)$, the following Lemma holds:

Lemma 61 *On the incoming sub-chain, only waves of the first family may be produced, while on the outgoing sub-chain only waves of the second family may be produced.*

From the last Lemma, assigned the initial datum, for each Riemann Solver it follows that

$$\begin{aligned} \hat{\rho}_i &= \varphi\left(\hat{\mu}_i\right), \quad i = 1, ..., n, \\ \hat{\mu}_j &= \mu_{j,0}, \qquad j = n+1, ..., n+m. \end{aligned} \tag{2.34}$$

where the function $\varphi(\cdot)$ describes the first family curve $\left(\rho_{i,0}, \mu_{i,0}\right)$ as function of $\hat{\mu}_i$. The expression of such curve changes at a particular value $\bar{\mu}_i$, given by:

$$\bar{\mu}_i = \begin{cases} \rho_{i,0}, & if\ \rho_{i,0} \leq \mu_{i,0}, \\ \frac{1+\varepsilon}{2}\rho_{i,0} + \frac{1-\varepsilon}{2}\mu_{i,0}, & if\ \rho_{i,0} > \mu_{i,0}. \end{cases}$$

The case of sequential supply chain.

Considering a node P_k with one incoming arc k and one outgoing arc $k+1$. Let us now to discuss how $\hat{\rho}_{k+1}$ and $\hat{\mu}_k$ (from 2.34 we set $i = k$ and $j = k+1$) can be chosen.

The conservation of flux at the node can be written as

$$f\left(\varphi\left(\hat{\mu}_k\right), \hat{\mu}_k\right) = f\left(\hat{\rho}_{k+1}, \mu_{k+1,0}\right). \tag{2.35}$$

We have:

Case α): $\mu_{k+1,0} < \bar{\mu}_k$;

Case β): $\bar{\mu}_k \leq \mu_{k+1,0}$.

In both cases $\bar{\mu}_k$ and $\mu_{k+1,0}$ individuate in the plane $\left(\hat{\rho}_{k+1}, \hat{\mu}_k\right)$ four regions so defined:

$$\begin{aligned} A &= \left\{\left(\hat{\rho}_{k+1}, \hat{\mu}_k\right) : 0 \leq \hat{\rho}_{k+1} \leq \mu_{k+1,0}, \bar{\mu}_k \leq \hat{\mu}_k \leq \mu_k^{\max}\right\}; \\ B &= \left\{\left(\hat{\rho}_{k+1}, \hat{\mu}_k\right) : \mu_{k+1,0} \leq \hat{\rho}_{k+1} \leq \rho_{k+1}^M, \bar{\mu}_k \leq \hat{\mu}_k \leq \mu_k^{\max}\right\}; \\ A &= \left\{\left(\hat{\rho}_{k+1}, \hat{\mu}_k\right) : 0 \leq \hat{\rho}_{k+1} \leq \mu_{k+1,0}, 0 \leq \hat{\mu}_k \leq \bar{\mu}\right\}; \\ B &= \left\{\left(\hat{\rho}_{k+1}, \hat{\mu}_k\right) : \mu_{k+1,0} \leq \hat{\rho}_{k+1} \leq \rho_{k+1}^M, 0 \leq \hat{\mu}_k \leq \bar{\mu}_k\right\}; \end{aligned}$$

The (2.35) is satisfied in case β) along the line depicted in Fig.2.9 and in case α) (Fig.2.8) there are solutions, only under some conditions, along the dashed line. For details, see [12].

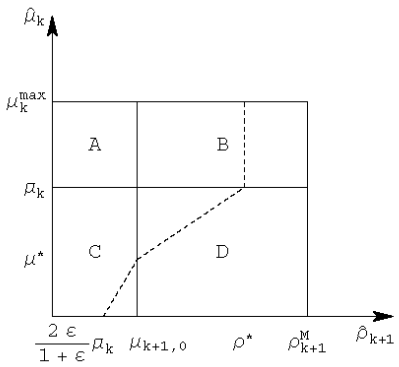

Figure 2.8: Case α)

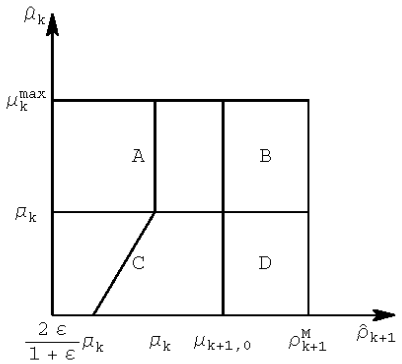

Figure 2.9: Case β)

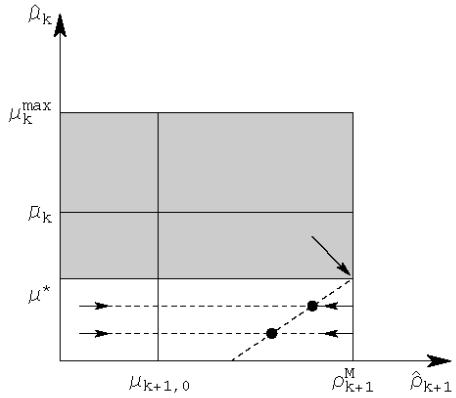

Figure 2.10: An example of Riemann Solver: case α).

A Riemann Solver according to rule SC1. Geometrically, in case β), we can define a Riemann Solver mapping every initial datum on the line $\hat{\mu}_k = c$ to the intersection of the same line with that drawn in Fig.2.9. While in case α), it may happen that there is no admissible solution on a given line $\hat{\mu}_k = c$. Therefore, we can use the same procedure if the line $\hat{\mu}_k = c$ intersects the dashed line of Fig.2.8, while mapping all other points to the admissible solution with the highest value of $\hat{\mu}_k$. This Riemann Solver is shown in Fig.2.10 and Fig.2.11.

Remark 62 *If $\hat{\rho}_{k+1} \leq \mu_{k+1,0}$, then the solution $\left(\hat{\rho}_{k+1}, \rho_{k+1,0}\right)$ is a contact discontinuity. The same happens if $\hat{\rho}_{k+1} \geq \mu_{k+1,0}$ and $\rho_{k+1,0} > \mu_{k+1,0}$. If $\hat{\rho}_{k+1} \geq \mu_{k+1,0}$ and $\rho_{k+1,0} < \mu_{k+1,0}$, the solution consists of two discontinuities.*

A Riemann Solver according to rule SC2. Rule SC2 identifies a specific Riemann Solver:

Theorem 63 *Fix a node P_k. For every Riemann initial datum $\left(\rho_{k,0}, \mu_{k,0}, \rho_{k+1,0}, \mu_{k+1,0}\right)$ at P_k there exists a unique vector $\left(\hat{\rho}_k, \hat{\mu}_k, \hat{\rho}_{k+1}, \hat{\mu}_{k+1}\right)$ solution of the Riemann Problem according to rule **SC2**.*

Proof. Given the initial datum $\left(\rho_{k,0}, \mu_{k,0}, \rho_{k+1,0}, \mu_{k+1,0}\right)$, it holds

$$\begin{aligned} \hat{\rho}_k &= \varphi\left(\hat{\mu}_k\right), \\ \hat{\mu}_{k+1} &= \mu_{k+1,0}, \end{aligned}$$

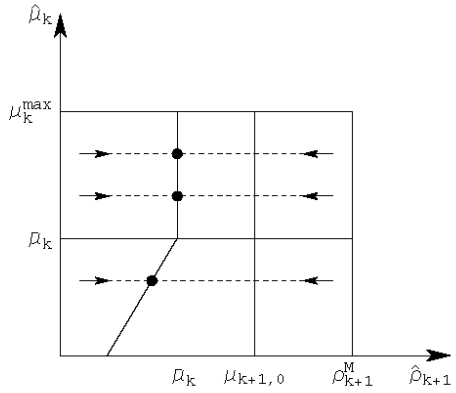

Figure 2.11: An example of Riemann Solver: case β).

where $\varphi(\hat{\mu}_k)$ has been defined by (2.34). We have to distinguish again two cases:

Case α): $\mu_{k+1,0} < \bar{\mu}_k$. Let

$$\rho^* = \frac{\bar{\mu}_k - (1-\varepsilon)\,\mu_{k+1,0}}{\varepsilon}, \tag{2.36}$$

we consider two subcases which correspond to the situation in which solutions in region B exist or do not exist.

Case α_1): $\rho^* \leq \rho^M(\mu_{k+1,0})$. Since $\mu_{k+1,0} < \bar{\mu}_k$ we get

$$\rho^* = \frac{\bar{\mu}_k}{\varepsilon} - \left(\frac{1}{\varepsilon} - 1\right)\mu_{k+1,0} > \frac{\bar{\mu}_k}{\varepsilon} - \left(\frac{1}{\varepsilon} - 1\right)\bar{\mu}_k = \bar{\mu}_k.$$

Considering the lines of Fig.2.8, to every μ it corresponds a value of the flux. We claim the following:

Claim 64 *If $\rho^* \leq \rho^M$ the flux increases with respect to μ along the dashed lines in region C,D and in B for $\mu_k^{\max} \leq \mu \leq \rho^*$ and, finally, it is constant along the dashed line in region B for $\rho^* \leq \mu \leq \mu_k^{\max}$.*

It holds

$$f(\rho^*, \mu) = \begin{cases} \varepsilon\rho^* + (1+\varepsilon)\,\mu, & 0 \leq \mu \leq \rho^*, \\ \rho^*, & \rho^* \leq \mu \leq \mu_k^{\max}, \end{cases}$$

whose derivative, with respect to μ, is given by

$$\frac{\partial f(\rho^*, \mu)}{\partial \mu} = \begin{cases} (1+\varepsilon), & 0 \le \mu \le \rho^*, \\ 0, & \rho^* \le \mu \le \mu_k^{\max}. \end{cases}$$

It follows that for $\rho^* \le \mu \le \mu_k^{\max}$ the flux is constant along the dashed line in region B.

Let us now prove that the flux is increasing with respect to μ along the dashed lines in regions C and D. The line connecting the points $\left(\frac{2\varepsilon}{1+\varepsilon}\bar{\mu}_k, 0\right)$ and $\left(\mu_{k+1,0}, \mu^*\right)$ with $\mu^* = \frac{1+\varepsilon}{1-\varepsilon}\left(\hat{\mu}_{k+1} - \frac{2\varepsilon}{1+\varepsilon}\bar{\mu}_k\right)$ has equation

$$\rho - \frac{1}{\mu^*}\left(\mu_{k+1,0} - \frac{2\varepsilon}{1+\varepsilon}\bar{\mu}_k\right)\mu - \frac{2\varepsilon}{1+\varepsilon}\bar{\mu}_k = 0,$$

and a directional vector is given by

$$r_{C_\alpha} = \begin{pmatrix} \frac{1}{\mu^*}\left(\mu_{k+1,0} - \frac{2\varepsilon}{1+\varepsilon}\bar{\mu}_k\right) \\ 1 \end{pmatrix}.$$

Therefore, the directional derivative of the flux is equal to

$$\begin{aligned} \nabla f(\rho, \mu) \cdot r_{C_\alpha} &= \begin{pmatrix} \varepsilon \\ 1-\varepsilon \end{pmatrix}\begin{pmatrix} \frac{1}{\mu^*}\left(\mu_{k+1,0} - \frac{2\varepsilon}{1+\varepsilon}\bar{\mu}_k\right) \\ 1 \end{pmatrix} = \\ &= \frac{\varepsilon}{\mu^*}\left(\mu_{k+1,0} - \frac{2\varepsilon}{1+\varepsilon}\bar{\mu}_k\right) + (1-\varepsilon) > 0. \end{aligned}$$

The latter inequality is fulfilled if $\mu_{k+1,0} > \frac{2\varepsilon}{1+\varepsilon}\bar{\mu}_k$, which is true whenever we have solutions in region C.

In region D a directional vector of the line connecting the points $\left(\mu_{k+1,0}, \mu^*\right)$ and $(\rho^*, \bar{\mu}_k)$ is the following

$$r_{D_\alpha} = \begin{pmatrix} \frac{\rho^* - \mu_{k+1,0}}{\bar{\mu}_k - \mu^*} \\ 1 \end{pmatrix}.$$

It implies that

$$\nabla f(\rho, \mu) \cdot r_{D_\alpha} = \begin{pmatrix} \varepsilon \\ 1-\varepsilon \end{pmatrix}\begin{pmatrix} \frac{\rho^* - \mu_{k+1,0}}{\bar{\mu}_k - \mu^*} \\ 1 \end{pmatrix} = \varepsilon\frac{\rho^* - \mu_{k+1,0}}{\bar{\mu}_k - \mu^*} + (1+\varepsilon) > 0,$$

since $\rho^* > \bar{\mu}_k > \mu_{k+1,0}$ and $\bar{\mu}_k - \mu^* > 0$.

In order to respect rule **SC2** we set

$$\begin{aligned}\rho_{k+1} &= \rho^*,\\ \hat{\mu}_k &= \min\left\{\mu_k^{\max}, \rho^*\right\}.\end{aligned}$$

Case α_2): If $\rho^* > \rho^M\left(\mu_{k+1,0}\right)$, there are not solutions in region B and since the flux increases with respect to μ in region D we set

$$\begin{aligned}\hat{\rho}_{k+1} &= \rho^M,\\ \hat{\mu}_k &= \tilde{\mu},\end{aligned}$$

where $\tilde{\mu}$ is obtained from

$$(1-\varepsilon)\,\mu_{k+1,0} + \varepsilon\hat{\rho}_{k+1} = (1-\varepsilon)\,\hat{\mu}_k + \varepsilon\hat{\rho}_k,$$

setting $\hat{\rho}_{k+1} = \rho^M$, i.e.

$$\begin{aligned}\tilde{\mu} &= \frac{\varepsilon\,(1+\varepsilon)}{1-\varepsilon}\rho^M - \frac{2\varepsilon}{1-\varepsilon}\bar{\mu}_k + (1+\varepsilon)\,\mu_{k+1,0} =\\ &= \frac{2\varepsilon}{1-\varepsilon}\left(\mu_k^{\max} - \bar{\mu}_k\right) + \mu_{k+1,0}.\end{aligned}$$

Case β): $\bar{\mu}_k \leq \mu_{k+1,0}$. Consider the line of Fig.2.9. In this case the flux is constant with respect to μ along the line in the region A and is an increasing function along the line in region C.

In fact, since the line in region A is given by $\hat{\rho}_{k+1} = \bar{\mu}_k$, it follows that

$$f\left(\hat{\rho}_{k+1}, \mu\right) = \begin{cases} \varepsilon\bar{\mu}_k + (1-\varepsilon)\,\mu, & 0 \leq \mu \leq \bar{\mu}_k,\\ \rho, & \bar{\mu}_k \leq \mu \leq \mu_k^{\max},\end{cases}$$

from which

$$\frac{\partial f\left(\hat{\rho}_{k+1}, \mu\right)}{\partial \mu} = \begin{cases} (1-\varepsilon), & 0 \leq \mu \leq \bar{\mu}_k,\\ 0, & \bar{\mu}_k \leq \mu \leq \mu_k^{\max}.\end{cases}$$

In region C the line connecting the points $\left(\frac{2\varepsilon}{1-\varepsilon}\bar{\mu}_k, 0\right)$ and $(\bar{\mu}_k, \bar{\mu}_k)$ has equation

$$\rho - \frac{1-\varepsilon}{1+\varepsilon} - \frac{2\varepsilon}{1+\varepsilon}\bar{\mu}_k = 0,$$

and a directional vector is given by

$$r_{C_\beta} = \begin{pmatrix} \frac{1-\varepsilon}{1+\varepsilon} \\ 1 \end{pmatrix}.$$

The directional derivative is the following

$$\nabla f(\rho,\mu)\cdot r_{C_\beta} = \begin{pmatrix} \varepsilon \\ 1-\varepsilon \end{pmatrix}\begin{pmatrix} \frac{1-\varepsilon}{1+\varepsilon} \\ 1 \end{pmatrix} = \varepsilon\frac{1-\varepsilon}{1+\varepsilon} + (1-\varepsilon) > 0.$$

It follows that rule **SC2** is satisfied if we define

$$\begin{aligned} \hat{\rho}_{k+1} &= \bar{\mu}_k, \\ \hat{\mu}_k &= \bar{\mu}_k. \end{aligned}$$

Finally the Riemann Solver is the following:

Case α): $\mu_{k+1,0} < \bar{\mu}_k$

Case α_1): $\rho^* \leq \rho^M\left(\mu_{k+1,0}\right)$

$$\begin{aligned} \hat{\rho}_{k+1} &= \rho^*, \\ \hat{\mu}_k &= \min\left\{\mu_k^{\max}, \rho^*\right\}. \end{aligned}$$

Case α_2): $\rho^* > \rho^M\left(\mu_{k+1,0}\right)$

$$\begin{aligned} \hat{\rho}_{k+1} &= \rho^M\left(\mu_{k+1,0}\right), \\ \hat{\mu}_k &= \tilde{\mu}. \end{aligned}$$

Case β): $\mu_{k+1,0} \geq \bar{\mu}_k$

$$\begin{aligned} \hat{\rho}_{k+1} &= \bar{\mu}_k, \\ \hat{\mu}_k &= \bar{\mu}_k. \end{aligned}$$

■

The Riemann Solver is shown in Fig.2.12 and Fig.2.13. In case α) we can define a Riemann Solver mapping every initial datum to the circle or to the square point if $\rho^* \leq \rho^M$ and to the filled point if $\rho^* > \rho^M$. In case β) we can define a Riemann Solver mapping every initial datum to the point $(\bar{\mu}_k, \bar{\mu}_k)$, indicated by the arrow.

A Riemann Solver according to rule SC3 Also with rule **SC3**, we have a precise Riemann Solver.

Theorem 65 *Fix a node P_k. For every Riemann initial datum $\left(\rho_{k,0}, \mu_{k,0}, \rho_{k+1,0}, \mu_{k+1,0}\right)$ at P_k there exists a unique vector $\left(\hat{\rho}_k, \hat{\mu}_k, \hat{\rho}_{k+1}, \hat{\mu}_{k+1}\right)$ solution of the Riemann Problem according to rule **SC3**.*

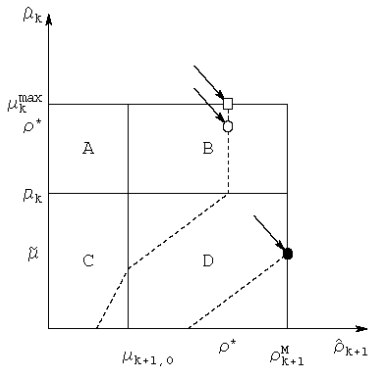

Figure 2.12: Case α) for the Riemann Solver **SC2.**

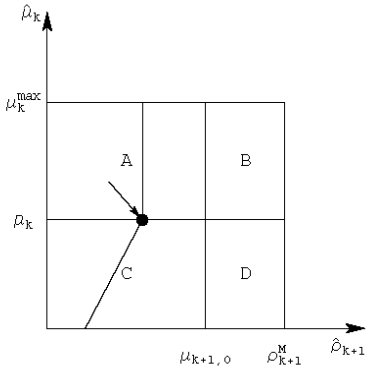

Figure 2.13: Case β) for the Riemann Solver **SC2**.

Proof. As for the Riemann Solver for rule **SC2**, given the initial datum $\left(\rho_{k,0}, \mu_{k,0}, \rho_{k+1,0}, \mu_{k+1,0}\right)$, we have

$$\begin{aligned}\hat{\rho}_k &= \varphi\left(\hat{\mu}_k\right),\\ \hat{\mu}_{k+1} &= \mu_{k+1,0},\end{aligned}$$

We distinguish:

Case α): This case is splitted in two subcases:

Case α_1): $\rho^* \leq \rho^M\left(\mu_{k+1,0}\right)$. In theorem 64 it was proved that the flux increases with respect to μ along the dashed lines in regions C, D and B for $\mu_k^{\max} \leq \mu \leq \rho^*$ and, finally, it is constant along the line in region B for $\rho^* \leq \mu \leq \mu_k^{\max}$. It follows that we have to consider two situations:

Case α_{11}): $\rho^* > \mu_k^{\max}$. According to rule **SC3** we set

$$\begin{aligned}\hat{\rho}_{k+1} &= \rho^*,\\ \hat{\mu}_k &= \mu_k^{\max}.\end{aligned}$$

Case α_{12}): $\rho^* \leq \mu_k^{\max}$. We set

$$\begin{aligned}\hat{\rho}_{k+1} &= \rho^*,\\ \hat{\mu}_k &= \max\left\{\rho^*, \mu_{k+1}\right\}.\end{aligned}$$

Case α_2): $\rho^* > \rho^M\left(\mu_{k+1,0}\right)$. In this case, there are not solutions in region B and since the flux increases with respect to μ in region D we set, as for the Riemann Solver **SC2**,

$$\begin{aligned}\hat{\rho}_{k+1} &= \rho^M\left(\mu_{k+1,0}\right),\\ \hat{\mu}_k &= \tilde{\mu}.\end{aligned}$$

Case β): The flux is constant with respect to μ along the line in the region A and is an increasing function along the line in region C, then we set

$$\begin{aligned}\hat{\rho}_{k+1} &= \bar{\mu}_k,\\ \hat{\mu}_k &= \begin{cases}\bar{\mu}_k, & \text{if } \mu_{k,0} < \bar{\mu}_k,\\ \mu_{k,0}, & \text{if } \mu_{k,0} \geq \bar{\mu}_k.\end{cases}\end{aligned}$$

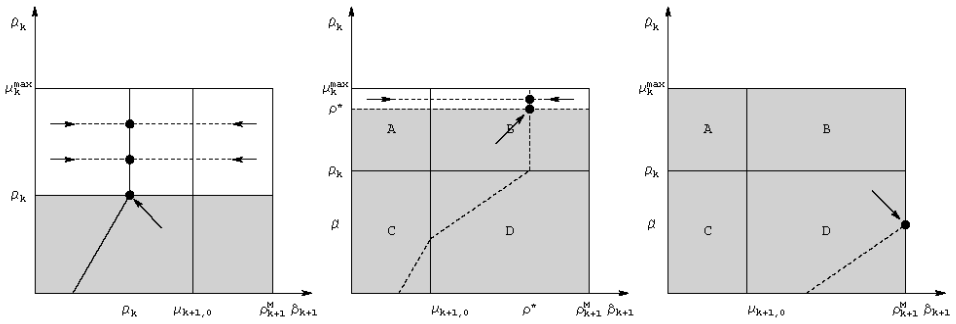

Figure 2.14: Case β) and α) (namely α_1) and α_2)) for the Riemann Solver **SC3**.

■

The obtained Riemann Solver is shown in Fig.2.14: all points of the white region are mapped horizontally and all points of the dark regions are mapped to the point indicated by the arrows.

Analogously to the case of rule **SC1**, we can give conditions for solvability of Riemann Problems, more precisely:

Lemma 66 *Consider a supply chain on which the initial datum verifies* $\mu_{k,0} = \mu_k^{\max}$*, i.e. the production rate is at its maximum. A sufficient condition for the solvability of all Riemann Problems, according to rule* ***SC2*** *or* ***SC3****, on the supply chain at every time is*

$$\rho_{k+2}^{\max} \geq \rho_k^{\max}, \ \forall k.$$

The case of a supply chain networks

Now, two different Riemann Solvers at junction are defined according to the routing algorithms **RA1** and **RA2**. For both these algorithms, the flux of goods can be maximized considering the two additional rules **SC2** and **SC3**.

In order to define Riemann problems according to **RA1** and **RA2** let us introduce the notation:

$$f_k = f\left(\rho_k, \mu_k\right).$$

The maximum flux obtainable by a wave solution on each production sub-chain:

$$f_k^{\max} = \begin{cases} \bar{\mu}_k, & k = 1, ..., n, \\ \mu_{k,0} + \varepsilon \left(\rho^M \left(\mu_{k,0} \right) - \mu_{k,0} \right), & k = n+1, ..., n+m. \end{cases}$$

Since $\hat{f}_i \in \left[f_i^{\min}, f_i^{\max} = \bar{\mu}_i \right]$, $i = 1, ..., n$ and $\hat{f}_j \in \left[0, f_j^{\max} = \mu_{j,0} + \varepsilon \left(\rho^M \left(\mu_{j,0} \right) - \mu_{j,0} \right) \right]$, $j = n+1, ..., n+m$ it follows that if

$$\sum_{i=1}^{n} f_i^{\max} > \sum_{j=n+1}^{n+m} f_j^{\max}$$

the Riemann Problem does not admit solution. For the solvability of the supply network the following conditions hold:

Lemma 67 *A necessary and sufficient condition for the solvability of the Riemann Problem is that*

$$\sum_{i=1}^{n} f_i^{\max} \leq \sum_{j=n+1}^{n+m} \mu_{j,0} + \varepsilon \left(\rho^M \left(\mu_{j,0} \right) - \mu_{j,0} \right).$$

Lemma 68 *A sufficient condition for the solvability of the Riemann Problems, independent of the initial data, is the following*

$$\sum_{i=1}^{n} \rho_i^{\max} \leq \sum_{j=n+1}^{n+m} \mu_j^{\max}.$$

Proof. Since $\hat{f}_i \in \left[f_i^{\min}, f_i^{\max} \right]$, $i = 1, ..., n$ and $\hat{f}_j \in \left[0, f_j^{\max} \right]$, $j = n+1, ..., n+m$, the worst case to fulfill the condition of Lemma XX(prec) happens when $f_i^{\min}$ assumes the greatest value and $f_j^{\max}$ the lowest one

$$\sum_{i=1}^{n} \varepsilon \rho_i^{\max} \leq \varepsilon \sum_{j=n+1}^{n+m} \mu_j^{\max}.$$

■

Now, considering a single junction P, we analyze two cases:

1. P with $n-1$ incoming arcs and 1 outgoing arc (i.e. $(n-1) \times 1$ node);
2. P with 1 incoming arc and $m-1$ outgoing arcs (i.e. $1 \times (m-1)$ node).

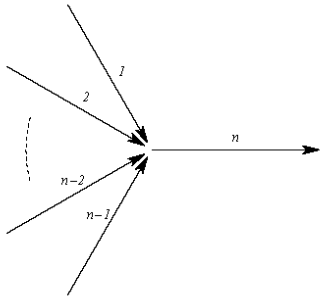

Figure 2.15: One outgoing sub-chain.

One outgoing sub-chain

In this case, since there is only one outgoing sub-chain, the algorithms **RA1** and **RA2** coincide.

Fixing a Riemann initial datum $(\rho_0, \mu_0) = \big(\rho_{1,0}, \mu_{1,0}, ..., \rho_{n-1,0}, \mu_{n-1,0}, \rho_{n,0}, \mu_{n,0}\big)$, let us denote the solution of the Riemann Problem with $(\hat{\rho}, \hat{\mu}) = \big(\hat{\rho}_1, \hat{\mu}_1, ..., \hat{\rho}_{n-1}, \hat{\mu}_{n-1}, \hat{\rho}_n, \hat{\mu}_n\big)$ and introduce the priority parameters $(q_1, q_2, ..., q_{n-1})$ which determine a *level of priority* at the junction sub-chains (see Fig.2.15).

Let us define

$$\begin{aligned} \Gamma_{inc} &= \sum_{i=1}^{n-1} f_i^{\max}, \\ \Gamma_{out} &= f_n^{\max}, \end{aligned}$$

and $\Gamma = \min\{\Gamma_{inc}, \Gamma_{out}\}$.

For simplicity, we analyze a junction with $n = 3$, so we need only one priority parameter $q \in]0, 1[$. Think, for example, of a filling station for soda cans. The sub-chain 3 fills the cans, whereas sub-chains 1 and 2 produce plastic and aluminium cans, respectively.

First, we compute $\hat{f}_i$ $i = 1, 2, 3$ and then $\hat{\rho}_i$ and $\hat{\mu}_i$, $i = 1, 2, 3$.

We have to distinguish two cases:

Case 1): $\Gamma = \Gamma_{inc}$.

Case 2): $\Gamma < \Gamma_{inc}$.

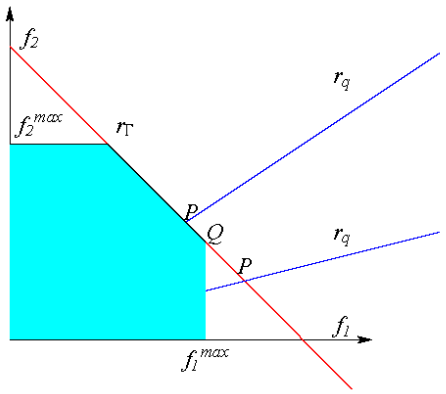

Figure 2.16: P belongs to Ω and P is outside Ω

In the first case we set $\hat{f}_i = f_i^{\max}$, $i = 1, 2$.

Instead, in the second case we have to use the priority parameter q. Since not all objects can enters the junction, letting C be the amount of objects that can go through, then qC and $(1-q)\,C$ are the objects coming respectively from first and second sub-chain.

Considering the space (f_1, f_2), we define the following line:

$$\begin{aligned} r_q &: \quad f_2 = \frac{1-q}{q} f_1, \\ r_\Gamma &: \quad f_1 + f_2 = \Gamma. \end{aligned}$$

Define P to be the point of intersection of the lines r_q and r_Γ. Recall that the final fluxes should belong to the region (as in Fig.2.16):

$$\Omega = \{(f_1, f_2) : 0 \leq f_i \leq f_i^{\max}, i = 1, 2\}.$$

We distinguish two cases:

a) P belongs to Ω,

b) P is outside Ω.

In the first case we set $\left(\hat{f}_1, \hat{f}_2\right) = P$, while in the second case we set $\left(\hat{f}_1, \hat{f}_2\right) = Q$, with $Q = proj_{\Omega \cap r_\Gamma}(P)$ where $proj$ is the usual projection on a convex set (Fig.2.16). Notice that $\hat{f}_3 = \Gamma$.

Remark 69 *The same reasoning can be done also in the case of $n-1$ incoming sub-chains. In $\mathbb{R}^{n-1}$ we get the line $r_q = tv_q$, $t \in \mathbb{R}$, with $v_q \in \Delta_{n-2}$ where*

$$\Delta_{n-2} = \left\{ (f_1, ..., f_{n-1}) : f_i \geq 0, i = 1, ..., n-1, \sum_{i=1}^{n-1} f_i = 1 \right\}$$

is the $(n-2)$ dimensional simplex and

$$H_\Gamma = \left\{ (f_1, ..., f_{n-1}) : \sum_{i=1}^{n-1} f_i = 1 \right\}$$

is a hyperplane. Since $v_q \in \Delta_{n-2}$, there exists an unique point $P = r_q \cap H_\Gamma$. If $P \in \Omega$, then we set $\left(\hat{f}_1, ..., \hat{f}_{n-1}\right) = P$. If $P \notin \Omega$, then we set $\left(\hat{f}_1, ..., \hat{f}_{n-1}\right) = Q = proj_{\Omega \cap r_\Gamma}(P)$, the projection over the subset $\Omega \cap H_\Gamma$. Observe that the projection is unique since $\Omega \cap H_\Gamma$ is a closed convex subset of H_Γ.

In order to compute $\hat{\rho}_i$ and $\hat{\mu}_i$, $i = 1, 2, 3$, on the incoming sub-chains we have to distinguish two subcases:

Case 2.1): $\hat{f}_i = f_i^{\max}$. We set according to rules $SC2$ and $SC3$,

$$\begin{array}{lll} SC2: & \begin{array}{l} \hat{\rho}_i = \bar{\mu}_i, \\ \hat{\mu}_i = \bar{\mu}_i, \end{array} & i = 1, 2, \\ SC3: & \begin{array}{l} \hat{\rho}_i = \bar{\mu}_i, \\ \hat{\mu}_i = \max\left\{\bar{\mu}_i, \mu_{i,0}\right\}, \end{array} & i = 1, 2. \end{array}$$

In this case $\hat{\rho}_i = \varphi(\hat{\mu}_i) = \bar{\mu}_i$, $i = 1, 2$.

Case 2.2): $\hat{f}_i < f_i^{\max}$. There exists an unique $\hat{\mu}_i$ such that $\hat{\mu}_i + \varepsilon(\varphi(\hat{\mu}_i) - \hat{\mu}_i) = \hat{f}_i$. According to (2.34), we set $\hat{\rho}_i = \varphi(\hat{\mu}_i)$, $i = 1, 2$.

On the outgoing sub-chain we have:

$$\hat{\mu}_3 = \mu_{3,0},$$

while $\hat{\rho}_3$ is the unique value such that $f_\varepsilon\left(\mu_{3,0}, \hat{\rho}_3\right) = \hat{f}_3$.

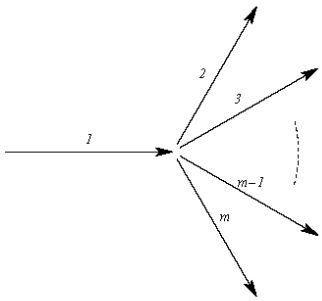

Figure 2.17: One incoming sub-chain

One incoming sub-chain

Fixing a node P with 1 incoming arc and $m-1$ outgoing ones (see Fig.2.17), and a Riemann initial datum $(\rho_0, \mu_0) = \big(\rho_{1,0}, \mu_{1,0}, \rho_{2,0}, \mu_{2,0}, ..., \rho_{m,0}, \mu_{m,0}\big)$, let us denote the solution of the Riemann Problem $(\hat{\rho}, \hat{\mu}) = (\hat{\rho}_1, \hat{\mu}_1, \hat{\rho}_2, \hat{\mu}_2, ..., \hat{\rho}_m, \hat{\mu}_m)$. For this configuration, we need to define the distribution of goods from the incoming arc. Then, we introduce the flux distribution parameters α_j, $j = 2, ..., m$, where

$$0 < \alpha_j < 1, \ \sum_{j=2}^{m} \alpha_j = 1.$$

The coefficient α_j represents the percentage of objects addressed from the arc 1 to the sub-chain j. The flux on the arc j is thus given by

$$f_j = \alpha_j f_1, \ j = 2, ..., m,$$

where f_1 is the incoming flux on the arc 1.

Let us define

$$\begin{aligned} \Gamma_{inc} &= f_1^{\max}, \\ \Gamma_{out} &= \sum_{j=2}^{m} f_j^{\max}, \end{aligned}$$

and $\Gamma = \min\{\Gamma_{inc}, \Gamma_{out}\}$.

We have to determine $\hat{\mu}_k$ and $\hat{\rho}_k$, $k = 1, ..., m$, for both algorithms **RA1** and **RA2**.

Riemann solver according to RA1 Analyze the general case with m sub-chains. For example, we refer to the filling station for orange and lemon fruit juice bottles as shown in Fig.2.4-a, where the dynamics at node v^1 is solved using the algorithm we are going to describe.

Since $f_j \leq f_j^{\max}$ it follows that

$$f_1 \leq \frac{f_j^{\max}}{\alpha_j},\ j = 2, ..., m.$$

We set

$$\begin{aligned} &\hat{f}_1 = \min\left\{f_1^{\max}, \tfrac{f_j^{\max}}{\alpha_j}\right\}, \\ &\hat{f}_j = \alpha_j \hat{f}_1, \end{aligned} \qquad j = 2, ..., m.$$

On the incoming sub-chain we have to distinguish two subcases:

Case 1): $\hat{f}_1 = f_1^{\max}$. According to rule **SC2** and **SC3**, respectively, we set:

$$\begin{aligned} SC2: \quad &\hat{\rho}_1 = \bar{\mu}_1, \\ &\hat{\mu}_1 = \bar{\mu}_1, \\ SC3: \quad &\hat{\rho}_1 = \bar{\mu}_1, \\ &\hat{\mu}_1 = \max\left\{\bar{\mu}_1, \mu_{1,0}\right\}. \end{aligned}$$

Case 2): $\hat{f}_1 < f_1^{\max}$. In this case there exists an unique $\hat{\mu}_1$ such that $\hat{\mu}_1 + \varepsilon\left(\varphi\left(\hat{\mu}_1\right) - \hat{\mu}_1\right) = \hat{f}_1$. According to (2.34), we set $\hat{\rho}_1 = \varphi\left(\hat{\mu}_1\right)$.

On the outgoing sub-chain we have:

$$\hat{\mu}_j = \mu_{j,0},\ j = 2, 3, .., m$$

while $\hat{\rho}_i$ is the unique value such that $f_\varepsilon\left(\mu_{j,0}, \hat{\rho}_j\right) = \hat{f}_j$, $j = 2, 3, .., m$.

Riemann solver according to RA2 For simplicity let us consider a node with $m = 3$ and in this case we need only one distribution parameter $\alpha \in]0, 1[$ (referred to the cups production as shown in Fig.2.4-b). The dynamics at the node is solved according to the algorithm **RA2**. Compute $\hat{f}_k$, $k = 1, 2, 3$.

We have to distinguish two cases:

Case 1): $\Gamma = \Gamma_{out}$.

Case 2): $\Gamma < \Gamma_{out}$.

In the first case we set $\hat{f}_j = f_j^{\max}$, $j = 2, 3$, while in the second one we use the priority parameter α.

Then, if we indicate with C the amount of objects that can go through the junction, let αC and $(1-\alpha)\, C$ be the objects that respectively coming from the first and second sub-chain. Considering the space (f_2, f_3), define the following lines:

$$r_\alpha : f_3 = \tfrac{1-\alpha}{\alpha} f_2,$$
$$r_\Gamma : f_2 + f_3 = \Gamma.$$

Define P to be the point of intersection of the lines r_α and r_Γ. Recall that the final fluxes should belong to the region:

$$\Omega = \left\{ (f_2, f_3) : 0 \leq f_j \leq f_j^{\max},\ j = 2, 3 \right\}.$$

We distinguish two cases:

a) P belongs to Ω,

b) P is outside Ω.

In the first case we set $\left(\hat{f}_2, \hat{f}_3\right) = P$, while in the second case we set $\left(\hat{f}_2, \hat{f}_3\right) = Q$, with $Q = proj_{\Omega \cap r_\Gamma}(P)$ where $proj$ is the usual projection on a convex set. Notice that $\hat{f}_1 = \Gamma$.

Again, we can extend the reasoning to the case of $m-1$ outgoing sub-chains as for the incoming ones defining the hyperplane

$$H_\Gamma = \left\{ (f_2, ..., f_m) : \sum_{j=2}^{m} f_j = \Gamma \right\}$$

and choosing a vector $v_\alpha \in \Delta_{m-2}$. Moreover, we compute $\hat{\rho}_k$ and $\hat{\mu}_k$ in the same way described for the Riemann Solver **RA1**.

Remark 70 *In alternative, assuming that a traffic distribution matrix A is assigned, then we can compute $\hat{f}_1$ and choose the vector $v_\alpha \in \Delta_{m-2}$ by*

$$v_\alpha = \Delta_{m-2} \cap \left\{ tA\left(\hat{f}_1\right) : t \in \mathbb{R} \right\}.$$

Remark 71 *The classical Kruzkov entropy inequalities at nodes [6] read*

$$\sum_{inc} sgn\left(\rho - k\right)\left(f\left(\rho\right) - f\left(k\right)\right) \geq \sum_{out} sgn\left(\rho - k\right)\left(f\left(\rho\right) - f\left(k\right)\right)$$

over the sums are respectively over incoming and outgoing sub-chains and k is arbitrary. The fluxes are always monotone with respect to ρ, while the precise values taken by fluxes and densities on the sub-chains may be different. Thus we can not expect the inequality to hold in general.

2.3.3 Waves production

In this section let us discuss the waves production on an incoming and an outgoing sub-chain with initial datum $\left(\rho_{i,0}, \mu_{i,0}\right)$ and $\left(\rho_{j,0}, \mu_{j,0}\right)$ respectively.

Since the load dynamic is described by a conservation law in ρ and an evolution equation in μ, we have ρ-waves and μ-waves of two types:

- shocks waves which are discontinuities in ρ and/or μ traveling at a constant speed,
- contact discontinuities, which separate two constant states with the same speed but different values.

The last one are contact discontinuities in ρ and μ with speed $\lambda = -1$ connecting the states $\rho_{i,0}$ and $\hat{\rho}_i$ and $\mu_{i,0}$ and $\hat{\mu}_i$.

On the outgoing sub-chain only ρ-waves of the second family can be produced. Then we must consider two cases:

Case a): $\rho_{j,0} \leq \mu_{j,0}$.

Case b): $\rho_{j,0} > \mu_{j,0}$.

For the case a), two subcases have to be distinguished:

Case a.1): If $\hat{\rho}_j \in \left[0, \mu_{j,0}\right]$ then the solution of the Riemann Problem consists of a contact discontinuity connecting $\hat{\rho}_j$ and $\rho_{i,0}$ with speed 1 (for $t = 1$);

Case a.2): If $\hat{\rho}_j \in \left]\mu_{j,0}, \mu_j^{\max}\right]$ then the solution of the Riemann Problem consists of two shocks: one connecting $\hat{\rho}_j$ and $\mu_{j,0}$ with speed ε (for $t = 1$) followed by another one connecting $\mu_{j,0}$ and $\rho_{j,0}$ traveling with speed 1 (for $t = 1$) (see Fig.2.18).In the case b) we have to consider two subcases:

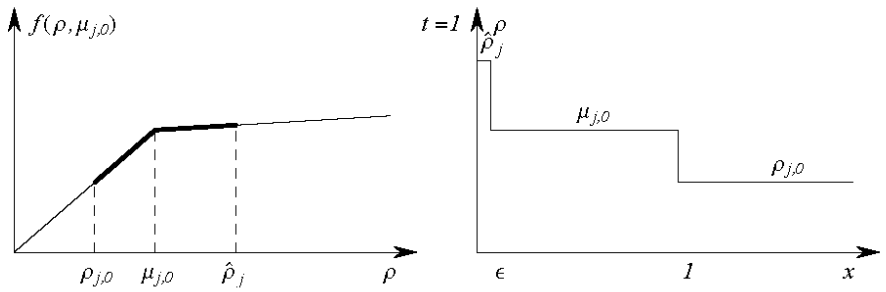

Figure 2.18: Waves production on an outgoing sub-chain: case a.2).

Case b.1): If $\hat{\rho}_j \in \left[0, \mu_{j,0}\right]$ then the solution of the Riemann Problem consists of a shock wave connecting the states $\hat{\rho}_j$ and $\rho_{j,0}$ with speed (for $t = 1$) equal to slope λ of the line connecting the two states:

$$\lambda = \frac{\mu_{j,0} + \varepsilon\left(\rho_{j,0} - \mu_{j,0}\right) - \hat{\rho}_j}{\rho_{j,0} - \hat{\rho}_j}.$$

Case b.2): If $\hat{\rho}_j \in \left]\mu_{j,0}, \mu_j^{\max}\right]$ then the solution of the Riemann Problem consists of a contact discontinuity connecting $\hat{\rho}_j$ and $\rho_{j,0}$ with speed ε (for $t = 1$).

2.4 Equilibrium analysis

Fixing a node P and a Riemann initial datum (ρ_0, μ_0), now we introduce some notions about the equilibria at nodes.

Definition 72 *Define* $(\hat{\rho}, \hat{\mu}) = RS\left((\rho_0, \mu_0)\right)$. *The datum* (ρ_0, μ_0) *is an equilibrium if*

$$(\hat{\rho}, \hat{\mu}) = RS\left((\rho_0, \mu_0)\right) = (\rho_0, \mu_0)\,.$$

Distinguishing two types of nodes, $(n-1) \times 1$ and $1 \times (m-1)$, and equilibria with active and not active constraints for the maximization problem, we consider generic equilibria for the Riemann Problem at a junction.

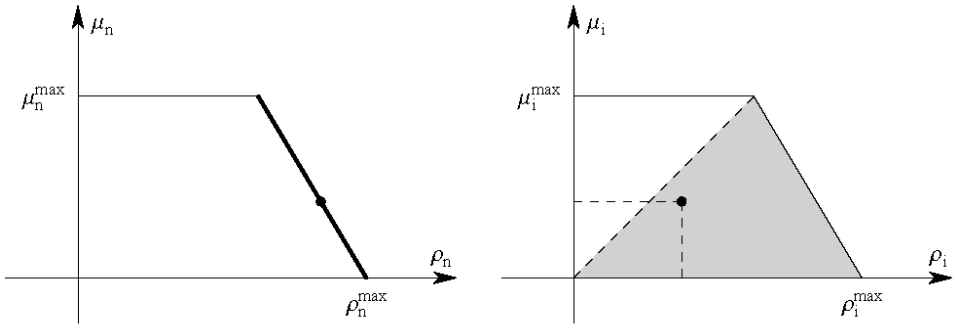

Figure 2.19: The outgoing sub-chain is an active constraint and the incoming ones are not active constraints.

2.4.1 A node with one outgoing sub-chain

If the n-th sub-chain is an active constraint then we have:

$$\rho_n = \rho^M(\mu_n),$$

otherwise, if it is not an active constraint, we have:

$$\rho_n < \rho^M(\mu_n).$$

For the incoming sub-chains I_i, $i = 1, ..., n-1$, it will be: if the i-th sub-chain is an active constraint then

$$\begin{array}{ll} SC2: & \mu_i = \rho_i \\ SC3: & \mu_i \geq \rho_i \end{array}, \ i = 1, ..., n-1,$$

otherwise

$$\rho_i \geq \mu_i.$$

In Fig.2.19 and Fig.2.20 the equilibria are shown. In the latter the equilibria for the algorithm **SC2** are depicted in bold, while for **SC3** in bold and grey.

The first type of equilibria (Fig.2.19) represents the situation in which the outgoing sub-chain exhibit the maximal production effort, while the incoming ones adjust accordingly their production flows.

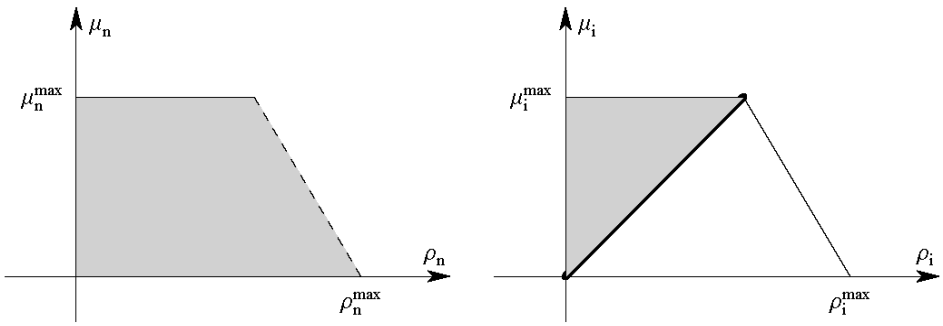

Figure 2.20: The incoming sub-chains are active constraints and the outgoing one is not an active constraint.

The second type (Fig.2.20) shows the situation in which the incoming sub-chains have a low level of part densities and, consequently, the outgoing sub-chain is not used at maximal level. In this case, then, since the whole plant is not used suitably, a re-building is in order, in fact it can be considered either the incoming sub-chains should be powered such that the production rate is improved or the outgoing ones should be restricted such that the production costs would be lower.

2.4.2 A node with one incoming sub-chain

The equilibria for the two algorithms **RA1** and **RA2** coincide. In particular, if the incoming sub-chain is an active constraint then

$$\begin{aligned} SC2: &\quad \rho_1 = \mu_1, \\ SC3: &\quad \rho_1 \leq \mu_1, \end{aligned}$$

otherwise $\rho_1 \geq \mu_1$.

Considering the outgoing sub-chains I_j, $j = 2, ..., m$, if I_j is an active constraint then $\rho_j = \rho^M\left(\mu_j\right)$ for both **SC2** and **SC3** algorithms, otherwise $\rho_j < \rho^M\left(\mu_j\right)$.

For both algorithms **RA1** and **RA2**, the case of incoming sub-chain as active constraint should happen only with $\rho_1 = \mu_1$, in such a way that the goods fill up appropriately the sub-chain. Otherwise the incoming sub-chain should be powered. For the outgoing sub-chains as active constraints, the situation is different. In fact, the latter represents a projecting error for the algorithm **RA1**, while it may well

happen for **RA2**.

2.4.3 Bullwhip effect

The Bullwhip effect is a well known oscillation phenomenon in supply chain theory, see [11]. Since this effect consists in oscillations moving backwards, the most interesting case consists of nodes with $n-1$ incoming sub-chains and one outgoing sub-chain.

Then, to study the Bullwhip effect, we have to compute the oscillations on incoming sub-chains produced by the interaction with the node of a wave from the outgoing one. Since the wave must have negative speed, it is a first family wave. Fixing the notation, we denote with $-$ and $+$ the values before and after the interaction, and with Δ the jump in the values from the left to the right along waves traveling on sub-chains. Let (ρ^-, μ^-) be an equilibrium configuration at the node and $\left(\left(\rho_n^-, \mu_n^-\right), \left(\tilde{\rho}_n, \tilde{\mu}_n\right)\right)$ the wave coming to the same node.

The effect of the interaction of the wave is the production of $n-1$ waves on the incoming sub-chains.

The oscillation amplitude in the production rate before the interaction is given by:

$$\Delta\mu^- = \tilde{\mu}_n - \mu_n^-.$$

The maximum flux on the outgoing sub-chain as function of μ is the following

$$f_n^{\max}(\mu) = \mu\frac{1-\varepsilon}{1+\varepsilon} + \varepsilon\rho_n^{\max},$$

thus it is an increasing function. The oscillation of the flux after the interaction is

$$\Delta f^+ = \frac{1-\varepsilon}{1+\varepsilon}\Delta\mu^-.$$

Now, assuming first that the incoming sub-chains are not active constraints, for both algorithms **SC2** and **SC3**, we have $\rho_i^- \geq \mu_i^-$, $i = 1, ..., n-1$. Then the first family curve passing through $\left(\rho_i^-, \mu_i^-\right)$, belonging to the region $\rho \geq \mu$, is given by

$$\rho = \rho_i^- + \left(\mu - \mu_i^-\right)\left(-\frac{1-\varepsilon}{1+\varepsilon}\right).$$

From which, for small oscillations we obtain

$$\Delta\rho^+ = -\frac{1-\varepsilon}{1+\varepsilon}\Delta\mu^+.$$

If the oscillation is not small the same relation holds with an inequality sign. Observe that

$$\Delta f^+ = \Delta\mu^+(1-\varepsilon) + \varepsilon\Delta\rho^+ = \frac{1-\varepsilon}{1+\varepsilon}\Delta\mu^+,$$

from which

$$\Delta\mu^+ = \frac{1+\varepsilon}{1-\varepsilon}\Delta f^+,$$

and then

$$\Delta\mu^+ = \Delta\mu^-.$$

Assume now that the incoming sub-chains are active constraints, which means that $\mu_i^- = \rho_i^-$ and $\mu_i^- = \rho_i^-$ respectively for **SC2** and **SC3** algorithm. Along the curve of the first family belonging to the region $\rho \leq \mu$ we have $\Delta f = 0$, i.e. a dumping effect is possible, while in the region $\rho \geq \mu$ we have

$$\Delta f = \frac{1-\varepsilon}{1+\varepsilon}\Delta\mu.$$

Considering the **SC2** algorithm, if the first family wave from the outgoing road increases the flux, then it is reflected as a second family wave. In the opposite case, we get the same estimates as above.

Considering the **SC3** algorithm, if the first family wave from the outgoing road increases the flux, then it is again reflected as a second family wave. In the opposite case, we get:

$$\Delta\mu^+ = \Delta\mu^- + \left(\mu_i^- - \rho_i^-\right)$$

with an increase in the production rate oscillation.

In conclusion we get the following:

Proposition 73 *The algorithm **SC3** may produce the Bullwhip effect. On the contrary, the algorithm **SC2** conserves oscillations or produce a dumping effect, thus not permitting the Bullwhip effect.*

Chapter 3

Numerical Schemes

In this chapter we present the numerical schemes for the Göttlich-Herty-Klar model and the continuum-discrete model for supply chains.

3.1 Numerical methods for Göttlich-Herty-Klar model

Considering the system (2.22a)-(2.22e), we want to obtain numerical results for parts dynamics inside a supply chain finding, for each arc j, a suitable approximation for the density $\rho_j(x,t)$ and the queue $q_j(t)$, with $0 \leq x \leq L_j$ and $t \in [0,T]$. In particular, we use the upwind scheme for densities (i.e referred to *PDE* of the model) and the explicit Euler scheme for queues (i.e referred to *ODE of the model*).

For each arc $j \in J$, define e numerical grid in $[0,L_j] \times [0,T]$ using the following notations:

- $\Delta x_j = \frac{L_j}{N_j}$ is the space grid size, where N_j is the number of segments into which we divide L_j (the length of j-th supplier);
- $\Delta t_j = \frac{T}{\eta_j}$ is the time grid size, where η_j is the number of segments into which we divide the interval $[0,T]$;
- $(x_i, t^n) = (i\Delta x_j, n\Delta t_j)$, $i = 0, ..., N_j$, $n = 0, ..., \eta_j$ are the grid points.

For the density function ρ_j defined on the grid, we set ${}^j\rho_i^n$ as the approximation of $\rho_j(x_i,t^n)$,with $j \in J$, $i = 0, ..., N_j$, $n = 0, ..., \eta_j$. For the queue q_j, q_j^n is the approximation of $q_j(t^n)$.

Without loss of generality, we can assume that for each arc j, $\Delta x_j = \Delta x$ and $\Delta t_j = \Delta t$, with Δx and Δt fixed.

A numerical scheme to solve conservation laws at each arc is the upwind method:

$$ {}^j\rho_i^{n+1} = {}^j\rho_i^n - \frac{\Delta t}{\Delta x}\frac{L_j}{T_j}\left({}^j\rho_i^n - {}^j\rho_{i-1}^n\right),\ j \in J,\ i = 0, ..., N_j,\ n = 0, ..., \eta_j. \tag{3.1} $$

The evolution of queues is described by the explicit Euler method:

$$ q_j^{n+1} = q_j^n + \Delta t\left(f_{j-1,out}^n - f_{j,inc}^n\right),\ j \in J - \{1\},\ n = 0, ..., \eta_j, \tag{3.2} $$

where $f_{j-1,out}^n$ and $f_{j,inc}^n$ are the approximation of $f_{j-1}\left(\rho_{j-1}\left(b_{j-1}, t^n\right)\right)$ and $f_j\left(\rho_j\left(a_j, t^n\right)\right)$, respectively, both depending on values of densities computed by (3.1).

In order to consider boundary data, we refer to equation (3.1) for $i = 0$. We proceed by inserting a ghost cell and defining

$$ {}^j\rho_0^{n+1} = {}^j\rho_0^n - \frac{\Delta t}{\Delta x}\frac{L_j}{T_j}\left({}^j\rho_0^n - {}^ju_0^n\right),\ j \in J,\ n = 0, ..., \eta_j, $$

where ${}^ju_0^n$ takes the place of ${}^j\rho_{-1}^n$. Two different cases can occur:

1. if the arc j is the incoming one to the supply chain (namely $a_j = -\infty$), and inflow profile $\varphi(t)$ is assigned, and we set ${}^ju_0^n = \varphi(t^n)$.
2. if the arc j is inside the supply chain, or $a_j \neq -\infty$, we set ${}^ju_0^n = \frac{T_j}{L_j} f_j^n$, where f_j^n obeys equation (2.22e).

3.1.1 Correction of numerical fluxes in case of negative queues

The following lemma holds:

Lemma 74 *Consider a supply chain evolution $\rho_j(x_i, t)$, $q_j(t)$, i.e. a solution of (2.22a)-(2.22e). Then for every $j \in J$, $t \geq 0$ and x, it holds $\rho_j(x_i, t) \geq 0$, $q_j(t) \geq 0$.*

Since the ODE numerical scheme does not necessarily maintain the positivity proprieties of the Lemma 1, we have to modify the Euler scheme.

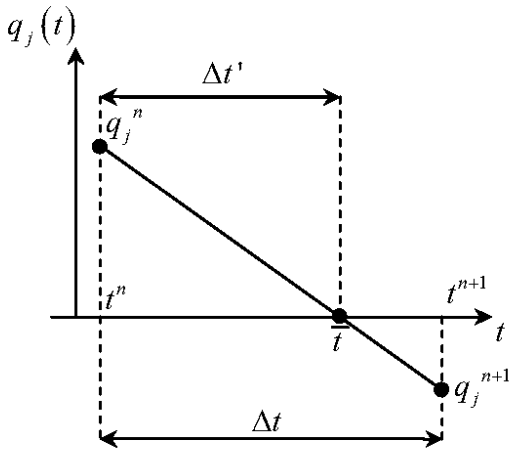

Figure 3.1: Negative queue buffer occupancy at t^{n+1}.

Consider the arc j of a supply chain and suppose that, in the time interval $\left[t^n, t^{n+1}\right[$, $\rho_j(x_i, t)$ is approximated by the constant value ${}^j\rho_i^n$. Then, from (3.2), $q_j(t)$ has a linear shape (see Fig.3.1), namely

$$q_j(t) = \frac{q_j^{n+1} - q_j^n}{\Delta t} t + \frac{q_j^n t^{n+1} - q_j^{n+1} t^n}{\Delta t},\ t \in \left[t^n, t^{n+1}\right[. \tag{3.3}$$

Assume that $q_j^n > 0$ and $q_j^{n+1} < 0$. Then, the queue vanishes at an instant of time $\bar{t} > t^n$, which is computed by (3.3):

$$\bar{t} = t^n + \Delta t',\ \Delta t' = \frac{q_j^n}{q_j^n - q_j^{n-1}} \Delta t = \frac{q_j^n}{\mu_j - f_{j-1,out}^n}.$$

Forcing to zero the behaviour of $q_j(t)$, $t \in \left[\bar{t}, t^{n+1}\right]$, the following numerical correction for the entering flux $f_{j,inc}^n$ is needed:

$$f_{j,inc}^n = \frac{1}{\Delta t}\left[\Delta t' \mu_j - \left(\Delta t - \Delta t'\right) f_{j-1,out}^n\right] \tag{3.4}$$

This correction on the boundary incoming data for the arc j influences the approximation of $\rho_j(x, t)$, with consequent effects on dynamics for following arcs and queues.

3.1.2 Different space and time grid meshes

Considering the general case in which L_j have not rational ratios, we have to consider the possibility of choosing different space and/or time grid meshes.

Different space meshes for different suppliers

For each supplier $j \in J$, the numerical grid in $[0, L_j] \times [0, T]$ is defined choosing a fixed grid mesh Δt, then different space grid meshes are necessary and we set $\Delta x_j = v_j \Delta t$, where $v_j := \frac{L_j}{T_j}$ is the processing velocity. In this case, grid points are $(x_i, t^n)_j = (i\Delta x_j, n\Delta t)$, $i = 0, ...N_j$, $n = 0, ..., \eta_j$. Then the upwind scheme for the parts density of the arc j now reads:

$$ {}^j\rho_i^{n+1} = {}^j\rho_i^n - \frac{\Delta t}{\Delta x_j} v_j \left({}^j\rho_i^n - {}^j\rho_{i-1}^n \right), \ j \in J, \ i = 0, ..., N_j, \ n = 0, ..., \eta_j. \tag{3.5} $$

To respect CFL condition (see [23]) the time mesh satisfy:

$$ \Delta t \leq \min \left\{ v_j \Delta x_j : j \in J \right\}. \tag{3.6} $$

For queues we refer again to equation (3.2).

Different time meshes for different suppliers

Now, fix two consecutive arcs $j-1$ and j. Then two different numerical grids are defined, whose points are, respectively:

$$ (x_k, t^{n_{j-1}})_{j-1} = (k\Delta x, n_{j-1}\Delta t_{j-1}), \ k = 0, ..., N_{j-1}, \ n_{j-1} = 0, ..., \eta_{j-1}, $$

$$ \left({}^jx_k, t^n \right) = (k\Delta x, n_j \Delta t_j), \ k = 0, ..., N_j, \ n_j = 0, ..., \eta_j. $$

For the queue buffer occupancy the explicit Euler is given by:

$$ q_j^{n_{j-1}} = q_j^{n_j} + \Delta t_j \left(f_{j-1,out}^{n_j} - f_{j,inc}^{n_j} \right), \tag{3.7} $$

where

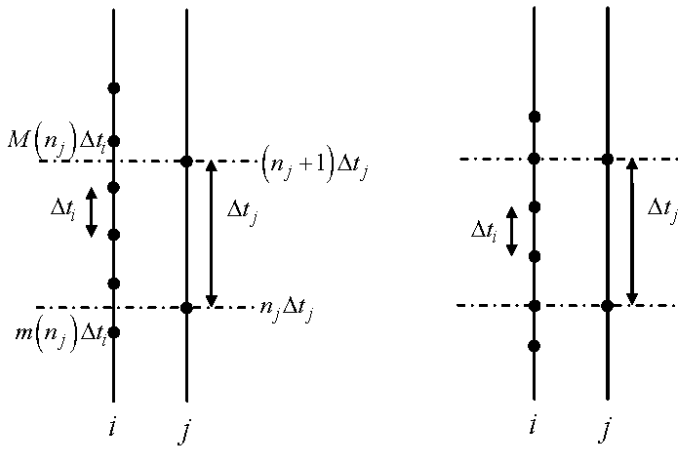

Figure 3.2: Case $\Delta t_{j-1} < \Delta t_j$. Left: not proportional case. Right: proportional case.

$$f_{j,inc}^{n_j} = \begin{cases} \min\left\{f_{j-1}\left({}^{j-1}\rho_{N_{j-1}}^{n}\right), \mu_j\right\}, & q_j^n(t) = 0, \\ \mu_j, & q_j^n(t) > 0, \end{cases} \tag{3.8}$$

while $f_{j-1,out}^{n_j}$ must be suitably defined. If $\Delta t_{j-1} < \Delta t_j$ (see Fig.3.2), we define $m(n_j)$ and $M(n_j)$ as:

$$m(n_j) = \sup\{m : m\Delta t_{j-1} \leq n_j \Delta t_j\},$$

$$M(n_j) = \inf\{M : M\Delta t_{j-1} \geq (n_j+1)\Delta t_j\},$$

and set

$$\begin{aligned} f_{j-1,out}^{n_j} \quad = \quad & \sum_{l=1}^{M(n_j)-m(n_j)-1} \Delta t_{j-1} f_{j-1}\left({}^{j-1}\rho_{N_{j-1}}^{m(n_j)+l}\right) + \\ & + \left[(m(n_j)+1)\Delta t_{j-1} - n_j \Delta t_j\right] f_{j-1}\left({}^{j-1}\rho_{N_{j-1}}^{m(n_j)}\right) + \\ & + \left[(n_j+1)\Delta t_j - (M(n_j)-1)\Delta t_{j-1}\right] f_{j-1}\left({}^{j-1}\rho_{N_{j-1}}^{M(n_j)-1}\right). \end{aligned}$$

Notice that, in the special case $\Delta t_j = \gamma \Delta t_{j-1}$, $\gamma \in \mathbb{N} - \{1\}$, we simply have:

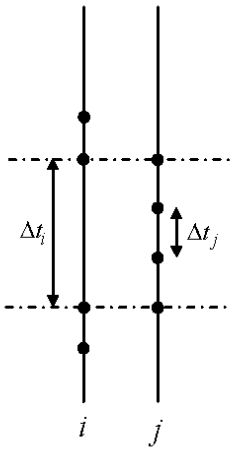

Figure 3.3: Case $\Delta t_{j-1} > \Delta t_j$.

$$f_{j-1,out}^{n_j} = \sum_{l=1}^{M(n_j)-m(n_j)-1} \Delta t_{j-1} f_{j-1}\left({}^{j-1}\rho_{N_{j-1}}^{m(n_j)+l}\right) = f_{j-1,out}^{n_j} =$$
$$= \sum_{l=1}^{\gamma} \Delta t_{j-1} f_{j-1}\left({}^{j-1}\rho_{N_{j-1}}^{\gamma n_j+l}\right).$$

If, on the contrary, $\Delta t_{j-1} > \Delta t_j$ (see Fig.3.3), we set

$$f_{j-1,out}^{n_j} = f_{j-1}^{\left|\frac{n_j \Delta t_j}{\Delta t_{j-1}}\right|},$$

where $|\cdot|$ indicates the floor function.

Finally, in this case, the approximation scheme for densities is the classical upwind method.

Fluxes corrections

In case of negative values of queues, flux corrections have to be considered also for the variants of numerical method seen before.

For the modified upwind scheme, fluxes corrections are the same as in the previous section.

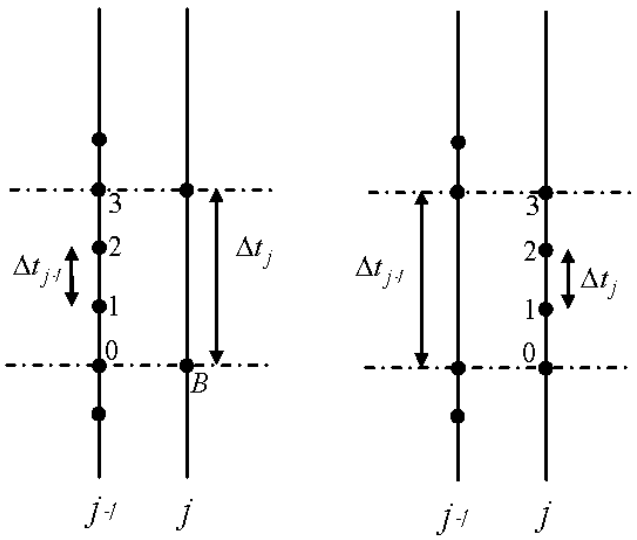

Figure 3.4: Different time meshes for fluxes corrections.

Now, for the modified Euler scheme for queue (3.7), we consider two consecutive arcs, $j-1$ and j, with approximation grids characterized by equal spatial meshes Δx and different temporal meshes Δt_{j-1} and Δt_j.

Assuming $q_j^{n_j} > 0$ and $q_j^{n_j+1} < 0$, if $\Delta t_{j-1} < \Delta t_j$ (see 3.4 left, for an example), more precisely $\Delta t_j = N\Delta t_{j-1}$, a possible correction for the flux entering the arc j is the following:

$$f_{j,inc}^B = \frac{\sum_{k=0}^{N-1} f_{j-1,out}^k}{N+1},$$

where f_{j-1}^k and f_j^B are, respectively, the approximations of $f_{j-1}\left(\rho_{j-1}\left(b_{j-2}, t^k\right)\right)$ and $f_j\left(\rho_j\left(a_j, t^B\right)\right)$. If $\Delta t_{j-1} > \Delta t_j$ (Fig.3.4 right), precisely $\Delta t_{j-1} = N\Delta t_j$, we indicate with $\bar{t}$ the instant such that $q_j\left(\bar{t}\right) = 0$.

Then if

$$t^{num} = \Delta t_j \delta, \quad \text{with } \delta = \left|\frac{\bar{t}}{\Delta t_j}\right|,$$

is the numerical approximation of $\bar{t}$, a suitable correction for the flux entering the arc j can be

$$f^k_{j,inc} = \begin{cases} \mu_j, & if\ q_j\left(t^k\right) > 0, \\ \frac{\mu_j(t^{num}=\Delta t_j\delta)+[(\delta+1)\Delta t_j - t^{num}]f_{j-1,out}}{\Delta t_j}, & otherwise, \end{cases} \quad \forall k = 0,..,N-1$$

3.1.3 Convergence

According to study the convergence of the previously presented numerical schemes, the main idea is to relate the solution to those produced by Wave Front Tracking (**WFT**) and control the norm of generalized tangent vectors as in [21].

Consider the Cauchy problem of type (2.22a)-(2.22e), with initial conditions $\rho_{j,0}$ in the space of bounded variation functions BV. For simplicity, we consider the case of equal processing velocity and equal space and time meshes for all suppliers; the general case is similar.

Fix an initial space mesh Δx_0 and define a sequence of approximate solutions ${}^{v,j}\rho^n_i$, generated sampling the initial datum $\rho_{j,0}$ on grids of mesh $\Delta x_v = 2^{-v}\Delta x_0$ and using the time mesh:

$$\Delta t_v = v\Delta x_v = v2^{-v}\Delta x_0, \tag{3.9}$$

where v is the common velocity to all suppliers. More precisely:

$${}^{v,j}\rho^0_i = \rho_{j,0}\left(\left(a_j + i2^{-v}\Delta x\right)+\right)$$

where $(\cdot+)$ indicates the limit from the right, which exists because of the assumption of BV initial data.

We can define a projection of the approximate solution over the space of piecewise constant functions by setting:

$$\pi_{PC}\left({}^{v,j}\rho^n\right) = \sum_{i=0}^{\frac{L_j}{2^{-v}\Delta x}-1} {}^{v,j}\rho^n\chi_{[a_j+i2^{-v}\Delta x, a_j+(i+1)2^{-v}\Delta x[}$$

where $\chi_{[a,b]}$ is the indicator function of the set $[a,b]$. Similarly we define the corresponding buffer occupancy approximations ${}^{v}q^n_j$. We will also consider the **WFT** solution ${}^{j}\rho^{WFT}_v$ starting from the initial datum:

$$\pi_{PC}\left({}^{v,j}\rho^0\right).$$

A **WFT** solution is given by:

- Solve the Riemann problems corresponding to discontinuities of $\pi_{PC}\left({}^{v,j}\rho_i^0\right)$, replacing rarefactions by a set of small non entropic shocks of size 2^{-v};
- Use the piecewise constant solution obtained piecing together the solutions to Riemann problems up to the first time of interaction of two shocks;
- Then solve a new Riemann problem created by interaction of waves and prolong the solution up to next interaction time, and so on.

In order to ensure the existence of **WFT** solutions and their convergence, it is enough to control the number of interactions, waves and the BV norm. In the scalar case, this is easily done since both number of waves and the BV norm are decreasing in time (for details [6]).

For queues we use the exact solutions to (2.22c) which are indicate by ${}^{v}q_j^{WFT}$. BV estimates for complete set of *ODE-PDE* model (2.22a)-(2.22e) are proved in [21].

We have:

Lemma 75 *Assume that all suppliers have the common velocity v, $\rho_{j,0}$ are BV functions, $\rho_{j,0}(x) \leq \mu_j$ for every x and (3.9) holds true. Then:*

$$\left|\left|\pi_{PC}\left({}^{v,j}\rho^n\right) -^{j} \rho_v^{WFT}(n\Delta t_v)\right|\right|_{L^1} + \sum_j \left|{}^{v}q_j^n -^{v} q_j^{WFT}(n\Delta t_v)\right| \leq C2^{-v}\Delta x_0 \sum_j TV\left(\rho_{j,0}\right)$$

where $C > 0$ and $TV(\cdot)$ indicates the total variation.

As in [21], we define generalized tangent vectors (v, ξ, η) to **WFT** solutions. As proved in the Lemma 2.7 of [21], the norms of tangent are decreasing along **WFT** solutions.

Now, we define the convergence error as:

$$\begin{aligned} E_v(n) &= \sum_j \sum_i 2^{-v}\Delta x_0 \left|{}^{v,j}\rho_i^n -^{v+1,j} \rho_i^n\right| + \sum_j \left|{}^{v}q_j^n -^{v+1} q_j^n\right| = \qquad (3.10) \\ &= \sum_j \left|\left|\pi_{PC}\left({}^{v,j}\rho_i^n\right) - \pi_{PC}\left({}^{v+1,j}\rho_i^n\right)\right|\right|_{L^1} + \sum_j \left|{}^{v}q_j^n -^{v+1} q_j^n\right|. \end{aligned}$$

Moreover, we have:

$$E_v(0) = \left|\left|{}^j\rho_v^{WFT}(0) -^j \rho_{v+1}^{WFT}(0)\right|\right|_{L^1} \leq 2^{-(v+1)}\Delta x_0 \sum_j TV\left(\rho_{j,0}\right). \tag{3.11}$$

We can notice that the initial datum $\pi_{PC}\left({}^{v+1,j}\rho_i^0\right)$ can be obtained from $\pi_{PC}\left({}^{v,j}\rho_i^0\right)$ by possible shifting waves with tangent vectors of the $2^{v+1}\Delta x$, in fact both functions are obtained sampling the same BV function on different subgrids.

Then, again by the Lemma 2.7 of [21], we can control the distance writing:

$$\left|\left|{}^j\rho_v^{WFT}(t) -^j \rho_{v+1}^{WFT}(t)\right|\right|_{L^1} + \sum_j \left|{}^v q_j^{WFT}(t) -^{v+1} q_j^{WFT}(t)\right| \leq \left|\left|{}^j\rho_v^{WFT}(0) -^j \rho_{v+1}^{WFT}(0)\right|\right|_{L^1}.$$

By the Lemma 75 and (3.11) we get:

$$\begin{aligned}
E_v(n) &= \left|\left|{}^j\rho_v^{WFT}(n\Delta t_v) -^j \rho_{v+1}^{WFT}(n\Delta t_v)\right|\right|_{L^1} + \sum_j \left|{}^v q_j^{WFT}(n\Delta t_v) -^{v+1} q_j^{WFT}(n\Delta t_v)\right| \\
&\quad + C\left(2^{-v} + 2^{-(v+1)}\right)\Delta x_0 \sum_j TV\left(\rho_{j,0}\right) \\
&\leq \left|\left|{}^j\rho_v^{WFT}(0) -^j \rho_{v+1}^{WFT}(0)\right|\right|_{L^1} + C\left(2^{-v} + 2^{-(v+1)}\right)\Delta x_0 \sum_j TV\left(\rho_{j,0}\right) \\
&\leq 2^{-(v+1)}\Delta x_0 \sum_j TV\left(\rho_{j,0}\right) + C\left(2^{-v} + 2^{-(v+1)}\right)\Delta x_0 \sum_j TV\left(\rho_{j,0}\right).
\end{aligned}$$

Finally we get the following:

Theorem 76 *Assume that all suppliers have the common velocity v, $\rho_{j,0}$ are BV functions, $\rho_{j,0}(x) \leq \mu_j$ for every x and (3.9) holds true. Then the convergence error $E_v(n)$ (defined in (3.10)) tends to zero uniformly in n with linear convergence rate in $\Delta x_v = 2^{-v}\Delta x_0$.*

3.2 Godunov scheme for 2×2 systems

In order to describe Godunov numerical method as applied to the system (2.30), we rewrite it as the 2×2 hyperbolic system (2.31).

The Godunov scheme is based on the construction of the Riemann problem for (2.31), $[U_L, U_R]$, which is the initial value problem for initial data given by a jump discontinuity

$$U(0,x) = \begin{cases} U_L, & x < 0, \\ U_R, & x > 0, \end{cases} \tag{3.12}$$

and it has a unique entropy solution

$$U(t,x) = U_R\left(\frac{x}{t}; U_L, U_R\right). \tag{3.13}$$

We discretize $[0,+\infty) \times \mathbb{R}$ by a time and spatial mesh length, respectively, Δt and Δx, and we let $t_n = n\Delta t$ and $x^j = j\Delta x$, so that $\left(t_n, x^j\right)$ denotes the mesh points of the approximate solution $v_\Delta(t,x) = v_n^j$. Starting by the approximation $v_n = \left(v_n^j\right)_{j\in\mathbb{Z}}$ of $U(t_n,\cdot)$, with v a column vector of $\mathbb{R}^2$, an approximation v_{n+1}^j, with $j \in \mathbb{Z}$, of $U(t_{n+1},\cdot)$ can be defined as follows:

- extension of the sequence v_n as a piecewise constant function $v_\Delta(t,\cdot)$:

$$v_\Delta(t,\cdot) = v_n^j, \quad x^{j-\frac{1}{2}} < x < x^{j+\frac{1}{2}}; \tag{3.14}$$

  solution of the Cauchy problem

$$\begin{cases} U_t + F(U)_x = 0, & x \in \mathbb{R},\ t > 0, \\ U(0,x) = v_\Delta(t_n,\cdot), \end{cases} \tag{3.15}$$

  in the cell $(t_n, t_{n+1}) \times \left(x^{j-1}, x^j\right)$;

- computation of the solution as the average value of the preceding solution in the interval $\left(x^{j-\frac{1}{2}}, x^{j+\frac{1}{2}}\right)$ obtained projecting $U(\Delta t,\cdot)$ onto the piecewise constant functions:

$$v_{n+1}^j = \frac{1}{\Delta x}\int_{x^{j-\frac{1}{2}}}^{x^{j+\frac{1}{2}}} U(\Delta t, x)\, dx. \tag{3.16}$$

To avoid the interaction of waves in two neighbouring cells before time Δt, we impose a CFL(*Courent-Friedrichs-Lewy*) condition as:

$$\frac{\Delta t}{\Delta x}\max\{|\lambda_0|, |\lambda_1|\} \le \frac{1}{2}, \tag{3.17}$$

where λ_0 and λ_1 are the eigenvalues. Since, in this case, we have that $|\lambda_0| = 1$ and $|\lambda_1| \le 1$, the CFL condition reads as:

$$\frac{\Delta t}{\Delta x} \leq \frac{1}{2}.$$

The solution of (3.15) is obtained by solving a sequence of neighbouring Riemann problems and we have

$$U(t,x) = U_R\left(\frac{x - x^{j+\frac{1}{2}}}{\Delta t}; v_n^j, v_n^{j+1}\right),\ x^j < x < x^{j+1},\ j \in \mathbb{Z}. \tag{3.18}$$

Then, a more explicit expression of the scheme can be obtained integrating the equation (3.15) over the rectangle $(0, \Delta t) \times \left(x^{j-\frac{1}{2}}, x^{j+\frac{1}{2}}\right)$. Since the function is piecewise smooth, we get:

$$\int_{x^{j-\frac{1}{2}}}^{x^{j+\frac{1}{2}}} \left(U(\Delta t, 0) - U(0,x)\right) dx +$$

$$+ \int_0^{\Delta t} \left(F\left(U\left(t, x^{j+\frac{1}{2}} - 0\right)\right) - F\left(U\left(t, x^{j-\frac{1}{2}} + 0\right)\right)\right) dt = 0.$$

Now, using (3.14) and projecting the solution on piecewise constant functions we obtain:

$$\Delta x\left(v_{n+1}^j - v_n^j\right) + \int_0^{\Delta t} \left(F\left(U\left(t, x^{j+\frac{1}{2}} - 0\right)\right) - F\left(U\left(t, x^{j-\frac{1}{2}} + 0\right)\right)\right) dt = 0 \tag{3.19}$$

and, recalling (3.18), we derive:

$$v_{n+1}^j = v_n^j - \frac{\Delta t}{\Delta x}\left\{F\left(U_R\left(0-; v_n^j, v_n^{j+1}\right)\right) - F\left(U_R\left(0+; v_n^{j-1}, v_n^j\right)\right)\right\}. \tag{3.20}$$

Since the function $\xi \to F\left(U_R\left(\xi; U_L, U_R\right)\right)$ is continuous at the origin due to the Rankine-Hugoniot conditions (see [16]), Godunov scheme can be written in the form:

$$v_{n+1}^j = v_n^j - \frac{\Delta t}{\Delta x}\left\{F\left(U_R\left(0; v_n^j, v_n^{j+1}\right)\right) - F\left(U_R\left(0; v_n^{j-1}, v_n^j\right)\right)\right\}, \tag{3.21}$$

and the numerical flux computed in $V = (v_1, v_2)$ and $W = (w_1, w_2)$, is

$$G(V,W) = F(U_R(0;V,W)). \tag{3.22}$$

The numerical flux can be written in a general form as:

$$G(V,W) = \begin{cases} \min_{z_1\in[v_1,w_1]} F(Z) & \text{if } v_1 \le w_1 \\ \max_{z_1\in[v_1,w_1]} F(Z) & \text{if } v_1 \ge w_1 \end{cases}$$

where the second variable z_2 in $Z = (z_1, z_2)$ is assumed to be fixed. The final expression of Godunov scheme for the problem (3.15) is:

$$v_{n+1}^j = v_n^j - \frac{\Delta t}{\Delta x}\left(G\left(v_n^j, v_n^{j+1}\right) - G\left(v_n^{j-1}, v_n^j\right)\right). \tag{3.23}$$

More precisely, for the system (2.31), the scheme reads as:

$$\begin{cases} \rho_{n+1}^j = \rho_n^j - \frac{\Delta t}{\Delta x}\left(g\left(\rho_n^j, \rho_n^{j+1}\right) - g\left(\rho_n^{j-1}, \rho_n^j\right)\right), \\ \mu_{n+1}^j = \mu_n^j - \frac{\Delta t}{\Delta x}\left(\mu_{n+1}^j - \mu_n^j\right), \end{cases} \tag{3.24}$$

where the approximate values of $\rho(x,t)$ and $\mu(x,t)$ on the numerical grid is indicated as, respectively, ρ_n^j and μ_n^j for $j = 0, ..., L$ and $n = 0, ..., M-1$. In the (3.24) we can observe that the Godunov scheme for the second equation reduces to forward upwind scheme.

3.2.1 Fast Godunov for 2×2 system

In order to find a simplified expression for the numerical flux of Godunov scheme, considering as numerical flux the function $F(U)$ with $f(\rho,\mu)$ defined in (2.30), we solve Riemann problems between the two states: (ρ_-, μ_-) on the left and (ρ_+, μ_+) on the right. In particular, referring to relation (3.22), we compute the value of $F(U)$ in the separation point between waves of different speed.

Theorem 77 *The numerical flux function $G(V,W) = F(U_R(0;V,W))$ is*

$$G(\rho_-,\mu_-,\rho_+,\mu_+) = \begin{cases} (\rho_-, -\mu_+) & \text{if } \rho_- < \mu_- \vee \rho_- \le \mu_+, \\ \left(\frac{1-\varepsilon}{1+\varepsilon}\mu_+ + \frac{2\varepsilon}{1+\varepsilon}\rho_-, -\mu_+\right) & \text{if } \rho_- < \mu_- \vee \rho_- > \mu_+, \\ \left(\frac{1+\varepsilon}{2}\rho_- + \frac{1-\varepsilon}{2}\mu_-, -\mu_+\right) & \text{if } \rho_- \ge \mu_- \vee \mu_+ > \tilde{\mu}, \\ \left(\frac{1-\varepsilon}{1+\varepsilon}\left(\mu_+ + \varepsilon\mu_-\right) + \varepsilon\rho_-, -\mu_+\right) & \text{if } \rho_- \ge \mu_- \vee \mu_+ \le \tilde{\mu}, \end{cases} \tag{3.25}$$

with

$$\tilde{\mu} = \mu_- + \frac{1+\varepsilon}{2}\left(\rho_- - \mu_-\right). \tag{3.26}$$

Proof. Let P be the intersection point between the first family curve passing through $\left(\rho_-, \mu_-\right)$ and the line $\rho = \mu$, namely $P = \begin{pmatrix} \rho_- \\ \rho_- \end{pmatrix}$. The second family curve passing through P splits the invariant region into two regions $A = \left\{(\rho,\mu) : \mu > \rho_-\right\}$ and $B = \left\{(\rho,\mu) : \mu \leq \rho_-\right\}$ as shown in Fig.3.5 and Fig.3.6. Each Riemann problem solution presents waves traveling with two velocities, namely $\lambda_0 = -1$ and $0 < \varepsilon \leq \lambda_1 \leq 1$. If (ρ_*, μ_*) is the intermediate state (see Fig.3.7), we compute the numerical flux function $G\left(\rho_-, \rho_+\right)$ given by $\left(f\left(\rho_*, \mu_*\right), \mu_*\right)$. We distinguish two different cases:

Case1: $\rho_- < \mu_-$. In this case, if $\left(\rho_+, \mu_+\right) \in A$ then $(\rho_*, \mu_*) = \left(\rho_-, \mu_+\right)$. If $\left(\rho_+, \mu_+\right) \in B$, the needed value of flux is that corresponding to $\left(f\left(\rho_*, \mu_+\right), -\mu_+\right)$ (see Fig.3.5). We have

$$(\rho_*, \mu_*) = \left(\rho_*, \mu_+\right) = \begin{pmatrix} \rho_- \\ \rho_- \end{pmatrix} + t \begin{pmatrix} -\frac{1-\varepsilon}{1+\varepsilon} \\ \rho_- \end{pmatrix} \tag{3.27}$$

and ρ_* is computed as:

$$\rho_* = \rho_- + \left(\rho_- - \mu_+\right)\frac{1-\varepsilon}{1+\varepsilon}. \tag{3.28}$$

Finally, since $\rho_* > \rho_- > \mu_+$ we get the expression in the second line of (3.25).

Case 2: $\rho_- \geq \mu_-$. In this case, if $\left(\rho_+, \mu_+\right) \in A$ then $(\rho_*, \mu_*) = \left(\tilde{\rho}, \mu_+\right)$, where

$$\tilde{\rho} = \frac{1+\varepsilon}{2}\rho_- + \frac{1-\varepsilon}{2}\mu_- \tag{3.29}$$

is obtained as follows. The point $(\tilde{\rho}, \tilde{\mu})$ is:

$$(\tilde{\rho}, \tilde{\mu}) = \begin{pmatrix} \rho_- \\ \mu_- \end{pmatrix} + t \begin{pmatrix} -\frac{1-\varepsilon}{1+\varepsilon} \\ 1 \end{pmatrix},$$

and, using that $\tilde{\rho} = \tilde{\mu}$, it is possible to get (3.29). Assuming $\left(\rho_+, \mu_+\right) \in B$, the value of flux we need is $f\left(\rho_*, \mu_+\right)$ with ρ_* given by

$$(\rho_*, \mu_*) = \left(\rho_*, \mu_+\right) = \begin{pmatrix} \rho_- \\ \mu_- \end{pmatrix} + t \begin{pmatrix} -\frac{1-\varepsilon}{1+\varepsilon} \\ 1 \end{pmatrix}, \tag{3.30}$$

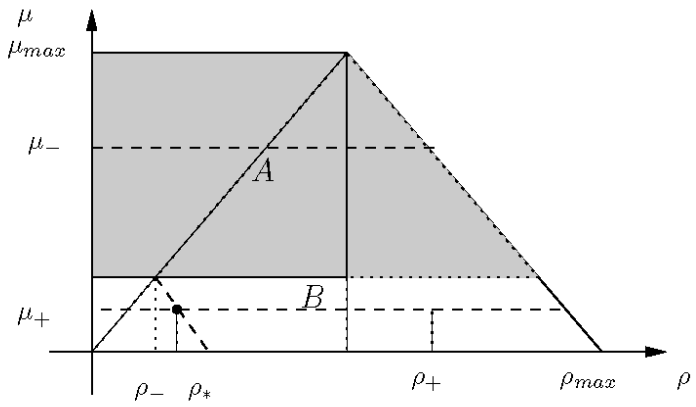

Figure 3.5: Case 1, with $(\rho_+, \mu_+) \in B$.

and, making simple computations, one gets:

$$\rho_* = \rho_- + (\mu_- - \mu_+) \frac{1-\varepsilon}{1+\varepsilon}. \tag{3.31}$$

Taking into account that $\rho_* > \mu_+$, we obtain the expression of flux as in the last line of (3.25).

■

3.3 Numerics for Riemann Solvers

In this sub-section, in order to describe the numerical framework for the solution of Riemann problems at junctions, we refer to the general Riemann solver called **SC1** [12] and to **SC2** and **SC3**.

For simplicity, we focus on a single supplier v^e, and on two consecutive sub-chains, e and $e+1$.

Let us introduce the following notations:

- $\rho_n^{e,L}$,$\mu_n^{e,L}$ are the approximate values, respectively, of density and processing rate at time t_n at the outgoing endpoint $x_L = L\Delta x$ of sub-chain e;
- $\rho_n^{e,0}$,$\mu_n^{e,0}$ are the approximate values, respectively, of density and processing rate at time t_n at the incoming endpoint $x_0 = 0$ of sub-chain $e+1$;

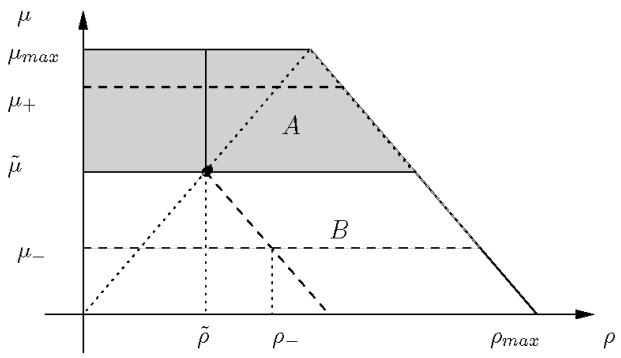

Figure 3.6: Case 2, with $(\rho_+, \mu_+) \in A$.

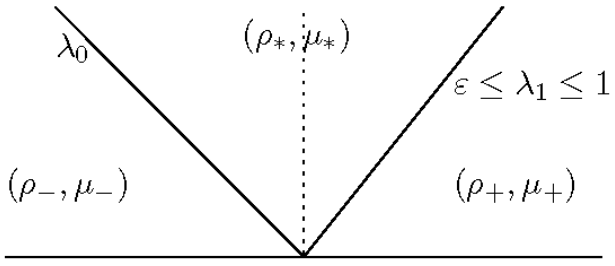

Figure 3.7: Intermediate state between the two waves.

3.3.1 Discretization of the Riemann Solver SC1

Setting

- $\hat{\gamma} = f\left(\rho_n^{e,L}, \mu_n^{e,L}\right)$,
- $\gamma_{\max}^{e+1} = f\left(\rho_{\max}^{e}, \mu_n^{e+1,0}\right)$,

we consider two cases:

Case α) If $\hat{\gamma} \leq \gamma_{\max}^{e+1}$:

$$\rho_n^{e,L+1} = \rho_n^{e,L},$$

$$\mu_n^{e,L+1} = \mu_n^{e,L},$$

$$\rho_n^{e+1,-1} = \begin{cases} f\left(\rho_n^{e,L}, \mu_n^{e,L}\right) & \text{if } f\left(\rho_n^{e,L}, \mu_n^{e,L}\right) \leq \mu_n^{e+1,0}, \\ \frac{f\left(\rho_n^{e,L}, \mu_n^{e,L}\right) - \mu_n^{e+1,0}}{\varepsilon} - \mu_n^{e+1,0} & otherwise, \end{cases}$$

$$\mu_n^{e+1,-1} = \mu_n^{e+1,0};$$

Case β) If $\hat{\gamma} > \gamma_{\max}^{e+1}$:

$$\rho_n^{e,L+1} = \rho_n^{e,L},$$

$$\mu_n^{e,L+1} = \frac{\gamma_{\max}^{e+1} - \varepsilon \rho_n^{e,L}}{1 - \varepsilon},$$

$$\rho_n^{e+1,-1} = \rho_{\max}^{e},$$

$$\mu_n^{e+1,-1} = \mu_n^{e+1,0}.$$

3.3.2 Discretization of the Riemann Solver SC2

Case α) We have two subcases:

α_1) if $\rho^* < \rho_M$, we set:

$$\rho_n^{e,L+1} = \rho_n^{e,L},$$

$$\mu_n^{e,L+1} = \min\left\{\rho^*, \mu_{\max}^{e}\right\},$$

$$\rho_n^{e+1,-1} = \rho^*,$$

$$\mu_n^{e+1,-1} = \mu_n^{e+1,0};$$

α_2) if $\rho^* \geq \rho_M$, the new values are:

$$\rho_n^{e,L+1} = \rho_n^{e,L},$$
$$\mu_n^{e,L+1} = \varepsilon \frac{1+\varepsilon}{1-\varepsilon} \tilde{\rho} - \frac{2\varepsilon}{1-\varepsilon} \bar{\mu}^e + (1+\varepsilon)\, \mu_n^{e+1,0},$$
$$\rho_n^{e+1,-1} = \tilde{\rho},$$
$$\mu_n^{e+1,-1} = \mu_n^{e+1,0};$$

Case β)

$$\rho_n^{e,L+1} = \rho_n^{e,L},$$
$$\mu_n^{e,L+1} = \bar{\mu}^e,$$
$$\rho_n^{e+1,-1} = \bar{\mu}^e,$$
$$\mu_n^{e+1,-1} = \mu_n^{e+1,0}.$$

3.3.3 Discretization of the Riemann Solver SC3

Case α) two subcases occur:

α_1) if $\rho^* < \rho_M$, we set:

$$\rho_n^{e,L+1} = \rho_n^{e,L},$$
$$\mu_n^{e,L+1} = \max\left\{\rho^*, \mu_n^{e,L}\right\},$$
$$\rho_n^{e+1,-1} = \rho^*,$$
$$\mu_n^{e+1,-1} = \mu_n^{e+1,0};$$

α_2) if $\rho^* \geq \rho_M$, we compute the new values as in **SC2**:

$$\rho_n^{e,L+1} = \rho_n^{e,L},$$
$$\mu_n^{e,L+1} = \varepsilon \frac{1+\varepsilon}{1-\varepsilon} \tilde{\rho} - \frac{2\varepsilon}{1-\varepsilon} \bar{\mu}^e + (1+\varepsilon)\, \mu_n^{e+1,0},$$
$$\rho_n^{e+1,-1} = \tilde{\rho},$$
$$\mu_n^{e+1,-1} = \mu_n^{e+1,0};$$

Case β)

$$\rho_n^{e,L+1} = \rho_n^{e,L},$$

β_1) if $\mu_n^{e,L+1} \geq \bar{\mu}^e$, we set:

$$\mu_n^{e,L+1} = \mu_n^{e,L},$$

β_2) otherwise, we assign:

$$\mu_n^{e,L+1} = \bar{\mu}^e,$$

$$\rho_n^{e+1,-1} = \bar{\mu}^e,$$

$$\mu_n^{e+1,-1} = \mu_n^{e+1,0}.$$

Chapter 4

Simulations and Optimization

In this section, first, we report some numerical results analyzing the use of the Klar model and the continuum-discrete model for supply chain. Then we will compare, via simulations, performances between the two previous model showing some differences.

Moreover, we show the behaviour of a supply chain network based on both models.

Finally we discuss about some optimization techniques related to Klar model for supply chain.

4.1 Numerical results

4.1.1 Example of Göttlich-Herty-Klar model for supply chain

Consider a supply chain with four arcs, i.e. $N = 4$, consisting of three processors with queues characterized by length L_j, capacity μ_j, and processing time T_j, for $i = 1, 2, 3, 4$ and an inflow arc. Then we summarize these quantities for each processor in the following table:

Processor j	μ_j	T_j	L_j
1	25	1	1
2	15	1	0.2
3	10	3	0.6
4	15	1	0.2

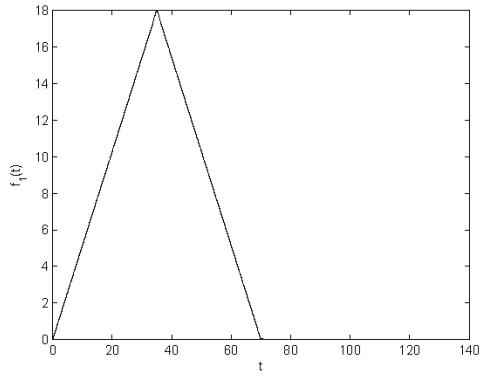

Figure 4.1: Inflow profile $f_1(t)$ prescribed as initial data on the first arc.

We suppose that at time $t = 0$, all arcs are empty, i.e. $\rho_{j,0} = 0 \; \forall x \in [0, L_j]$ and the queues are assumed zero, i.e. $q_{j,0} = 0$, $j = 2, 3, 4$. The initial inflow profile

$$f_1(t) = \begin{cases} \frac{18}{35}t, & 0 \leq t \leq \frac{T}{4}, \\ 36 - \frac{18}{35}t, & \frac{T}{4} < t < \frac{T}{2}, \\ 0, & \frac{T}{2} \leq t \leq T. \end{cases} \tag{4.1}$$

is such that it exceeds the maximum capacity of processor (see Fig.4.1).

Assuming a total simulation time $T = 140$ and discretization spatial and time step constants for each arc, respectively $\Delta x = 0.0125$ and $\Delta t = 0.5\Delta x = 0.00625$ (such that the CFL condition is satisfied), we get the numerical solution to the *ordinary* (i.e. without considering different space meshes and time mesh) supply chain model (as shown in Fig.4.2 and Fig.4.3).

In 4.2 we observe that queue q_4 remains empty, since the maximal capacity is such that $\mu_4 > \mu_3$, while in the queues q_2 and q_3 it is evident the buffering of an exceeding demand.

4.3 shows the behaviour of the final density in which the density ρ_2 of processor two corresponds to the strip $0 \leq x \leq 10$, $t > 0$, ρ_3 for processor three to $10 \leq x \leq 40$, $t > 0$ and ρ_4 for processor four to the remaining part of the plot.

Now, if we consider the supply chain model with different spatial steps and different time steps choosing, respectively, $\Delta x = 0.0125$ and $\Delta x = 0.0125$, we can notice that, for the same parameters configuration, different numerical approximations give rise to very similar results. In the Fig.4.4 the comparison between

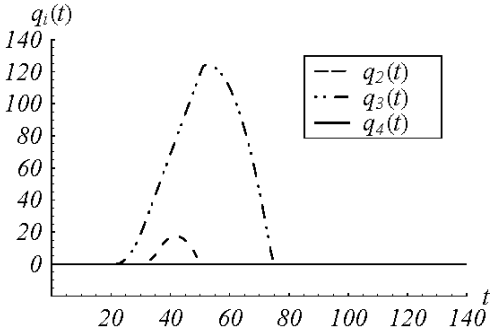

Figure 4.2: Behaviour of queues

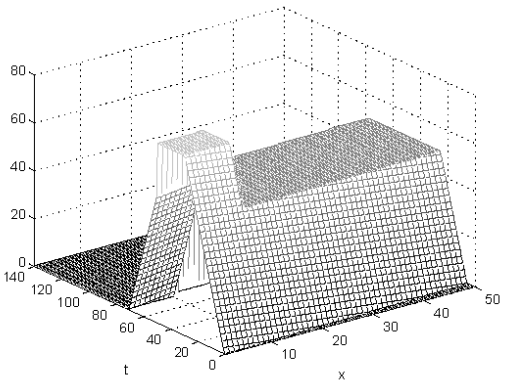

Figure 4.3: Behaviour of final density

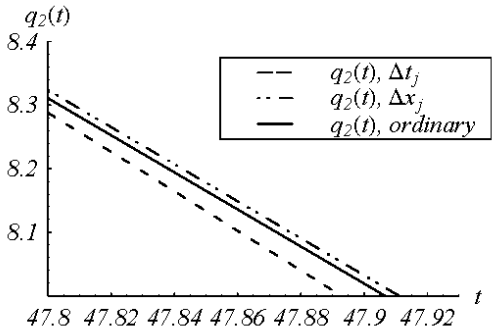

Figure 4.4: Comparison between ordinary and other methods for q_2.

ordinary and other methods of the queue buffer occupancy $q_2(t)$ is shown.

4.1.2 Example of continuum-discrete model for supply chain

In order to compare the continuum-discrete model and the Klar model, we refer to the previous example, considering the flux function with different slopes m_k (see **Remark 54**). The expression of numerical flux $G\left(\rho_-, \mu_-, \rho_+, \mu_+\right)$ of fast Godunov scheme for supplier I_k is:

$$G = \begin{cases} \left(m_k\rho_-, -\mu_+\right) & \text{if } \rho_- < \mu_- \vee \rho_- \leq \mu_+, \\ \left(\left(m_k - \frac{2\varepsilon}{1+\varepsilon}\right)\mu_+ + \frac{2\varepsilon}{1+\varepsilon}\rho_-, -\mu_+\right) & \text{if } \rho_- < \mu_- \vee \rho_- > \mu_+, \\ \left(m_k\left(\frac{1+\varepsilon}{2}\rho_- + \frac{1-\varepsilon}{2}\mu_-\right), -\mu_+\right) & \text{if } \rho_- \geq \mu_- \vee \mu_+ > \tilde{\mu}, \\ \left(\left(m_k - \frac{2\varepsilon}{1+\varepsilon}\right)\mu_+ + \frac{1-\varepsilon}{1+\varepsilon}\varepsilon\mu_- + \varepsilon\rho_-, -\mu_+\right) & \text{if } \rho_- \geq \mu_- \vee \mu_+ \leq \tilde{\mu}, \end{cases} \tag{4.2}$$

with $\tilde{\mu}$ as in (3.26). Then, we have $N = 4$ processors described by the following table:

Processor k	μ_k	m_k	L_k
1	25	1	1
2	15	0.2	0.2
3	10	0.2	0.6
4	15	0.2	0.2

Let us assume the initial data as $\rho_1(t,x) = \rho_2(t,x) = \rho_3(t,x) = \rho_4(t,x) = 0$ and the boundary data is given by

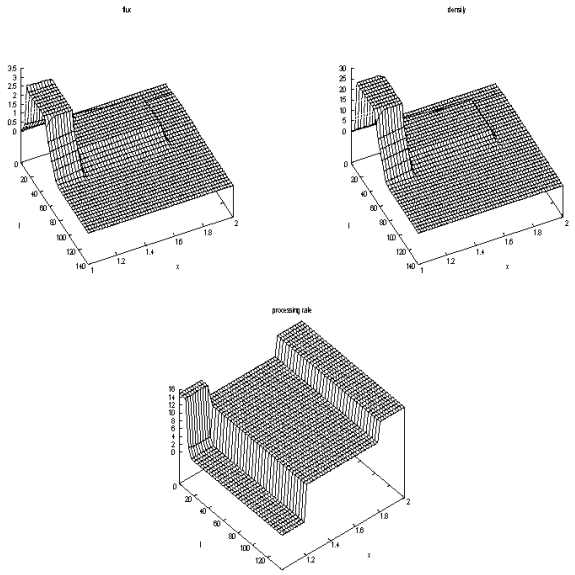

Figure 4.5: Evolution of flux f, density ρ, and processing rate μ, on processors 2, 3, 4, with Riemann Solver **SC1** and $\varepsilon = 0.1$.

$$\rho_1(t,0) = \begin{cases} \frac{18}{35}t, & 0 \le t \le \frac{T}{4}, \\ 36 - \frac{18}{35}t, & \frac{T}{4} < t < \frac{T}{2}, \\ 0, & \frac{T}{2} \le t \le T. \end{cases}$$

The simulation time is assumed to be $T = 140$, with $\Delta x = 0.02$ and $\Delta t = 0.01$. On each processor the initial datum $\mu(0,x)$ is the value μ_k with $k = 1, 2, 3, 4$.

The evolution in time of flux, density and processing rate on processors 2, 3, 4, considering the Riemann Solver **SC1** for $\varepsilon = 0.1$ is shown in Fig.4.5. In particular, in this case we can observe that the processing rate is minimized and the flux and density are considerably lowered on processors 3 and 4.

Instead, in case of the Riemann Solver **SC2** with $\varepsilon = 0.1$, shown in Fig.4.6, the flux and the density are correctly developed on processors 2, 3, 4, due to the behaviour of the processing rate μ, which assumes the minimum possible value in order to maximize the flux.

The Riemann Solver **SC3** is shown in Fig.4.7 and Fig.4.8, respectively with $\varepsilon = 0.1$ and $\varepsilon = 0.01$.

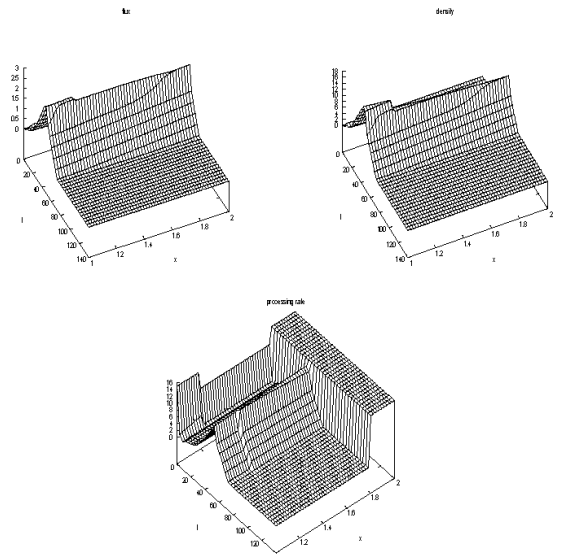

Figure 4.6: Evolution of flux f, density ρ, and processing rate μ, on processors 2, 3, 4, with Riemann Solver **SC2** and $\varepsilon = 0.1$.

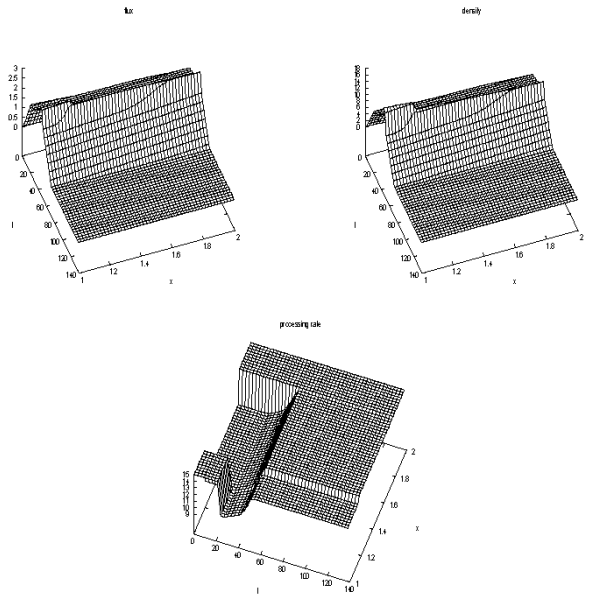

Figure 4.7: Evolution of flux f, density ρ, and processing rate μ, on processors 2, 3, 4, with Riemann Solver **SC3** and $\varepsilon = 0.1$.

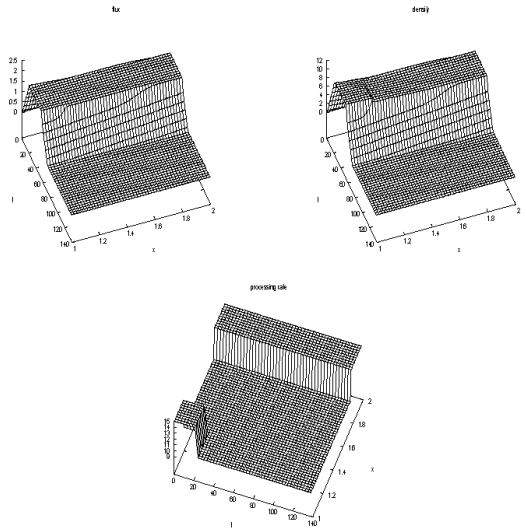

Figure 4.8: Evolution of flux f, density ρ, and processing rate μ, on processors 2, 3, 4, with Riemann Solver **SC3** and $\varepsilon = 0.01$.

As we can see by the last two graphs, different values of ε determines different behaviour of the quantities f, ρ and μ; in particular for $\varepsilon \to 0$, the maximum values assumed by the flux and density decrease.

Finally, if we compare the behaviour of the density for Riemann Solver **SC3** with that one of the example for Klar model shown in Fig.4.3, we can observe that the two modellistic approach are in accordance as we expect.

4.1.3 Example of Klar model for supply chain network

Consider a supply chain network with $N = 16$ arcs and $V = 10$ processors (i.e. nodes) as shown in Fig.4.9.

In the following table we report the characteristics of each arc, i.e. length L_j, capacity μ_j, processing time T_j and the distribution coefficient α_j.

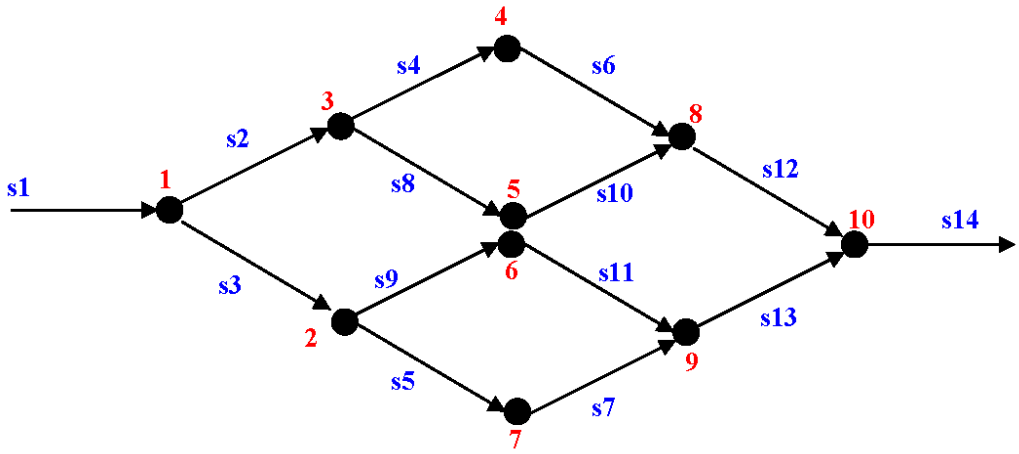

Figure 4.9: Supply chain network with 16 arcs and 10 nodes.

Processor j	μ_j	T_j	L_j	α_j
$s1$	0.0005	1	1	1
$s2$	0.01	1	1	0.6
$s3$	0.015	1	1	0.4
$s4$	0.02	1	1	0.5
$s5$	0.008	1	1	0.3
$s6$	0.02	1	1	0.4
$s7$	0.0005	1	1	0.2
$s8$	0.01	1	1	0.5
$s9$	0.017	1	1	0.7
$s10$	0.01	1	1	0.6
$s11$	0.012	1	1	0.8
$s12$	0.001	1	1	0.7
$s13$	0.0005	1	1	0.3
$s14$	0.0001	1	1	1

We assume that for each arc the initial data and the queue are equal to zero, and the boundary data is given by

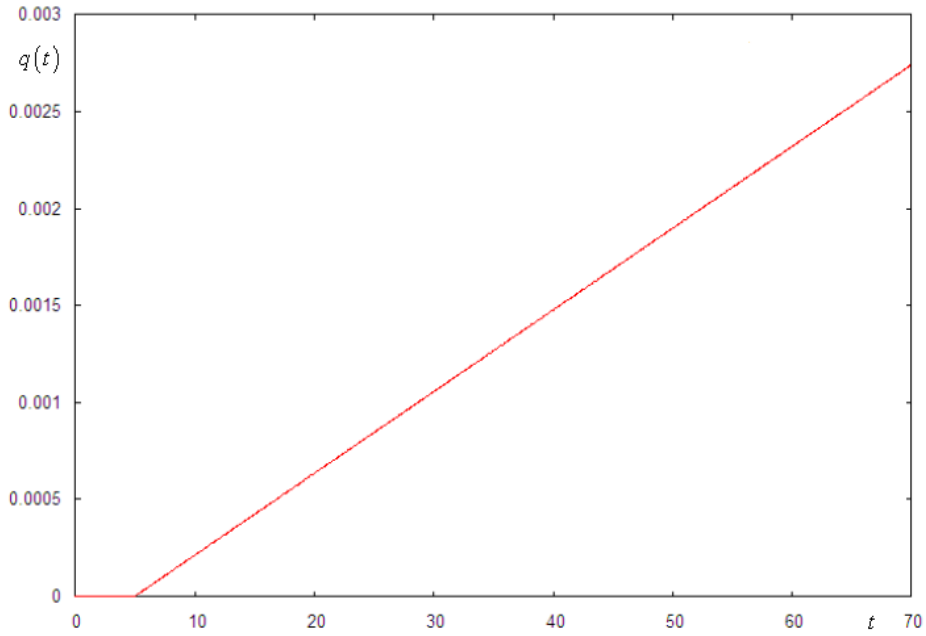

Figure 4.10: Queue on the last processor with $\alpha_{12} = 0.7$ and $\alpha_{12} = 0.3$.

$$\rho_1(t,0) = \begin{cases} \frac{18}{35}t, & 0 \le t \le \frac{T}{2}, \\ 36 - \frac{18}{35}t, & \frac{T}{2} < t < T, \end{cases}$$

with total simulation time $T = 70$. Moreover we set the spatial and time discretization step are, respectively, $\Delta x = 0.0125$ and $\Delta t = 0.0125$.

In the Fig.4.10 the behaviour of queue on the last processor (node 10) is shown. If we reverse the distribution coefficients of the arc $s12$ and $s13$, i.e. $\alpha_{12} = 0.3$ and $\alpha_{12} = 0.7$, we obtain the value of the same queue is lower that the previous case (as shown in Fig.4.11). Then, we can observe that the behaviour of the network can be managed through the control of few parameters such as the distribution coefficients.

4.1.4 Example of continuum-discrete model for supply chain networks

Now we report the densities and production rates at $t = 0$ and after some times (at $t = 1$) for different initial data using different routing algorithms. Since

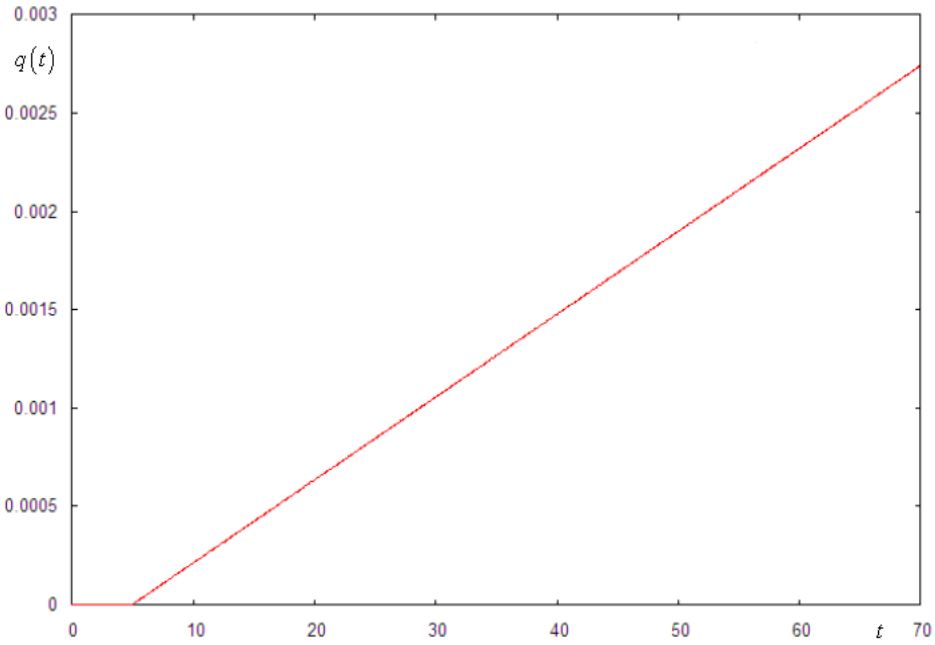

Figure 4.11: Queue on the last processor with $\alpha_{12} = 0.3$ and $\alpha_{12} = 0.7$.

a constant state is an equilibrium for the single line model, a modification of the state may only appear initially at the junction.

Assuming a node of type 1×2 with $\varepsilon = 0.2$, $\mu_i^{\max} = 1$, $i = 1, 2, 3$, $\alpha = 0.8$, $(\rho_{1,0}, \rho_{2,0}, \rho_{3,0}) = (0.7, 0.1, 0)$, $(\mu_{1,0}, \mu_{2,0}, \mu_{3,0}) = (1, 0.2, 1)$ we report the corresponding Riemann Solver (shown in Fig.4.12 - Fig.4.13).

We can observe that the algorithm **RA2** redirects the goods, in fact taking into account the initial loads of the outgoing sub-chains, the number of goods processed by the sub-chain with density $\rho_{3,0} = 0$ increases.

In the case of a node of type 2×1, assuming $\varepsilon = 0.2$, $\mu_i^{\max} = 1$, $i = 1, 2, 3$, $q = 0.6$, $(\rho_{1,0}, \rho_{2,0}, \rho_{3,0}) = (0.3, 0.7, 0.8)$, $(\mu_{1,0}, \mu_{2,0}, \mu_{3,0}) = (0.8, 0.7, 0.4)$, the numerical results are shown in Fig.4.14 and Fig.4.15.

4.1.5 Simulation of a simple supply network using both models

Consider a supply network formed by two junctions (nodes) and five processors (arcs) linked as in Fig.4.16

We suppose that at time $t = 0$ all processors are empty and the queues are

	RA1		RA2	
	SC2	SC3	SC2	SC3
$\hat{f}_i$	$(0.58, 0.47, 0.12)$	$(0.58, 0.47, 0.12)$	$(0.7, 0.47, 0.23)$	$(0.7, 0.47, 0.23)$
$\hat{\rho}_i$	$(0.82, 1.53, 0.12)$	$(0.82, 1.53, 0.12)$	$(0.7, 1.53, 0.23)$	$(0.7, 1.53, 0.23)$
$\hat{\mu}_i$	$(0.52, 0.2, 1)$	$(0.52, 0.2, 1)$	$(0.7, 0.2, 1)$	$(1, 0.2, 1)$

TABLE 1. A node of type 1×2.

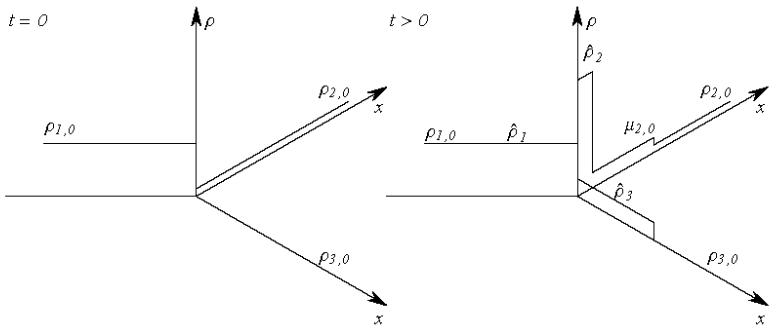

Figure 4.12: A Riemann Problem for the **RA2-SC3** algorithm: the initial density and the density after some times.

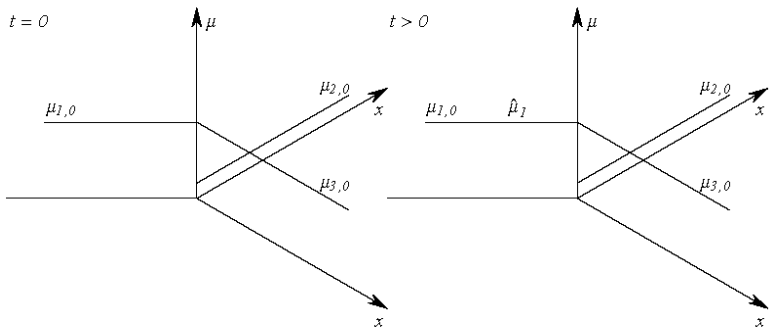

Figure 4.13: A Riemann Problem for the **RA2-SC3** algorithm: the initial production rate and the production rate after some times.

	RA1=RA2	
	SC2	SC3
$\hat{f}_i$	$(0.3, 0.3, 0.6)$	$(0.3, 0.3, 0.6)$
$\hat{\rho}_i$	$(0.3, 1.1, 1.4)$	$(0.3, 1.1, 1.4)$
$\hat{\mu}_i$	$(0.3, 0.1, 0.4)$	$(0.8, 0.1, 0.4)$

TABLE 2. A node of type 2×1.

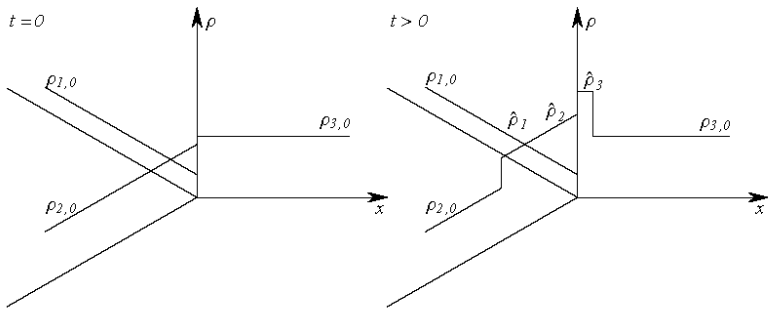

Figure 4.14: A Riemann Problem for the **SC2** algorithm: the initial density and the density after some times.

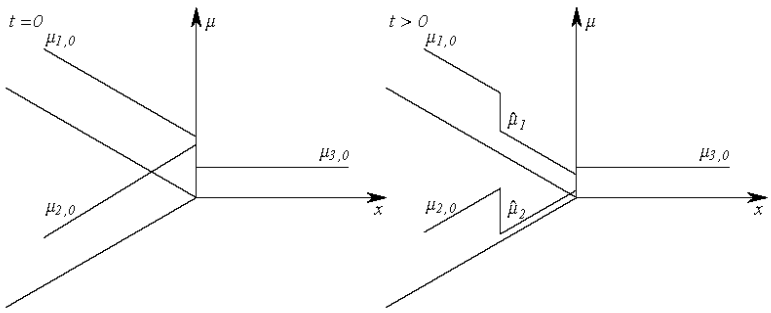

Figure 4.15: A Riemann Problem for the **SC2** algorithm: the initial production rate and the production rate after some times.

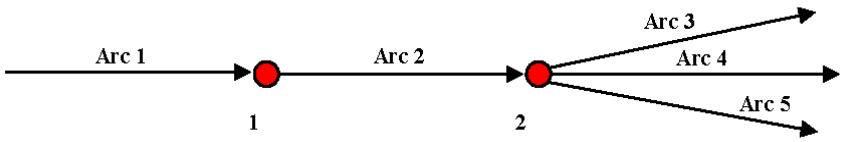

Figure 4.16: aaaaa

assumed zero. Moreover we use an initial inflow profile as:

$$\rho_1(t,0) = \begin{cases} \frac{18}{35}t, & 0 \le t \le \frac{T}{4}, \\ 36 - \frac{18}{35}t, & \frac{T}{4} < t < \frac{T}{2}, \\ 0, & \frac{T}{2} \le t \le T. \end{cases} \qquad ((4.3))$$

Each processor is characterized by the parameters shown in the following table:

Processor j	μ_j	T_j	L_j	α_j
Arc_1	15	10	10	1
Arc_2	10	50	30	1
Arc_3	10	50	10	0.3
Arc_4	20	50	10	0.2
Arc_5	8	50	10	0.5

Then, using the Klar model, the results for the densities versus time and space for each outgoing processor are in Fig.4.17.

Fig. 4.18 show the evolution of densities for the entire supply networks.

Now, if we consider the continuum-discrete model using the routing algorithm **RA1** in combination with the rule **SC2** and the inflow profile as in (4.3), and we set the boundary conditions for the processing rate of each arc as in the following table:

Processor j	μ_j_IN	μ_j_OUT	μ_j_MAX	T_j	L_j	α_j
Arc_1	10	10	15	10	10	1
Arc_2	7	8	10	50	30	1
Arc_3	7	7	10	50	10	0.3
Arc_4	15	16	20	50	10	0.2
Arc_5	5	6	8	50	10	0.5

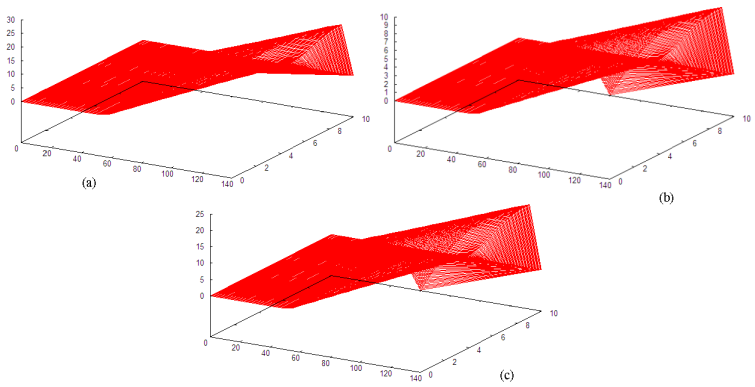

Figure 4.17: Results for Klar model. $Case(a)$: density for the first processors; $Case(b)$: density for the second processors; $Case(c)$: density for the third processors.

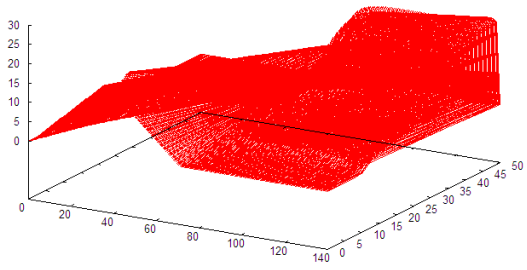

Figure 4.18: Behaviour of the final density: ρ_1 for $0 \leq x \leq 10$, $t > 0$, ρ_2 for $10 \leq x \leq 40$, $t > 0$, and ρ_3, ρ_4, ρ_5 for $40 \leq x \leq 50$, $t > 0$.

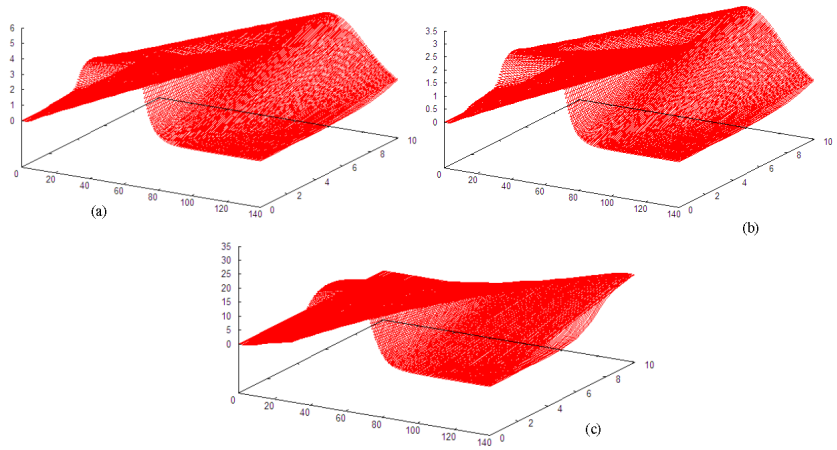

Figure 4.19: Results for the continuum-discrete model. $Case(a)$: density for the first processors; $Case(b)$: density for the second processors; $Case(c)$: density for the third processors.

The results for densities of each outgoing arc and evolution of densities for the entire supply networks are respectively shown in Fig. 4.19 and Fig 4.20.

4.2 Optimization of Klar model

According to consider the optimization problem for the Klar fluid dynamic model for supply chain, the aim is to adjust the production in order to minimize queues length and to obtain an expected pre-assigned outflow. The optimization is realized by minimizing a cost functional which takes into account the final flux of production and the queues representing the stores.

Since this functional is not linear, it is very difficult to determine its minimum, so to solve this problem, we use the tangent vector method as optimization technique.

Considering a supply chain with N arcs, and $N-1$ vertices, the cost functional is defined as:

$$J\left(\rho_j, q_j\right) = \sum_j \int_0^T q_j\left(t\right) dt + \int_0^T \left[f_N\left(\rho_N\left(t, b_N\right)\right) - \varphi\left(t\right)\right]^2 dt$$

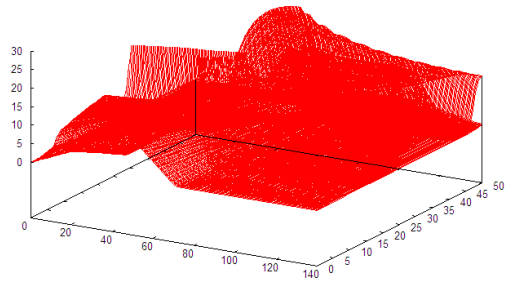

Figure 4.20: Behaviour of the final density: ρ_1 for $0 \leq x \leq 10$, $t > 0$, ρ_2 for $10 \leq x \leq 40$, $t > 0$, and ρ_3, ρ_4, ρ_5 for $40 \leq x \leq 50$, $t > 0$.

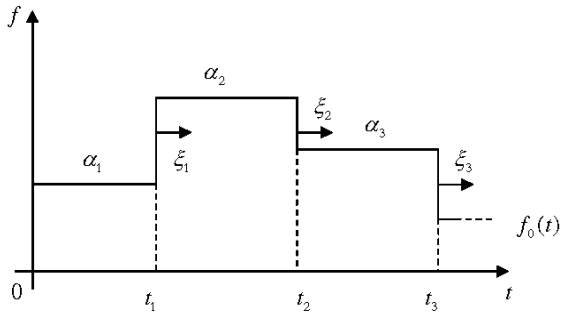

Figure 4.21: Profile of input flow with displacement of discontinuities

with $j = 1, .., N$ and where each arc is represent by intervals $[a_j, b_j]$, q_j is the queue between the arc $(j-1)$ and j, $f_N(\rho_N(t, b_N))$ is the final flux of production on the last arc N, $\varphi(t)$ is the pre-assigned output flux and T is the total time of observation. In order to optimize the production costs, we want to find

$$\min_{f \in L^2} \left[J\left(\rho_j, q_j\right) \right].$$

We choose the space L^2 because the definition of functional considers the distance in this space.

In order to compute this minimum, in what it follows, we show the tangent vector method. We consider an initial input flux f_0 as a piecewise constant function, where t_k are the discontinuity points (see Fig.4.21)

Let ξ_k be the infinitesimal displacement of discontinuities t_k .Each ξ_k produces

a reconfiguration of the function f_0 and changing the system, whose effect are visible both on fluxes and on the queues. Therefore time shifts on the processors and shifts on the queues are produced. In particular those shifts are generated by the interactions occurring at different times in the system as result of initial infinitesimal variations. We consider two kinds of interactions:

a) interaction of a wave flow with queue;

b) emptying of the queue.

The interaction time is denoted by $\bar{t}$. The time shift generated by the infinitesimal displacement ξ_k on the processor I_j is denoted by ${}^k\xi_j$, while the shifts on the queue q_j are, respectively before and after the interaction, ${}^k\eta_j^-$ and ${}^k\eta_j^+$.

For the case a), we distinguish two sub-cases:

1. $q_j(\bar{t}) = 0$;
2. $q_j(\bar{t}) > 0$.

Let us consider the case 1.a). For $t < \bar{t}$, for t sufficiently close to $\bar{t}$, $q_j(t) = 0$ and $\dot{q}_j(t) = 0$. Since $\dot{q}_j(t) = f\left(\rho_1^{j-1}\right) - f_{out} = 0$, where ρ_1^{j-1} is the density on arc $j-1$ before the interaction time, $f_{out} = \rho_1^{j-1}$, but if $f_{out} := \rho_1^j$, then $\rho_1^{j-1} = \rho_1^j$, i.e. the incoming flux are equal to outgoing flux before the interaction. For $t > \bar{t}$ it can be:

i) $\rho_2^{j-1} < \rho_1^{j-1}$; in this case the flux is decreasing and the queue still remains empty. Since $q_j(t) = 0$ for $t > \bar{t}$, we have $\rho_2^{j-1} = \rho_2^j$ (see Fig.4.22)A wave $\left(\rho_2^j, \rho_1^j\right)$ is produced on arc j. The time shifts do not change on arc $j-1$ and j, i.e.

$$\xi^+ = \xi^-.$$

There is no shift for the queue, so $\eta_j^+ = \eta_j^- = 0$.

ii) $\rho_2^{j-1} > \mu_j$. Then, $f_{out} = \min\left\{f\left(\rho_2^{j-1}\right), \mu_j\right\} = \mu_j$ and $\dot{q}_j(t) = f\left(\rho_2^{j-1}\right) - \mu_j > 0$, i.e. the queue increases and a wave $\left(\mu_j, \rho_1^j\right)$ is produced on arc j. The time shifts are equal on arcs $j-1$ and j, i.e. $\xi^+ = \xi^-$ (as shown in Fig.4.23).Moreover a shift for the queue j is produced; in particular it is $\eta_j^- = 0$ (before interaction there is no shift), while for $t > \bar{t}$ we have $\eta_j^+ = \left(\bar{t} + \xi^- - \bar{t}\right)\left(\rho_2^{j-1} - \mu_j\right) = \xi^-\left(\rho_2^{j-1} - \mu_j\right)$, as shown in Fig.4.24.

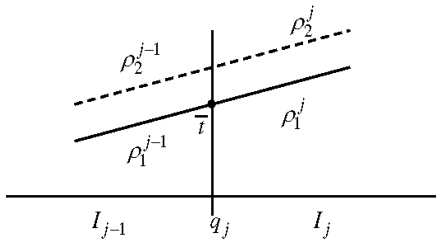

Figure 4.22: $\rho_2^{j-1} < \rho_1^{j-1}$.

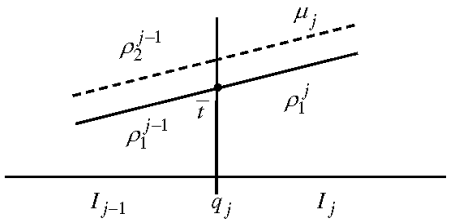

Figure 4.23: $\rho_2^{j-1} > \mu_j$.

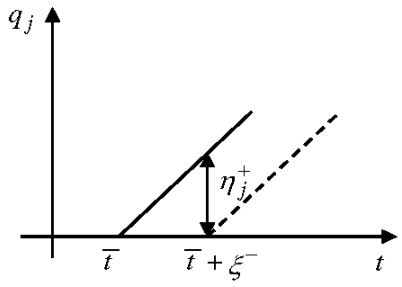

Figure 4.24: Shift of the queue j.

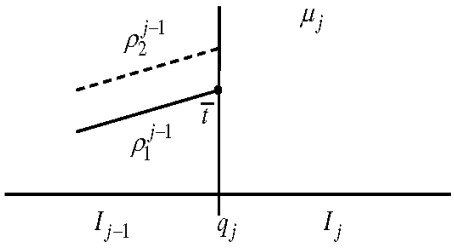

Figure 4.25: $q_j(\bar{t}) > 0$.

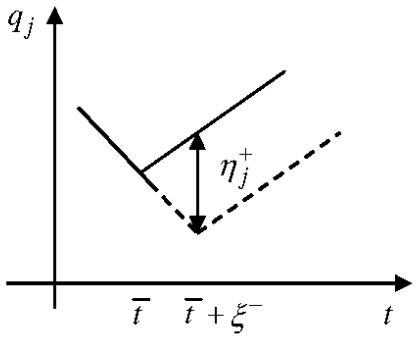

Figure 4.26: Shift of the queue q_j.

Consider the case 2.a). For $t < \bar{t}$, for t sufficiently close to $\bar{t}$, $q_j(t) > 0$, so $f_{out} = \mu_j$ and $\dot{q}_j(t) = f\left(\rho_1^{j-1}\right) - \mu_j$. For $t > \bar{t}$, since the queue is still not empty, we have that $f_{out} = \mu_j$ and $\dot{q}_j(t) = f\left(\rho_2^{j-1}\right) - \mu_j$. In this case no wave is produced on arc j and $\xi^+ = 0$ (see Fig.4.25).

A shift for the queue is produced,
i.e. $\eta_j^+ = \left(\bar{t} + \xi^- - \bar{t}\right)\left(\dot{q}_j^+ - \dot{q}_j^-\right) = \xi^-\left(f\left(\rho_2^{j-1}\right) - f\left(\rho_1^{j-1}\right)\right)$, as shown in Fig.4.26.

Finally, let us consider the case b), in which the queue is decreasing so $q_j(\bar{t}) = 0$. For $t < \bar{t}$, $q_j(t) < 0$ and $\dot{q}_j(t) < 0$, then $f_{out} = \mu_j$ and $\dot{q}_j(t) = f\left(\rho_1^{j-1}\right) - \mu_j$. While for $t > \bar{t}$, with t sufficiently close to $\bar{t}$, we have $q_j(t) = 0$ and $f_{out} = \min\left\{f\left(\rho_1^{j-1}\right), \mu_j\right\} = \rho_1^{j-1}$ (see Fig.4.27).

We can observe that $\eta_j^+ = 0$, while $\xi^- = 0$ and $\xi^+ = -\frac{\eta_j^-}{\rho_1^{j-1} - \mu_j}$ (see Fig.4.28).

Now, for the cost functional we can write

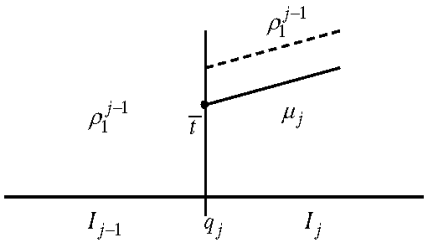

Figure 4.27: $q_j(\bar{t}) = 0$.

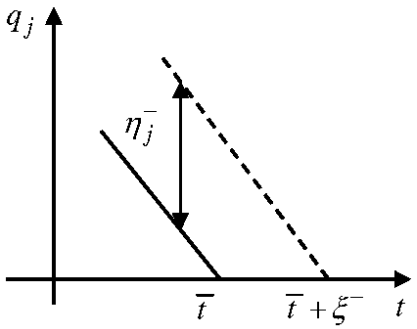

Figure 4.28: $q_j(\bar{t}) = 0$.

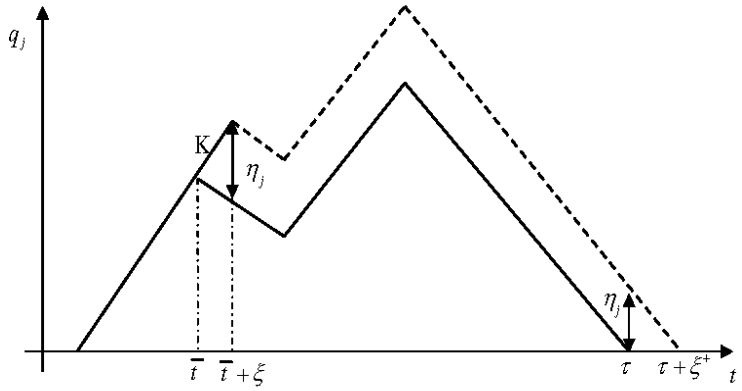

Figure 4.29: case 1).

$$J\left(\rho_j, q_j\right) = \sum_j \int_0^T q_j\left(t\right) dt + \int_0^T \left[f_N\left(\rho_N\left(t, b_N\right)\right) - \varphi\left(t\right)\right]^2 dt = J_1 + J_2,$$

where $J_1 = \sum_j J_{1,j} = \sum_j \int_0^T q_j\left(t\right) dt$. Starting from an empty chain, if we indicate with τ the time of emptying of the queue, $\xi_{\bar{t}}$ the time shift at $\bar{t}$ and ξ_τ the time shift at τ, four cases regarding to the signs of the tangent vectors $\xi_{\bar{t}}$ and η_j can be discussed.

1. $sgn\left(\eta_j\right) = sgn\left(\xi_{\bar{t}}\right) = 1$. In this case $q_j\left(\bar{t}\right) > 0$ and

$$\Delta J_{1,j} = \eta_j\left(\tau - \bar{t} - \xi_{\bar{t}}\right) + \frac{\xi_\tau \eta_j}{2} + K$$

where $\xi_\tau = \frac{\eta_j}{\mu_j - \rho_1^{j-1}}$ and K is the area shown in Fig.4.29.

Remark 78 *If* $q_j\left(\bar{t}\right) = 0$ *then* $sgn\left(\eta_j\right) = -sgn\left(\xi_{\bar{t}}\right)$.

We are considering a situation in which for $t > \bar{t}$, the queue is decreasing, so if t^- and t^+ are the left and right neighbourhoods of $\bar{t}$ respectively, then $\dot{q}\left(t^-\right) > \dot{q}\left(t^+\right)$, where $\dot{q}\left(t^-\right) = f\left(\rho_1^{j-1}\right) - \mu_j$, $\dot{q}\left(t^+\right) = f\left(\rho_2^{j-1}\right) - \mu_j$. Then $K = \frac{\left(\xi_{\bar{t}}\right)^2}{2}\left(f\left(\rho_1^{j-1}\right) - f\left(\rho_2^{j-1}\right)\right)$, and

$$\Delta J_{1,j} = \eta_j\left(\tau - \bar{t} - \xi_{\bar{t}}\right) + \frac{\xi_\tau \eta_j}{2} + \frac{\left(\xi_{\bar{t}}\right)^2}{2}\left(f\left(\rho_1^{j-1}\right) - f\left(\rho_2^{j-1}\right)\right).$$

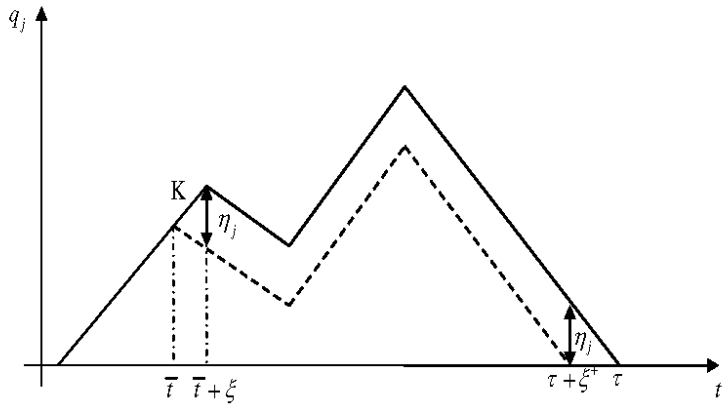

Figure 4.30: case 2).

2. $sgn\left(\eta_j\right) = -1$, $sgn\left(\xi_{\bar{t}}\right) = 1$.

$$\Delta J_{1,j} = \eta_j\left(\tau + \xi_\tau - \bar{t} - \xi_{\bar{t}}\right) - \frac{\xi_\tau \eta_j}{2} + \frac{\left(\xi_{\bar{t}}\right)^2}{2}\left(f\left(\rho_1^{j-1}\right) - f\left(\rho_2^{j-1}\right)\right).$$

3. $sgn\left(\eta_j\right) = 1$, $sgn\left(\xi_{\bar{t}}\right) = -1$.

$$\Delta J_{1,j} = \eta_j\left(\tau - \bar{t}\right) + \frac{\xi_\tau \eta_j}{2} + \frac{\left(\xi_{\bar{t}}\right)^2}{2}\left(f\left(\rho_1^{j-1}\right) - f\left(\rho_2^{j-1}\right)\right).$$

Remark 79 *If* $f\left(\rho_1^{j-1}\right) > f\left(\rho_2^{j-1}\right)$ *then* $sgn\left(\eta_j\right) = sgn\left(\xi_{\bar{t}}\right)$. *If* $f\left(\rho_1^{j-1}\right) < f\left(\rho_2^{j-1}\right)$ *then* $sgn\left(\eta_j\right) = -sgn\left(\xi_{\bar{t}}\right)$.

4. $sgn\left(\eta_j\right) = sgn\left(\xi_{\bar{t}}\right) = -1$.

$$\Delta J_{1,j} = \eta_j\left(\tau + \xi_\tau - \bar{t}\right) - \frac{\xi_\tau \eta_j}{2} - \frac{\xi_{\bar{t}} \eta_j}{2}.$$

We can see that $\Delta J_{1,j}$ has the same value in each case, or

$$\Delta J_{1,j} = \eta_j\left(\tau - \bar{t} + \frac{\xi_\tau - \xi_{\bar{t}}}{2}\right).$$

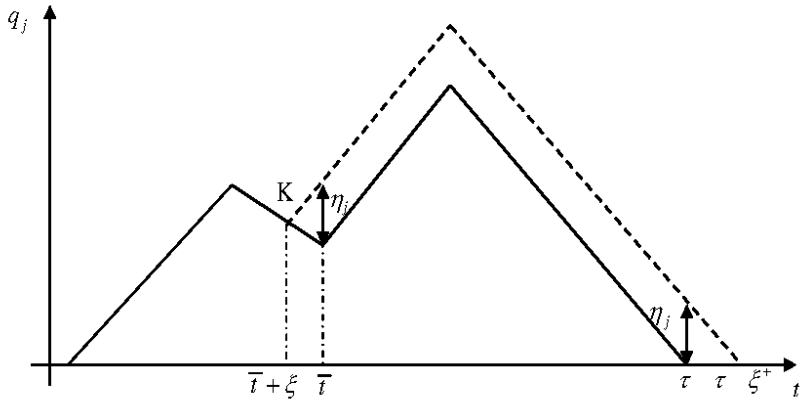

Figure 4.31: case 3).

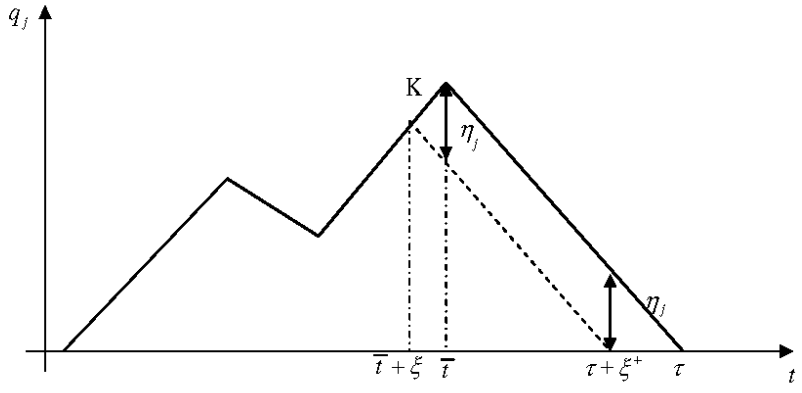

Figure 4.32: case 4).

Since $\xi_\tau = \frac{\eta_j}{\mu_j - \rho_1^j}$, $\Delta J_{1,j}$ assumes the following expression:

$$\Delta J_{1,j} = \eta_j (\tau - \bar{t}) - \frac{\eta_j^2}{2} \left(\frac{1}{\mu_j - \rho_1^j} + \frac{1}{f\left(\rho_2^{j-1}\right) - f\left(\rho_1^{j-1}\right)} \right) = \eta_j c_1(\rho) + \eta_j^2 c_2(\rho),$$

where ρ is the solution.

Finally the variation of $J_{1,j}$ is

$$\frac{\partial J_{1,j}}{\partial \xi_0} = \frac{\partial \eta_j}{\partial \xi_0} c_1(\rho).$$

For the variation of J_2, calling ξ_N the generic N-th shift, we have:

$$\Delta J_2 = \int_{\bar{t}}^{\bar{t}+\xi_N} \left(\left[\rho_1^N - \varphi(t)\right] - \left[\rho_2^N - \varphi(t)\right] \right) dt.$$

If $f \in C^0$, then ξ_N is sufficiently small and it results that

$$\Delta J_2 = \xi_N \left[\left(\rho_1^N - \varphi(t)\right)^2 - \left(\rho_2^N - \varphi(t)\right)^2 \right] + o(\xi_N).$$

The variation of J_2 is

$$\frac{\partial J_2}{\partial \xi_0} = \frac{\partial \xi_N}{\partial \xi_0} c_N(\rho).$$

4.3 Numerical method

Some numerical methods for the evolution of the tangent vectors ξ and η, and for the functional J, are necessary to obtain simulative results. In particular, since for each arc there are two distinct equations, i.e. a conservation law (for density) and an ordinary differential equation (for the queue), two numerical methods have to be used. Starting by the numerical methods for the discretization of Klar model shown in subsection 3.1, now we consider the numerics for tangent vectors. Let f_0^n be the discrete version of the input function $f_0(t)$ e let t_k be its discontinuity points. For a generic arc j and t_k, ${}^{k,j}\xi_i^n$ is the approximation of vector ${}^k\xi_j(x_i, t^n)$, while ${}^{k,j}\eta^n$ approximates the vector ${}^k\eta_j(t^n)$. Shift starting values are zero, i.e. ${}^{k,j}\xi_i^0 = {}^{k,j}\eta^0 = 0$. In the ghost cell of the first arc I_1, if $n\Delta t = t_k$ then ${}^{k,j}\xi_1^n = 1$. In the inner arc, instead, we have that

$${}^{k,j}\xi_i^{n+1} = {}^{k,j}\xi_{i-1}^n.$$

Based on the analytical results in the previous section, we have the following four cases:

a-1.*i*)

$$\begin{cases} {}^{k,j}\eta^{n+1} = 0 \\ {}^{k,j}\xi_1^{n+1} = {}^{k,j-1}\xi_{N_{j-1}}^{n} \end{cases}$$

a-1.*ii*)

$$\begin{cases} {}^{k,j}\xi_1^{n+1} = {}^{k,j-1}\xi_{N_{j-1}}^{n} \\ {}^{k,j}\eta^{n+1} = {}^{k,j-1}\xi_{N_{j-1}}^{n}\left({}^{j-1}\rho_{N_{j-1}}^{n+1} - \mu_j\right) \end{cases}$$

a-2)

$$\begin{cases} {}^{k,j}\xi_1^{n+1} = 0 \\ {}^{k,j}\eta^{n+1} = {}^{k,j-1}\xi_{N_{j-1}}^{n}\left({}^{j-1}\rho_{N_{j-1}}^{n+1} - {}^{j-1}\rho_{N_{j-1}}^{n}\right) + {}^{k,j}\eta^{n} \end{cases}$$

b)

$$\begin{cases} {}^{k,j-1}\xi_{N_{j-1}}^{n} = 0 \\ {}^{k,j}\eta^{n+1} = 0 \\ {}^{k,j}\xi_1^{n+1} = -\frac{{}^{k,j}\eta^{n}}{{}^{j-1}\rho_{N_{j-1}}^{n} - \mu_j} \end{cases}$$

Now, in order to consider the numerics related to the variation of the cost functional, from $J = \sum_j J_{1,j} + J_2$, we have that

$$\frac{\partial J}{\partial \xi_k} = \sum_j \frac{\partial J_{1,j}}{\partial \xi_k} + \frac{\partial J_2}{\partial \xi_k}.$$

We indicate the numerical approximations $\frac{\partial J_{1,j}}{\partial \xi_k}$ and $\frac{\partial J_2}{\partial \xi_k}$, respectively, with ${}^{k,j}Y_1^n$ and ${}^{k}Y_2^n$.

If $q_j^{n+1} > 0$ then

$${}^{k,j}Y_1^{n+1} = {}^{k,j}Y_1^n + {}^{k,j}\eta^n \Delta t.$$

If $q_j^{n+1} = 0$ we have two cases:

1. if $q_j^n = 0$ then
$${}^{k,j}Y_1^{n+1} = {}^{k,j}Y_1^n;$$
2. if $q_j^n > 0$ then
$${}^{k,j}Y_1^{n+1} = {}^{k,j}Y_1^n + \frac{1}{2}{}^{k,j}\xi_1^{n+1}\,{}^{k,j}\eta^n.$$

For ${}^{k}Y_2^n$ we have that:

$$ {}^{k}Y_2^{n+1} = {}^{k}\, Y_2^n + {}^{k,N}\, \xi_{N_N}^n \left[\left({}^{N}\rho_{N_N}^n - \varphi^n \right)^2 - \left({}^{N}\rho_{N_N}^{n+1} - \varphi^n \right)^2 \right] $$

where φ^n is the numerical approximation of $\varphi\,(t)$.

We can observe that through the tangent vector method, we are able to determine the numerical first derivative of functionals J_1 and J_2. Then using the Steepest Descent algorithm, we can find the optimum configuration of the discontinuities of input flow that minimizes the entire functional J; in formula we have:

$$ t_{n+1} = t_n + h \frac{\partial J}{\partial t}, $$

where h is a pre-fixed scalar quantity, which represents the step of this algorithm.

The following example shows the use of this optimization technique. Consider a supply chain with two arcs, each of them characterized respectively by maximal processing times $\mu_1 = 200$, $\mu_2 = 75$ and lengths and processing times of each processor equal to 1. We assume that arcs and queues are empty at $t = 0$, the total simulation time is $T = 20$ and spatial and time discretization steps are equal, i.e. $\Delta x = \Delta t = 0.02$. For the input flow we consider three different levels, $\rho_1 = 100$, $\rho_2 = 80$, $\rho_3 = 50$, and two discontinuities, whose starting values are $t_1 = 6$ and $t_2 = 13$. The aim is to minimize the queue handling a pre-assigned piecewise constant outflow $\varphi(t)$ defined as follows:

$$ \varphi(t) = \begin{cases} 100, & 0 \leq t \leq 10, \\ 50, & 10 \leq t < T. \end{cases} $$

The results, obtained via simulation, are presented in the following figures. In particular Fig. 4.33 shows the values assumed by J at each iteration step of the steepest descent algorithm, while in the Fig. 4.34 it is shown the "path", point to point, followed by the algorithm in the plane (t_1, t_2). As shown in Fig. 4.33 J is decreasing until reaching its minimum (its value is equal to zero) in the point $(t_1, t_2) = (0, 0)$.

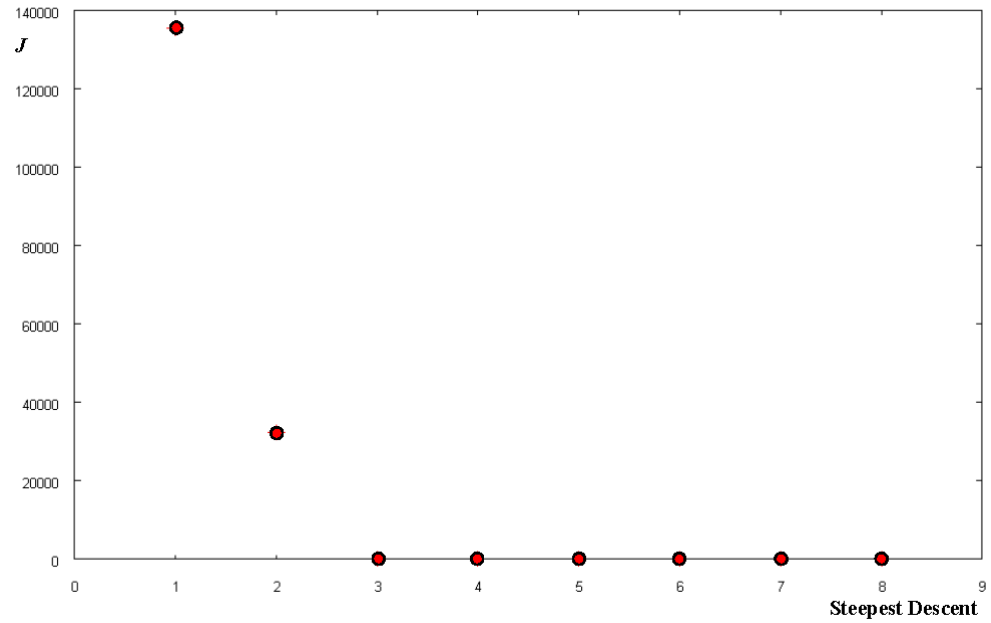

Figure 4.33: J versus Steepest Descent.

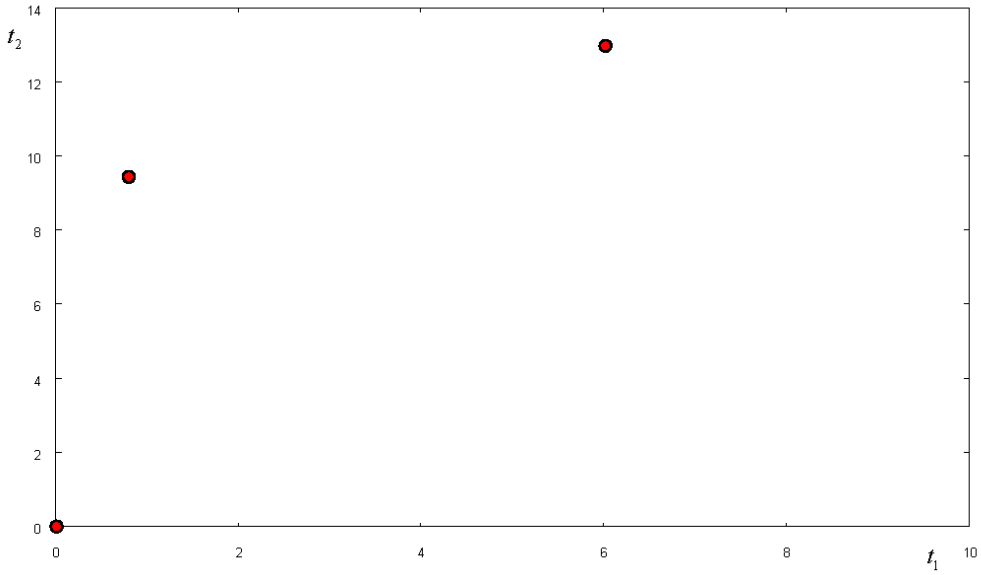

Figure 4.34: Evolution of points (t_1, t_2).

Bibliography

[1] E. J. Anderson, *A new continuous model for job shop scheduling*, International J Systems Science 12: 1469-1475 (1981).

[2] D. Armbruster, P. Degond and C. Ringhofer, *A model for the dynamics of large queuing networks and supply chains.*, SIAM J. Appl. Math., 66 (2006), pp. 896-920.

[3] D. Armbruster, D. Marthaler, C. Ringhofer, *Kinetic and fluid model hierarchies for supply chains*, SIAM J. on Multiscale Modeling, 2 (1), pp. 43 - 61, 2004.

[4] W.-J. Baumol, *Economic Dynamics*, Macmilan, New York, 1970.

[5] R. Billings, J. Hasenbein, *Applications of fluid models to semiconductor fab operations*, preprint, (2001).

[6] A. Bressan, *Hyperbolic Systems of Conservation Laws*, Oxford Univ. Press, 2000.

[7] A. Bressan, G. Crasta, B. Piccoli, *Well Posedness of the Cauchy Problem for $n \times n$ Systems of Conservation Laws*, Memoirs of the American Mathematical Society, vol. 146, n. 694, 2000.

[8] G. Bretti, C. D'Apice, R. Manzo and B. Piccoli, *A continuum-discrete model for supply chains dynamics*, Networks and Heterogeneous Media, (2007).

[9] C. Dafermos, *Hyperbolic Conservation Laws in Continuum Physics*, Springer - Verlang, 1999.

[10] C.F. Daganzo, *A continuum theory of traffic dynamics for freeways with special lanes*, Trans. Res. B, 31 (1997), p. 83.

[11] C.F. Daganzo, *A Theory of Supply Chains*, Springer Verlang, New York, Berlin, Heidelberg, 2003.

[12] C. D'Apice, R. Manzo, *A fluid-dynamic model for supply chain*, Networks and Heterogeneous Media (NHM) (2006), Vol. 1, No. 3, pp. 379-398.

[13] C. D'Apice, R. Manzo, B. Piccoli, *Modelling supply networks with partial differential equations*, submitted to CMS.

[14] P. Degond, S. Göttlich, M. Herty and A. Klar, *A network model for supply chains with multiple policies*, SIAM J. on Multiscale Models, (2007).

[15] J. W. Forrester, *Industrial Dynamics*, MIT Press, MA, 1964.

[16] E. Godlewski and P.A. Raviart, *Hyperbolic systems of conservation laws*, Mathématiques & Applications [Mathematics and Applications], 3/4. Ellipses, Paris, 1991.

[17] S. Göttlich, M. Herty and A. Klar, *Modelling and optimization of Supply Chains on Complex Networks*, Communication in Mathematical Sciences, 4(2), pp. 315-330, 2006.

[18] D. Helbing, D. Armbruster, A. Mikhailov and E. Lefeber, *Information and material flows in complex networks*, Physica A, 363 (2006).

[19] D. Helbing, S. Lammer, *Supply and production networks: from the bullwhip effect to business cycles*, in: D. Armbruster, A. S. Mikhailov and K. Kaneko (eds.) *Networks of Interacting Machines: Production Organization in Complex Industrial Systems and Biological Cells*, World Scientific, Singapore, 2005, pp. 33-66.

[20] D. Helbing, S. Lammer, T. Seidel, P. Seba, T. Platkowski, *Physics, stability and dynamics of supply networks*, Physical Review E 70 (2004), 066116.

[21] M. Herty, A. Klar, B. Piccoli, *Existence of solutions for supply chain model based on partial differential equations*, SIAM J. Math. An., 39(1), pp. 160-173, 2007.

[22] S. N. Kruzkov, *First order quasi linear equations in several independent variables*, Math. USSR Sbornik, 10 (1970), p. 217.

[23] R. J. Leveque, *Finite Volume Methods for Hyperbolic Problems*, Cambridge, 2002.

[24] G. F. Newell, *A simplified theory of kinematic waves in highway traffic*, Transportation Research B, 27 (1993), pp. 281-313.